INFORMATION TO USERS

This manuscript has been reproduced from the microfilm master. UMI films the text directly from the original or copy submitted. Thus, some thesis and dissertation copies are in typewriter face, while others may be from any type of computer printer.

The quality of this reproduction is dependent upon the quality of the copy submitted. Broken or indistinct print, colored or poor quality illustrations and photographs, print bleedthrough, substandard margins, and improper alignment can adversely affect reproduction.

In the unlikely event that the author did not send UMI a complete manuscript and there are missing pages, these will be noted. Also, if unauthorized copyright material had to be removed, a note will indicate the deletion.

Oversize materials (e.g., maps, drawings, charts) are reproduced by sectioning the original, beginning at the upper left-hand corner and continuing from left to right in equal sections with small overlaps.

Photographs included in the original manuscript have been reproduced xerographically in this copy. Higher quality 6" x 9" black and white photographic prints are available for any photographs or illustrations appearing in this copy for an additional charge. Contact UMI directly to order.

ProQuest Information and Learning
300 North Zeeb Road, Ann Arbor, MI 48106-1346 USA
800-521-0600

Université d'Ottawa · University of Ottawa

Seismic Response of Existing Buildings Constructed Using Semi-rigid Riveted Connections

by

Kevin C. Chessman

Thesis submitted to the Faculty of Graduate and Postdoctoral Studies
in partial fulfilment of the requirements for the
Master of Applied Science Degree in Civil Engineering
under the auspices of the
Ottawa-Carleton Institute for Civil Engineering

January 2001

Department of Civil Engineering, University of Ottawa
Ottawa, Canada, 2001

À ma famille

Abstract

The use of riveted semi-rigid connections was wide spread in building construction in the first half of the 20th century at a time when earthquake design was not required. It is therefore legitimate to question the seismic response of these historic buildings. Recent experimental work has shown that these connections can develop stable hysteretic moment rotation behavior, but must undergo large rotations in order to reach moderate moment capacity. This raises important concerns about the ability of buildings having such connections to withstand earthquakes while undergoing large drifts.

An 18-story building located in Eastern Canada has been surveyed and modeled using a non-linear inelastic dynamic analysis program. It was investigated whether this type of building can survive major earthquakes in spite of having low-strength semi-rigid connections such as those described above. Other generic structures of different heights, based on this existing building, have also been considered and modeled. Seismic ground motions typical of Eastern and Western Canada have been used to generalize the results obtained.

It was observed that old buildings of the type modeled in this study have much larger masses due to heavier floors and thicker cladding than their modern counterparts. The buildings also have considerably less rigidity, as a result of semi-rigid connections. The ensuing large period favorably impacts their seismic response. However, results demonstrate that small earthquakes cause considerable drifts, which can translate into non-structural damage in spite of the survival of the primary structure.

Acknowledgments

I wish to express my sincere gratitude to my research supervisor, Dr. Michel Bruneau for his insight and patience throughout this work, and his assistance in preparing this thesis. Funding for this research was provided in part by the National Sciences and Engineering Research Council, and is appreciated. I would also like to thank Mr. Luc Jolicoeur from the Engineering Department of the City of Quebec for providing useful information on the type of buildings considered in this study and the additional funding.

My deepest thanks go to my wife and my family for their continuous encouragement and support.

Table of Contents

Chapter 3

Chapter 4

Chapter 5

List of Tables

List of Figures

Notations

A_{net}	Net area of stem, mm^2
A_{rivet}	Cross-sectional area of rivet, mm^2
$F_{u\ rivet}$	Ultimate strength of rivet = 480 MPa
$F_{y\ rivet}$	Yield strength of rivet = 220 MPa
$F_{u\ steel}$	Ultimate strength of base steel = 400 MPa
$F_{y\ steel}$	Yield strength of base steel = 206 MPa
M	Applied moment, kN·m
M^+	Positive moment causing tension in top connection assembly, kN·m
M^-	Negative moment causing tension in bottom connection assembly, kN·m
SF	Safety factor used in connection redesign = 0.6
T	Tension applied to connection assembly, kN
θ	Connection rotation, radians
V	Applied shear force, kN

Chapter 1

Introduction

1.1 General

The designers of early high rise steel framed buildings were generally not required to incorporate lateral load resisting systems into their structures. Building codes of that era did not include provisions against earthquakes. Accordingly most of the steel framed buildings of the first half of the 20th century were constructed with connections that would be considered flexible, or at the very most semi-rigid, according to today's standards.

Building codes now have very stringent requirements for seismic design, as the importance of safeguarding the public against seismic hazards has been recognized over the years. However, pre-1950 structures are still very much part of our daily lives and engineers have been confronted with the need of assessing the survivability of these buildings in the event of a major earthquake.

When evaluating these older structures, many engineers typically consider the existing flexible and semi-rigid connections as simply not having any moment resistance. This conservative approach could require substantial retrofitting which always proves to be intrusive, disruptive and generally very costly. Where seismic retrofit is required by legislation, and when these retrofits are too costly to implement, the owner may have no other recourse than demolition, which may be undesirable for historic buildings. This could be

avoided with a clearer understanding of the behavior of buildings incorporating semi-rigid connections.

Recent studies have demonstrated that these semi-rigid connections can in fact develop some moment resistance in a ductile manner. Due to the number of connections found in a structure, their contribution to lateral load resistance could add up to be significant. These connections are present at every beam-to-column assembly of every frame. This inherent lateral resistance could minimize the amount of retrofitting or even avoid it altogether in areas of lower seismic activity.

1.2 Knowledge of Buildings Constructed with Semi-rigid Connections

Recent experimental work attests that these connections are able to develop stable hysteretic moment rotation behavior, but must first undergo large rotations in order to reach moderate moment capacity. It is therefore legitimate to question the seismic response of buildings incorporating these types of connections.

1.3 Objectives of this Research

It is the objective of the study presented in this thesis to:

i. Investigate the seismic response of an existing turn-of-the-century steel framed building, incorporating riveted connections, to moderate and high levels of seismic excitation, namely seismic activity expected in Eastern and Western Canada;

ii. Investigate the seismic response of other structures based on the aforementioned existing building and subjected to the same levels of excitation.

iii. Assess, based on this limited case study, whether these older steel structures have inherent properties that significantly impact their seismic behavior compared to more modern types of construction.

1.4 Scope of Work

In this analytical study, four frames of different sizes based on an existing building were analyzed. The analyses were performed using a non-linear inelastic dynamic analysis program. The four frames were subjected to earthquakes which represented the expected levels of excitation for Eastern and Western Canada. Six different earthquakes were scaled to the peak ground acceleration (PGA) expected in Victoria, British-Colombia, and four scaled to the PGA expected in Quebec City.

Moreover, two different types of connections were incorporated (separately) in all four frames: riveted stiffened seat angles and riveted stiffened tee-stubs. To account for possible second-order stability effects, the analyses were also performed with and without consideration of P-Δ effects. Finally, two different mass scenarios were used for comparison, the first using the as-built conditions (large masses) and the second using more modern construction materials (lighter overall mass).

Mean and maximum inter-story drifts as well as the maximum rotations will be computed for each of the analysis scenarios given above, and behavior of the various systems will be compared to identify the key factors that impact seismic response in these cases.

1.5 Outline of Thesis

Chapter 2 reviews the existing literature available on semi-rigid connections as well as the background of the model used in the analysis program. A description of the structures, analytical approach and the different scenarios used for the analysis is presented in Chapter 3. Chapter 4 presents both the analysis results and observations. Finally, Chapter 5 draws on these analytical results to present recommendations and a conclusion.

CHAPTER 2

Literature Review

2.1 General

For practical reasons nowadays, when analyzing a structure, connections in buildings are generally assumed, by design engineers, to be either fully rigid or fully flexible. Yet all types of assemblies allow some degree of flexibility and some degree of restraint. Connections which offer very little resistance to rotation would naturally fall in the flexible category and connections able to resist moment while allowing little rotation in the other. Semi-rigid connections, which fall somewhere in between the above connection types, allow some rotation but also display a certain amount of moment resistance.

Many researchers have demonstrated that semi-rigid connections do develop some moment resistance, albeit in some cases of limited magnitude compared to the connected beam. All of the early research has been strictly limited to developing the monotonic behavior of these connections. However with the importance of seismic survivability of older structures, more recent work has focused on the cyclic behavior of semi-rigid connections. These studies have resulted in a number of experimental and analytical models to describe the cyclic moment-rotation (M-θ) of various semi-rigid connection types.

Since the advent of computerized analysis tools, engineers have been able to predict more accurately the behavior of buildings during seismic excitation. As the aforementioned M-θ models became increasingly complex, the software available kept pace. In the following

sections some of the observations on the monotonic tests and findings from the cyclic experiments are presented along with brief descriptions of selected hysteresis models developed by other researchers, and the hysteretic element found in the software package used in the present study.

2.2 Experimental Investigations

In order for engineers to properly evaluate the performance of a given connection it is important to have accurate and reliable models describing its behavior. Experimental studies are essential in developing these models and to allow improved understanding of connection behavior.

2.2.1 Monotonic Tests

The first tests specifically performed on steel frame connections were done to examine the effect of wind on structures. These tests subjected the specimens to monotonic loads with small load reversals. Tests were performed in the early 1900's by Wilson and Moore (1917) and different types of connections were later tested by Young and Jackson (1934). These tests were also done to examine possible weight savings due to continuity at the beam-to-column joint. Rathbun (1936) performed an extensive study on riveted connections, examining three common connection types used at the time, namely, standard clip-angle connections, seat-angle connections and shallow wind-braced connections (tee-stubs). He concluded that these connections could incur large deformations without major loss in shear capacity.

Forty-seven separate specimens were tested by Hechtman and Johnston (1947). Their testing program mainly focused on top and seat angle connections but they included other types of connections, namely those using tees as beam flange connectors. They examined the effects of various factors in the connections by changing the beam depth, top angle thickness and beam flange thickness. They determined that most of the rotation was caused by bending of

the top flange connection assembly, slippage between connected elements and extension of the rivets.

Lewitt, Chesson and Munse (1969) investigated the role of angles in the behavior of semi-rigid connections. They applied direct tension and compression to angles in order to observe their response. They developed an exponential formulation to express the load-deformation characteristics of these angles. They also determined that angles subjected to tension develop three plastic hinges (Figure 2.1) as they reach their maximum capacity.

More recently, many other researchers undertook studies to better understand the behavior of semi-rigid connections under monotonic loading (Hetchman and Johnston 1948; Marley 1982; Maxwell et al. 1981). The results from these studies have been used to develop experimentally based models. These models will be briefly discussed in a subsequent section.

2.2.2 Cyclic Test

The tests performed by Young and Jackson (1934) were among the first to incorporate loading reversal. Although the riveted connections were subjected to small amounts of load reversal (to simulate the effects of wind), significant pinching[1] was observed in the M-θ curves even at small magnitudes of rotation. In more recent years, research on semi-rigid connections have been directed towards the determination of their M-θ behavior when subjected to larger cyclic loading expected from seismic excitation.

Astaneh, Nader and Malik (1989) performed a series of tests on bolted and welded double angle web connections. They subjected the connections to increasingly larger magnitudes of

[1]Pinching of hysteretic loops typically develops when certain components of a structural member or system can only contribute once (i.e in one loading direction) to the global energy dissipation mechanism. Higher stiffness is usually recovered when deformations increase beyond the maximum value previously obtained, as these components can now further dissipate energy.

cyclic rotations until failure. One of the conclusions of their research was that although the specimens demonstrated ductile behavior, they all showed signs of pinching in their hysteresis loops. This pinching was more evident in the bolted connections.

A series of tests on bolted semi-rigid connections were performed by Bernuzzi, Zandonini and Zanon (1992). Three connection types were tested among which top and seat angles were subjected to cyclic loading. They observed that slippage was the major cause of pinching in the M-θ curves.

Roeder, Leon and Preece (1994) constructed and tested a series of twenty-three specimens to simulate the existing conditions found in a San Francisco building. The study included tests on tee-stubs as well as top and bottom seat angles with web clips, some of which had columns encased in concrete with continuous concrete slabs. The specimens were all constructed using new materials. The riveted connections were constructed in some instances using an in-laboratory riveting machine and at other times using over-tightened mild steel bolts to simulate the rivets. It was assumed that the concrete encasement originally designed to 17 MPa would have increased over time. The encasement was thus designed to have a 24 MPa 28-day compressive strength. The encasement was also reinforced with a light welded-wire mesh. The experimental results showed pinched and deteriorating M-θ curves (Figure 2.2). The mode of rupture for the top and seat angle connections was the shear failure of the rivets in the flange of the beam. The tee-stubs had two modes of rupture occurring, the shearing of the rivets in the tee's stem and yielding of the tee's flange accompanied with tensile yielding of the rivets connected to the column. Figure 2.3 shows the deformations observed during the testing of the tee-stubs. It was observed that the concrete encasement and presence of continuous slab improved the joint rigidity by as much as 300% for the clip angle connections and up to 30% for the tee-stubs.

Several joint assemblies were salvaged during the demolition of an early 1900's building in Ottawa. The specimens were riveted stiffened seat-angle connections (Figure 2.4). Two

series of test were performed on these connections. The first test by Bruneau and Sarraf (1996) tested the specimens cyclically to failure. The concrete encasement used as fireproofing was removed for this test. The results obtained showed severely pinched M-θ curves. The connection failed by the shearing of the rivets in the outstanding leg of the upper angle. Among other tests performed, the basic material properties for the base metal and the rivets were determined. Figure 2.5 gives the stress-strain relationship of a $^3/_4$" rivet obtained by tensile tests. Bruneau and Bisson (2000) later tested another specimen from the same building. This test examined the effects of the concrete encasement on the overall resistance of the connections. Samples of the concrete were tested in order to replace some of the fireproofing removed during instrumentation. The compressive strength was determined to be around 8 MPa. Pinched M-θ curves were also obtained during this second test. The hysteresis curves are presented in Figure 2.6. It was concluded that the concrete encasement did not provide any additional stiffness to the connections.

2.2.3 Retrofit Strategies

Having demonstrated the ability of semi-rigid connections to develop stable hysteresis loops, researchers attempted to increase the energy dissipation capabilities of these connections. Creating effective ways of retrofitting these semi-rigid connections will allow older structures to continue functioning without major disruptions due to earthquakes.

Roeder, Leon and Preece (1994) presented in their study a relatively simple retrofit strategy. They added angles at the top and the bottom of the beam-to-column intersection clamping them together with threaded rods to increase the concrete confinement and provide composite action at larger rotations (Figure 2.7). The results obtained demonstrated an increase in maximum resistance of approximately 25%. However, it was observed that initial shear failure of the rivets occurred at the same rotation as the non-retrofitted specimens.

Bruneau and Sarraf (1996) and Bruneau and Bisson (2000) suggested various strategies for retrofitting their specimens, either by simply replacing selected rivets by high strength bolts, by performing selective welding of specific areas, by adding knee braces or by adding fuse plates. In all four cases, encouraging results were obtained. The strategies relying on high strength bolts and on welding greatly reduced pinching in the M-θ curves by eliminating the slip between the elements and reducing yielding of the fasteners. The knee braces demonstrated large moment resistance and considerable energy dissipation capabilities in both positive and negative rotations. The knee braces, however, require special design considerations and significant on-site preparation. Furthermore, the braces also take up significant space once installed, especially on the top of the connections. The use of steel band fuse plates (a steel band wrapped around the column and a fuse plate welded to the beam) does not require the removal of concrete from the column thus minimizing some of the preparation required on site. The fuse plate acts as an energy dissipater during cyclic loading. The results from the experimental testing shows M-θ curves which are still pinched but overall dissipate a much larger amount of energy. Figures 2.8 and 2.9 show configuration of the knee braces and steel band fuse plates. Figure 2.10 compares the M-θ curves of the existing connection and the retrofitted connection using the steel band fuse plates.

2.3 Hysteresis Models

Various connection types have been modeled successfully using simple models. Double web angle connections for example have been modeled considering the tensile load deformation of the angles (Lewitt et al. 1966). The monotonic behavior of top and seat angle connections have been also modeled by Youssef-Agha et al. (1989). The monotonic non-linear M-θ curve for this connection is simplified to a bi-linear form which includes the initial stiffness and the strain hardening. This model includes the effects of the column flange deformation and the bolt elongation while ignoring their slippage.

Fry and Morris (1976) have proposed polynomial models which use curve fitting constants and standardized parameters based on the type of connection and its geometry. This model was successfully applied to various connection types with, however, certain values of moment creating a negative stiffness. Proposed B-spline curve fitting models also match experimental M-θ curves well. However, they require large number of data points to properly calibrate, and are more computationally intensive and complex than multi-linear models.

De Stephano, De Luca and Astaneh-Asl (1994) developed a cyclic response model for double web angle connections. The connection is modeled by using rigid elements for the beam and column and non-linear springs for the web angles. The model accounts for strain hardening and alternating contact between the column flange and the top and bottom of the web angles during reverse loading. This model was later expanded by De Luca (1995) to represent top and seat angle connections. The model predicts well the strength of the top and seat angle connections without, however, including the characteristic pinching of this semi-rigid connection (Figure 2.11).

Roeder, Leon and Preece (1994) developed analytical models to represent the connections tested in the study previously described. Their models consider the formation of plastic hinges in the legs of the connecting elements (angles or tees), the tensile yielding of the rivets and prying action. Figures 2.12 and 2.13 show the local equilibrium of the bending and prying forces in the clip angle and the tee-stub connections.

Bruneau and Sarraf (1996) have developed a model for top and stiffened seat angle connections. Their model is also based on the formation of a plastic mechanism in the top angle but replaces the simple horizontal yield line (considered by other researchers) by a more complex yield pattern (Figure 2.14). The capacity of the top angle and stiffened seat angle are calculated based on the principles of virtual work. The hinging mechanism of the seat angle follows the same pattern described above with the addition of a plastic hinge

forming in the stiffeners (Figure 2.15). The calculated resistance of the stiffened seat angle connection is in good agreement with the capacities observed experimentally.

2.4 Inelastic Non-linear Analysis Programs

The research studies discussed above described the behavior of top and seat angle connections and of tee-stub connections as having severely pinched hysteretic M-θ curves (see for example, Figure 2.6). This type of hysteretic element is, however, not easily found in commercially available non-linear inelastic analysis software.

Roeder, Leon and Preece (1994) have developed an element which can be incorporated in *Drain-2DX*. Figure 2.16 shows their riveted connection hysteresis rule. Another software package also offers an hysteretic element with a similar behavior. *Ruaumoko*[2] offers over 30 different hysteretic models for its elements. These range from the simple bi-linear model to the complex steel brace member hysteresis model. Of particular interest here is the Mehran Keshavarzian Degrading and Pinching Hysteresis model (Figure 2.17). This hysteresis model can be adjusted to resemble the characteristic M-θ curve of the typical semi-rigid connection described earlier. To illustrate this capability, the Mehran Keshavarzian Degrading and Pinching Hysteresis rule is superimposed over an experimentally obtained M-θ curve (Bruneau and Sarraf, 1996) in Figure 2.18. As shown, the computer model follows closely the experimental curve envelope.

[2] *Ruaumoko* is a non-linear inelastic analysis software developed by Dr. Athol Carr from the University of Canterbury in New Zealand.

CHAPTER 3

Analytical Approach

3.1 Existing Structure

For this analytical study, an existing structure is used as the model for the generic frames analyzed. The structure was built in the late 1920s and is still in use today. It is located in Eastern Canada in a zone of moderate seismicity. The structure was built using riveted connections without any bracing. The modeling of the structure was done using the original architectural and structural drawings as well as additional information collected during a five-week site visit of the existing building.

The structure is an 18-story office building (Figure 3.1) and its height is 250.7 ft (76.4 m). In its East-West direction the structure has five bays tapering to three on the fifth floor and further down to two on the upper levels (15^{th} to 18^{th}). In the North-South direction it has 6 bays which taper to 4 bays on the 15^{th} level. The first level was originally used as commercial space and has a larger story height to accommodate a mezzanine at the South end. The floor to floor height of 23 ft makes this level more susceptible to seismic excitation (soft story). The original corporate offices were located on the 14^{th} floor which also has a larger inter-story height (18 ft). The average height of the office floors is just under 12 ft. The upper floors house the mechanical and electrical equipment (17^{th} and 18^{th}). The structure has a sloped copper roof with a large steel framed, stone-clad chimney.

The spacing of the columns changes four times over the height of the building. In all cases, deep beams are used to transfer the loads to the levels below. These transfer girders are situated on the 2nd, 13th and 15th and 18th floors.

The types of material used in the construction of this structure make for very large floor masses. The typical floor was constructed using 2" concrete slabs over 10" concrete joists, $2^1/_2$" cinder fill plus the floor finishing. The corridors have a $1^1/_2$" terrazzo floor finish. The partitions are all terra cotta bricks covered on both sides with plaster. The exterior walls are 4" stone, over 6" bricks, over 3" terra cotta furring over plaster. The weight of the exterior walls is 165 lbs/ft^2!

All the sizes for the steel members were given on the architectural and structural drawings. Some shop drawings showing typical stiffened tee-stub connection details were also available for the lower floors. The drawings gave rivet dimensions, and some of the sizes for the tee connectors. Unfortunately not all the required information was found on these drawings. Tee thicknesses and stiffener sizes were not indicated for example. Likewise, none of the connection information was available for the remainder of the building.

It was thus decided to redesign the connections using early 1900's design methods, to obtain representative sizes this redesign was done based on the architects specifications. The architect provided all the design loads to be used including a 30lbs/ft^2 wind load. *The Structural Engineer's Handbook* (Ketchum, 1924) was used for help with 1920's design philosophy. The rivet layout was assumed constant for each connection throughout the majority of the structure (Figure 3.2). The rivet layout had to be modified for the upper floors as the columns became narrower. This was verified during the site visit and with historical photos of the construction.

Appendix A gives an example of the calculations used in the design. The assumptions made are also explained in the Appendix. The same design process was followed for the twenty

different connections of the 18-story structure. All the connection sizes obtained are listed in Table 3.1.

3.2 Generic Frames

The same type of connections are found in both the East-West and North-South frames making the narrower frame more susceptible to seismic excitation. It was decided to use the East-West frame as the model generic frame analyzed in the present study. However, four frames of different heights are analyzed to broaden the findings of this parametric study.

The first frame analyzed represents the existing structure. It is a simplified version of the East-West frames of the building. A side by side comparison of the two frames is given in Figure 3.3. The bays at either end of the existing structure have simple pinned connections and have thus been removed. The sloped roof framing has also been removed to further simplify the analysis as this detail was deemed to be of little significance on seismic behavior. The roof masses have been lumped at the top floor. Other simplifications were made regarding modeling of the transfer girders and their connections. It was assumed that transfer girders behave as a rigid body and that the columns supporting them are rigidly connected to the girder. The other elements framing into the transfer girders are all assumed to be simply connected. These assumptions are also shown on Figure 3.3.

The computer model was created assuming that the beams and columns remain elastic. The connections are modeled using spring elements. This effectively doubled the number of nodes as the springs are attached to two superimposed nodes. The model has 179 nodes and 229 elements with 20 different spring stiffnesses.

In its existing condition the 18-story frame has a period of 5.04 sec. This is quite high for such a building but the structure has very large story masses which tend to lengthen the period.

Three other frames are analyzed in the present study. The frames vary in height but are all based on the 18-story structure (Figure 3.4). The upper stories of the 18-story frame are used in modeling the lower frames. The beam and column sizes are identical as are the spring stiffnesses. All three frames also have higher than expected periods.

The second frame analyzed has 7 stories and its period is 2.33 sec. This frame is equivalent to the 8^{th} to 15^{th} floors of the existing structure. The input file is composed of 84 nodes and 105 elements with 11 different spring stiffnesses. The third frame has 4 stories and a period of 2.30 sec. The 4-story frame is much more flexible than the 7-story frame because of it's geometry. The 4-story frame tapers to two bays on the second floor making the upper floors less rigid. The frame is equivalent to the top floors of the existing structure. This additional flexibility is responsible for the period being almost the same as that of the 7-story frame. The model for the 4-story frame is composed of 42 nodes and 47 elements with 3 different spring stiffnesses. The final frame analyzed has 2 stories with a period of 1.23 sec. It is the same as the penthouse of the existing building. The input file has 17 nodes and 18 elements with a single spring stiffness.

3.3 Connections

As previously stated the connections found throughout the existing building are stiffened tee-stubs. This rigid connection was used in the lateral load resisting system of the structure. The rotational behavior of this connection is similar to the behavior of stiffened seat-angle connections. As seen in Chapter 2, the hysteretic M-θ curves of seat angle connections display severe pinching while still offering some energy dissipation at large rotations. The pinching in the tee-stubs, much like the seat-angle, is caused mainly by the elongation of the rivets and the lack of integrity between the stiffeners and the bottom tee. Rivet elongation results in the top tee separating from the column flange. This separation will cause the tee to offer little resistance until it reaches the elongated rivets in positive bending or the column face in negative bending during subsequent loading. The lack of integrity between the

bottom tee and the stiffeners will behave in a similar fashion. Little resistance will be developed until the tee reaches the deformed stiffeners in one direction or the column in the other.

Calculations are necessary to confirm the above reasoning and to obtain the capacity of the tee-stub connection. A total of ten possible modes of failure are calculated for the connections (six for the top connector and four for the bottom connection assembly) Table 3.2 lists all the failure modes that are calculated for each connection in the 18-story frame. It is observed that for the top tee, the onset of yielding is caused by the tensile yielding of the rivets connecting the tee to the column. Other modes of initial yielding include the net area yielding of the stem, and the formation of a hinge mechanism in the flange of the tee. The modes of rupture for the top tee include tensile rupture of rivets in the flange and shear failure of the rivets in the stem. However all the springs are modeled to behave in an identical manner even though in some cases rivets fail in shear. This is deemed acceptable because in all of those cases the rivets yield in tension prior to shear failure, ensuring some inelastic action in the connectors. This greatly simplifies modeling. Nonetheless, the results from the non-linear analyses are interpreted by comparing the rotation demands with the actual rotation capacities of the connections. Thus, the above failure mechanisms were converted into equivalent rotations for the purpose of that comparison. The initial yielding of the bottom assemblies is caused by either the net area yielding of the stem or tensile yielding of the rivets and plastification of the stiffeners. The ultimate capacity of the bottom connection assembly is caused by the tensile rupture of the stem or shear failure of the rivets connecting the beam's flange to the tee. Table 3.3 lists the yield and ultimate capacities of the connections used in the analyses. Appendix B gives an example of the failure mode calculations.

As stated in Chapter 2, the riveted stiffened seat angle was a popular type of connection for buildings in the early part of the 1900's. For this reason and to further generalize the present

study it was decided to also analyze the four frames using seat angle connections as an alternative.

Certain assumptions have been made to simplify the modeling of these four new frames. The geometry of the frames and the size of the elements remain the same. The only difference occurs in the connections, the spring elements. The stiffness of the new springs must be less than the stiffness of the tee-stubs as the seat angle connections are more flexible. The stiffness of the specimens tested experimentally (Bruneau and Sarraf 1996, Bruneau and Bisson 2000) was compared to the calculated stiffness of the tee-stub and an order of magnitude difference was observed. All connection stiffnesses in the model (spring stiffnesses) were therefore reduced by a factor of 10.

Another characteristic which could change is the capacity (yield and rupture) of the connections. It was however deemed acceptable to keep the same capacities. This assumes that the seat angle connections can sustain the large ductility demand required to reach failure.

3.4 Seismic Excitation

One of the objectives of this study is to subject the frames to moderate and high levels of seismic excitation. To this end, seismic excitation representative of those that would be expected in Quebec City (Eastern Canada) and Victoria, B.C. (Western Canada) were used in the analyses.

For the frames located in Victoria, records from earthquakes that occurred along the Pacific rim were used. They are the 1995 Kobe earthquake, two different time-histories from the 1994 Northridge earthquake (New Hall Fire Station and Pacoima Dam records), the 1971 San Fernando earthquake, the 1966 Parkfield earthquake and the 1949 Olympia earthquake. The time-histories of these earthquakes are presented in Figure 3.5.

The time-histories available for Eastern Canada are not as plentiful, and only four earthquake time-histories were used in the analyses. They include the 1988 Saguenay earthquake, the 1985 Nahanni earthquake and two synthetic earthquakes generated by Atkinson (1996) for Eastern Canada. The Nahanni earthquake occurred in the North-West Territories but its frequency content is considered to be similar to Eastern Canadian earthquakes. Figure 3.6 shows the time-histories of the Eastern Canada earthquakes. All the earthquakes are listed in Table 3.4 with their peak ground acceleration (PGA).

The earthquakes were scaled to represent the design seismicity level expected at the two selected cities. Normally, the scaling would be done to match the peak spectral acceleration (PSA) of each earthquake at the given building period with the PSA expected in each region. For example, for the 18-story, building the expected PSAs are approximately 0.10g for Quebec City and 0.20g for Victoria. However, to obtain these values, the scaling factors are not realistic. For example, the Kobe earthquake would need a scaling factor of 4.6. The PSA graphs for all the unscaled earthquakes are shown in Figure 3.7 (Eastern) and Figure 3.8 (Western), along with the period of each structure. Clearly, using the values presented, the scaling factors would need to be unrealistic to obtain the proper PSA for each earthquake. Instead, it was therefore decided to linearly scale the earthquakes to the PGA expected for the two cities. The National Building Code of Canada's Seismic Hazard Map (NBCC 1995), Figure 3.9, shows that the PGA for Quebec City is 0.19g and for Victoria 0.34g. These given PGA values represent a probability of exceedance of 10% in 50 years. Higher values would be obtained for a 2% probability of exceedance in 50 years, as is being considered for the next edition of the seismic maps.

For the other frames considered (2, 4 and 7 stories), scaling the earthquakes to the expected PSA would give more realistic factors, but it was decided, for consistency, to use the same scaling method. The scaling factors for all the earthquakes are listed in Table 3.4 and are the same for each frame. Figure 3.10 and 3.11 shows the scaled earthquakes.

3.5 Analysis Program

Overall, each frame described above (i.e., four frames, and two different types of connections) was thus analyzed with 10 earthquakes. Moreover, four additional analysis scenarios were also considered. The first two accounted for 2nd order effects, P-Δ, for both types of connections. The frames' floor masses remain the same for these scenarios but P-Δ effects are included. Ruaumoko accounts for P-Δ by changing the rigidity matrix of the structures thus increasing their periods. Effect of P-Δ on the hysteresis curves, and large displacements theory, were not considered. The other two scenarios investigate the effect of the floor masses on the structure's behavior. The heavy construction materials used in the original building are replaced by more modern materials. The heavy exterior walls are replaced by lighter glass curtain walls and the terra cotta partitions are replaced with the lighter modular wall system found in today's offices. The resulting periods for these new structures are listed in Table 3.5.

Finally a seventh scenario is used to analyze the four frames in their original condition using the unscaled earthquakes. This scenario has no real comparative value other than to ask the question: What would happen to such a structure should it be subjected to the full force of these earthquakes?

These seven scenarios amount to a very large number of analyses and an equally large number of results to compare. A total of 280 analyses are performed. The results of all of these analyses are compared with each other following the comparison matrix presented in Figure 3.12. The as-built or existing condition is the focal point of the matrix. This scenario is compared with the as-built P-Δ scenario to see the change in behavior due to 2nd order effects. The existing structure is also compared to the one with modern masses and tee-stubs connections to investigate the relative effects of mass on the observed behavior. Finally, the existing structure's behavior is also compared against the structure having seat angle connections, to assess the significance of the two connection types on seismic performance.

For this same reason, the two scenarios which include P-Δ effects are compared, as are the two scenarios using the modern construction materials. The as-built structure with seat angle connections is also compared to both P-Δ and modern materials structures having the same seat angles. Finally the original as-built scenario is briefly compared with the unscaled earthquake scenario to see if any particular effects are amplified by the stronger ground motion.

CHAPTER 4

Analyses and Observations

4.1 *Ruaumoko* Analysis

The *Ruaumko* non-linear inelastic analysis software was used in this research project. This program was selected because it contained the hysteretic element needed to analyze the structural frames having the semi-rigid connections considered in this study (as described earlier), but also because it provided easy to use and powerful post-processing capabilities. Although not normally done in a technical report such as the current document, the input and output features of that program are briefly described here to highlight how *Ruaumoko* differs in user friendliness from other non-linear inelastic time-history analysis programs more frequently used in earthquake engineering (such as Drain-2DX).

The analysis results obtained from *Ruaumoko* are produced in two formats. The first format is an ASCII text file that is readily read by any text editor or spreadsheet and the second format is a graphical representation of the results.

Among the results presented by the ASCII text file an echo of the input allows for an easy verification of the parameters entered for the analysis. The input file for *Ruaumoko* is of the typical preset position type. The data must be entered in a predetermined position, similar to most DOS-based analysis software. The input echo, however presents the parameters with their appropriate captions which allows the user to immediately verify the input for the analysis. The program also gives the structure's natural frequency and period for numerous

mode shapes. The analysis results are divided in many sub-sections. A maximum displacement envelope is presented for each node for each major axis, x and y and rotation, z. Envelopes for the maximum member forces and maximum member deformations are also given. The member deformations given include strain and curvature for beam members and rotation for spring elements. Finally the results also give maximum connection ductility. All these envelopes are given for both positive and negative reactions.

The graphical aspect of *Ruaumoko* is shown during the analysis and in the second output files. Before the analysis starts a graphical representation of the structure is available for the user's review. A number of animated mode shapes are also available for display. This screen also displays the structure's period (Figure 4.1). During the analysis the deformed shape of the structure is displayed for each time-step.

The software package includes an application which uses the second output file to graphically display some of the results. These results include deformed structure shape at any time-step, time-history plots (node displacement or base shear vs time) and many other graphs, hysteresis plots and work-energy plots to name a few. Figures 4.2 and 4.3 give an example of results for the as built 18-story structure subjected to the Saguenay earthquake and the Kobe earthquake, scaled as described in Chapter 3.

4.2 Results

The large number of analyses executed here requires that a few significant results be compiled for observation of behavior and better understanding of trends. It was decided that two aspects of the structure's behavior are to be considered in the present study: the inter-story drifts and connection rotations.

The inter-story drifts need to be calculated separately as they are not automatically evaluated by the program. The displacement time-histories of selected nodes at subsequent stories are

used to calculate the relative displacement for each floor. The resulting inter-story drifts are presented in Figures 4.4 to 4.9 for all analyses and discussed in more detail below. Each figure separately displays the results obtained for the analyses subjected to Eastern and Western North American type of earthquakes. It is important to note that the scales used for the horizontal axis of the graphs are not the same for both regions. The scales are however chosen to remain constant from Figures 4.4 to 4.9 to simplify the comparison of the results, i.e. they are the same for each frame size and each analysis scenario. The inter-story drifts obtained from analyses using the Western North American type of earthquakes are all plotted on a scale running from -3.0% to 3.0% drift while the scale for those analyses using the Eastern North American type of earthquakes is from -1.0 % to 1.0 %.

To further clarify the plots only the mean, mean plus one standard deviation and maximum inter-story drift results for all the earthquakes used for each region are displayed on the figures. The maximum and mean inter-story drifts averaged over the entire height of the structure are also summarized in Tables 4.1 to 4.4. The sign of the values only represent the maximum values obtained in each sway direction , i.e. Eastward (positive) or Westward (negative).

For each level of the structures, only the connections subjected to the maximum rotation are considered for further observation. The output file gives for each element its maximum deformation, and in the case of spring elements or connections, their maximum net rotation. These connection rotations are presented in Figures 4.10 to 4.15. The layout of these figures is similar to those for inter-story drifts. The results for eight frames are shown on each figure, four frames subjected to the Eastern North American (ENA) type of earthquakes and four to Western North American (WNA) type of earthquakes. The scales for these plots are also chosen to simplify the comparison of the results. For the analyses using the WNA type of earthquakes, the scale is from -0.05 to 0.05 radians, and for those using ENA type of earthquakes from -0.006 to 0.006 radians.

For the rotation plots the mean and maximum connection rotations obtained at each floor are drawn. The ultimate capacity of the critical connections are also indicated (see Table 3.3)

The analysis results for the frames subjected to non-scaled earthquakes are presented in Figures 4.16 and 4.17. These plots cannot be as easily compared to the previous figures as their scales do not always match the scales used for plotting the results of the other six analysis scenarios.

4.3 Observations of the Analysis Results

The observations for the analysis results are separated in two categories, global behavior of the structure and comparison of analysis scenarios. For each of these categories both the inter-story drift and connection rotation results are discussed.

4.3.1 Global Behavior of the Structure

4.3.1.1 Inter-story Drifts

Certain general behavioral traits can be easily identified on the plots representing the inter-story drifts. These general observations are mostly true for all the frames independent of the frame location or analysis scenario. The overall shape of the plots for each frame does not significantly change. The same stories on each graph are observed to deflect the most. It is these same stories that consistently dissipate the largest amounts of energy.

All the 2-story frames exhibit the same behavior. They all have larger inter-story drifts on the first level followed by a small decrease at the roof. The 4-story frames also have larger inter-story drifts on the first level, which tapers to a more or less constant inter-story drift for the three upper floors. The first floor of the 4-story frames should normally be stiffer because of the column layout, however, here, it also has a much larger inter-story height.

This larger story height creates a relatively softened story in the frame, making it drift much more than the upper floors. The inter-story drift plot for the 7-story frame is triangular in shape for the first six floors, i.e. the first floor's inter-story drift is the largest and values gradually decrease with height. The top floor however is softer than the floor underneath it, given that it has a larger story height.

Unlike the lower frames, the 18-story frames have some differences in behavior depending on the earthquake location (Eastern or Western North America). Firstly, for the frames subjected to the WNA type of earthquakes, the positive inter-story drifts obtained are consistently larger than their negative counterparts. The frames subjected to ENA type of earthquakes on the other hand have a more "symmetrical" inter-story drift distribution. However, in ali cases, the first level, a soft story, has a larger inter-story drift followed by a considerably lesser one on the second level. It is in the middle floors that behavior of these frames differ most significantly from the other ones. The frames subjected to the ENA type of earthquakes have inter-story drift values that rapidly increase from the second floor upwards, to reach a maximum on the 5^{th} and 6^{th} floor and then slowly decreases up to the 14^{th} level. For example, this behavior is most clearly seen on Figure 4.8. However, the frames subjected to the WNA type of earthquakes generally have two zones of higher values of inter-story drifts in the middle floors, one occurring at the same level as for the ENA type of earthquakes (the 5^{th} and 6^{th} floors) and a second occurring at the 12^{th} floor. The top portion of the frame in all cases are another part of the frame that undergoes large inter-story drifts. For the frame subjected to ENA type of earthquakes, this peak is concentrated on the 17^{th} floor, while the WNA type of earthquakes generally cause the peak to be distributed over the 15^{th}, 16^{th} and 17^{th} floors on the positive side only of the frame.

Many of the observations common for both seismic regions are caused by the peculiarities of the frame geometry, which have been described in Chapter 3. First, the 1^{st} level is a soft story which has a tendency to drift more. Second, two additional columns are added at the 13^{th} floor which increases the 14^{th} floor's stiffness and decreases its inter-story drift. While

these same columns extend over the 14th floor, the additional story height that exists there increases the 15th floor's deflection. Third, the 16th and 17th floors have two factors playing against them, namely the elevation setback at the 15th floor and the fact that both the 16th and 17th floors are mechanical rooms with increased floor masses. Both of these factors contribute to increased inter-story drifts. Fourth, the 18th floor has very little mass compared to the 16th or 17th floor, hence the lower lateral forces and smaller inter-story drifts observed there. Finally, although all the mass of the sloped copper roof is lumped at the top level, the story height there is significantly less than for the average floor, making for lesser inter-story drift values.

4.3.1.2 Connection Rotations

The values of rotations given in Figures 4.10 to 4.15 are for the total rotation of the critical connection. Both the elastic and plastic rotations are combined in the results. A connection was deemed critical when its ratio of demand over capacity was the highest for its level. A connection is considered to have failed when its demand over capacity ratio is higher than one.

For the 2-story frames, the trends in location of the maximum rotations follow closely those observed for the inter-story drift results. In other words, the connections on the first level are subjected to higher rotations than those on the second level. For the other frames, however, this is not the case. The levels exhibiting the highest rotations do not always match the levels with the highest inter-story drifts. *Ruaumoko* uses both the connection rotation and element (beams and columns) flexibility when it calculates the structure's inter-story drift. When the connections are rigid, as is the case for the tee-stubs, the element flexibility plays a major role in the drift behavior of the structure. This is apparent when comparing the inter-story drift and connection rotation figures for a given scenario, (Figures 4.5 and 4.11 for example). The peaks that are seen on the inter-story drift plots do not always occur at the

same levels for the rotation plots. The rigidity of the connection is such that some of the lateral deflection comes from the connection itself while the remainder is provided by the connected elements. However, for the less rigid connections (seat angles), their flexibility is responsible for the majority of the frame's deformation. As a result, the shape of the rotation plots resembles the inter-story drift plots much more closely. This is evident when examining the appropriate figures (Figures 4.6 and 4.10 for example).

As previously stated, the connection rotation capacities are also indicated on the figures of rotation demand. One will notice two levels where no capacity values are given. These two levels, the 2nd and 18th floors, are where deep transfer girders are located. Neither capacity nor rotation demand are indicated at these levels as the connections there have either been modeled as fully rigid or fully flexible (see Figure 3.3).

It is observed that the majority of the connections in the frames subjected to ENA type of earthquakes fall well below the rotation limit calculated. The exception occurs in the 2-story frame where the maximum positive rotation of the second floor connection exceeds the calculated rotation capacity. However, the mean rotation is still below the rotational capacity. The frames subjected to WNA type of earthquakes are much more vulnerable. Almost all the connections in the 2, 4 and 7-story frames exceeded their calculated rotation capacity. The damage levels for the 18-story frame connections are dependent on the analysis scenarios. Some connections in the lower and middle levels can withstand the rotation demand resulting from the consideration of some analysis scenarios.

4.3.2 Comparison of Analysis Scenarios

4.3.2.1 General

The different analysis scenarios are compared to observe specific behavioral changes in the frames. The comparison matrix (Figure 3.12) presented earlier is used in comparing the various frames. From this matrix emerges seven different comparisons. The difference for

the averaged means and maximums for these comparisons are presented in Tables 4.5 to 4.8. The comparisons can further be regrouped to observe the influence of the connection types, the P-Δ effects, and changes in the building's mass.

However before comparing the various analysis scenarios, a cursory comparison should be done between the results obtained considering the different seismic characteristics of the earthquakes in both geographical regions and their influence on the behavior of the frames. The comparison between the results obtained for the frames located in Quebec City and Victoria is straight forward. The lateral forces applied to the frames considered are much stronger when due to the WNA type of earthquakes, thus the obtained inter-story drifts and rotations are of greater amplitude than those resulting from the consideration of ENA type of earthquakes. All the plots of inter-story drifts or rotation demands confirm this assessment. This is partly attributable to the higher frequency content of the earthquakes in Eastern North America which have a much lesser effect on long period structures such as the ones considered in this study.

4.3.2.2 Connections Types

The first comparison focuses on the influence of connection types on the response of the frames. Six different analyses are performed to examine this influence. The connection types are changed from riveted stiffened tee-stubs to riveted stiffened seat angles in the as-built, the P-Δ, and the modern mass analysis scenarios. The initial expectation was that the frames incorporating the semi-rigid connections would be more flexible and thus generate larger inter-story drifts and connection rotations.

In the 18-story frames, the influence of changing connection type is immediately apparent in the inter-story drift plots of the P-Δ scenarios (significant increase in inter-story drifts). The increases in inter-story drifts are in the 20 to 40% range. The changes in the as built scenario are also quite significant, the maximums increasing by up to 45%, and the means by a more

moderate 11 to 30%. Changing the connection type has the least effect on the "modern mass" frames as the increases are approximately 10% when comparing both connections on this type of frame.

The connection rotation is significantly increased for all three analysis scenarios. However in the frames subjected to ENA type of earthquakes, the connection rotation demands are still within their allowable rotation capacity. For the frames subjected to WNA type of earthquakes, increases in rotation only pushed some connections further passed their rotation capacity. In the P-Δ scenarios, the low and mid-level connections only have a small increase in rotation and do not reach their rotation capacity.

For the lower frames (2, 4 and 7 stories), the increases in inter-story drift varies widely, with increases of over 110% in some frames while others experienced decreased inter-story drifts. The decrease in inter-story drift is usually observed in one direction while inter-story drifts in the other direction increases. These reductions are most likely caused by a larger inelastic deformation in the initial cycle causing the center line of the building to shift in one direction, with the resulting permanent offset creating the appearance of decreased inter-story drifts in the opposite direction.

The connection rotation for all four frames also increases significantly when changing from the tee stub connection to the seat angle connection. The connection rotation for the frames subjected to ENA type of earthquakes incorporating seat angles have increased many times the original rotation demand observed for the frames incorporating tee-stubs, yet none have reached their rotation capacity. The connections of the frames subjected to WNA type of earthquakes do not experience as significant an increase, but the connections in those frames are already stressed beyond their capacity, making any increase due to the change in connection stiffness not that important.

4.3.2.3 P-Δ Effects

In order to observe the effects of P-Δ, four analyses are performed. The P-Δ effects are included in the analysis scenario of the as built structure and of the structure incorporating semi-rigid connections.

In the 18-story frames located in Quebec City, the maximum inter-story drift values increase by 15 to 20% while the mean values increase up to 15%. The frames in Victoria on the other hand, have a decrease in inter-story drifts of up to 20%. This decrease in inter-story drift is also apparent in some of the lower frames whether located in Victoria or Quebec City. There appears to be no physical characteristics that could conclusively explain this lack of consistent trend between results obtained for Eastern and Western North America. Consideration of P-Δ effects translate into an elongation of the structures's period, with expected reduction on magnitude of lateral forces acting on the buildings. The trend observed for analyses using the ENA type of earthquakes may be due to spurious trends for the few time-histories selected for Eastern North America.

The connections for the frames subjected to ENA type of earthquakes incorporating the tee-stubs demonstrate a significant increase in rotation demand. Nonetheless none reach their rotation capacities other than the connection on the first floor of the 2-story frame. There is little noticeable change in behavior for the 2 and 7-story frames using the seat angle connections. The 4-story frame experienced a small increase, while the 18-story frame has a decrease in connection rotation demands. The frames subjected to WNA type of earthquakes behave in a similar manner, with the three lower frames having a rotation demand increase and the 18-story frame a decreased demand over capacity ratio.

4.3.2.4 Modern Construction Materials

To observe the impact of heavy versus lighter construction materials, four analyses are performed. The cladding and floor masses of the as built structure and the structure

incorporating the semi-rigid connections are replaced by lighter construction materials typically found in modern construction.

The lighter frames are observed to have much smaller resulting inter-story drifts than their heavier counterparts. Although the frames have shorter periods, thus increasing the applied spectral accelerations (see PSA graphs, Figures 3.7 and 3.8), the lighter floors generate smaller forces, thus leading smaller inter-story drifts. The decrease in inter-story drifts for the frames subjected to ENA type of earthquakes are in excess of 50%. The majority of the frames analyzed with the WNA type of earthquakes also have a decrease in inter-story drift of up to 40%. The 18-story frame located in Victoria does not entirely follow this trend, with larger inter-story drifts occurring in the top floors.

Much like the inter-story drift behavior, there is a slight reduction in the connection rotation demands. The reductions in the frames subjected to ENA type of earthquakes are not all that significant, with the 2-story frame having the greatest reduction of rotation demand. For the frames subjected to WNA type of earthquakes, the 2 and 4-story structures have the most reduction. Yet, little change is noticeable in the 7-story frame, and some increases occur in the upper floors of the 18-story frame.

4.4 Observation Summary

4.4.1 General

A summary of the above observations is required to have a clear picture of the behavior of the frames analyzed. Some of the frames have a behavior that does not change with the variation in seismic regions or analysis scenarios. The behavior of other frames, however, vary with the change of earthquake types (ENA or WNA) and analysis scenario. The following sections summarizes some general observations on the effect of frame size and analysis scenario. The potential seismic survivability of the structures is also addressed.

4.4.2 Frame Behavior

The 2-story frame has a very predictable behavior. The structure's inter-story drift or rotation distribution did not change from one analysis scenario to the next. The second floor (the first level) always experienced larger inter-story drifts and connection rotation demands than at the level above. Furthermore, the inter-story drift and rotation plots are generally found to be symmetrical.

The 4-story frame also has a stable behavior. No level exhibited a tendency to have significantly greater inter-story drift or rotation demand (results at all the levels are more or less constant), the second floor being the only exception for inter-story drifts. Most plots are symmetrical in nature, having the floors deflect by about the same amounts in each direction or the connections equally rotate in the positive and negative direction.

As the structure's height increases, so does complexity of the behavior. The 7-story frames tend to drift in the same manner independent of seismic region or analysis scenario. The maximum inter-story drift was always observed to occur at the first and last (top) level. However the rotation demand plots vary with the connection type and seismic region. The rigid (tee-stub) frames located in Quebec City have small rotations on all but the 7th floor (6^{th} level). This level happens to have the least amount of inter-story drift, which is explained by the increased number of columns (shorter beams require a larger magnitude of rotation to obtain a given inter-story drift value). The frames subjected to WNA type of earthquakes have larger connection rotations at the base, with minimal connection rotation demand on the upper floors. The more flexible (seat angle) frames all have constant rotation demands along the height of the structure, with the exception of the 5^{th} level which was observed to have smaller rotation demand.

The 18-story frame is much harder to generalize. The structure's behavior is much more dependent on the seismic region than the lower frames. The different analysis scenarios

change the magnitude of inter-story drifts and rotation demands, however, the distribution of the maximums (inter-story drifts or rotation demands) remain essentially the same. The frames subjected to ENA type of earthquakes generally have two zones of higher values of inter-story drifts, a first occurring around the 4th and 5th levels (5th and 6th floors) and a second towards the top. The frames subjected to the WNA type of earthquakes have the same zones of higher inter-drift values, with the addition of a third around the 12th floor. The higher inter-story drift values occurring at the top of the frame are generally distributed over three floors (15th, 16th and 17th) for the analyses using the WNA type of earthquakes, while the analyses using the ENA type of earthquakes produce a maximum value occurring on the 17th floor only. The inter-story drift distribution of the frames subjected to ENA type of earthquakes is generally symmetrical while the distribution for the frames subjected to the WNA type of earthquakes usually favors one direction. The rotation behavior is not dependent on seismic region but on connection type, as would be expected. There is one exception, the rigid P-Δ analysis scenario using the ENA type of earthquake has a behavior similar to the semi-rigid connections.

4.4.3 Analysis Scenarios

Three major changes in the basic configuration of the frames are analyzed: the connection types, the inclusion of P-Δ effects and the use of modern construction materials. The purpose of changing these elements was to observe the impact each has on the structure's behavior. As one may expect changing the type of connection for a more flexible one, increases the magnitudes of inter-story drifts and rotation demands. The change in connection type also shifted the centerline of the building (permanent inelastic offsets) creating asymmetrical inter-story drift plots. The inclusion the P-Δ effects did not significantly change the behavior of the structures. However, the inconsistent inter-story drift trends could not be conclusively explained through physical characteristics of the frames and earthquake types. Finally changing to lighter construction materials has a tendency to decrease the magnitudes of both the inter-story drifts and connection rotation demands.

There is one additional comparison which is not indicated on the matrix (Figure 3.12) and that has not yet been discussed. This comparison looks at the structures subjected to the unscaled earthquakes. The inter-story drifts obtained using the unscaled earthquakes are higher than for the scaled earthquakes. The frames subjected to WNA type of earthquakes have a large asymmetrical increase. The eastern sway direction increasing by approximately 120% for both the maximum and mean inter-story drifts while the western sway direction has much smaller increases, 26%(maximum) and 52%(mean). The frames subjected to ENA type of earthquakes also have an increase in inter-story drifts of up to 160% for the maximum inter-story drifts and a smaller 44% increase in the mean inter-story drifts. The increase in inter-story drift for the frames subjected to unscaled WNA type of earthquakes was expected, as all of these earthquakes needed to be scaled down to the PGA expected in Victoria. However, the majority of ENA type earthquakes needed to be scaled upward to the expected PGA in Quebec City, but the inter-story drift nonetheless increased. This increase is caused solely by the Nahanni earthquake which needed to be scaled down to only 20% of its original PGA.

The connections of the frames subjected to the unscaled ENA type of earthquakes also have large increases in rotation demand. The lower frames all experience rotation demands far exceeding the connection capacity. The 18-story frame, however, only has one upper floor connection with maximum rotation reaching its capacity while all mean rotation demands are well below their respective capacity. The lower frames subjected to the WNA type of earthquakes also have significant increases in connection rotation demand, with all but a few connections exceeding their capacity. The rotation demand increase for the connections of the 18-story frame is not as significant, although most connections exceed their available rotation capacity. The increase is once again asymmetrical, where the positive rotations exceeds the negative ones.

It is interesting to note that as the magnitude of the ENA type of seismic excitation increases, the 18-story frame behaves in a fashion similar to the frames subjected to WNA type of

earthquakes, with larger inter-story drifts also starting to concentrate on the 12th floor, and progressively larger inter-story drifts developing on the three upper levels.

This last comparison was done for curiosity and to assess the significance of previous results and was not intended to argue that earthquakes similar to the 1995 Kobe earthquake, for example, could occur in Canada.

4.4.4 Seismic Survivability

The NBCC gives the following expression as an arbitrary limit for the inter-story drifts of non-post-disaster buildings:

$$R\Delta<0.02h_s$$

where: R= force modification factor,

Δ= inter-story drift, and

h_s= story height.

The NBCC does not specifically provide an R value for the types of structures studied here. However, here, because inelastic analyses are performed, the displacements obtained from analysis directly correspond to the RΔ specified by the NBCC. This limit of 2% h_s can easily be verified on the inter-story drifts plots presented in this Chapter. It is observed that none of the frames subjected to ENA type of earthquakes reach this limit. However, the 2, 4 and 7-story frames subjected to WNA type of earthquakes all have inter-story drifts in excess of 2%. For the 18-story frames in Victoria, only the maximum values of inter-story drifts reach the limit set by the NBCC.

Limiting the inter-story drift values does not necessarily ensure survivability of a structure. Connections must also be able to withstand the rotation demands resulting from the seismic

excitation. The capacity of the connections incorporated in the frames considered in the present study are summarized in Table 3.3 and were shown in Figures 4.10 to 4.15, and have been discussed previously. It is found that the rotation limits indicated are not exceeded by any of the frames subjected to ENA type of earthquakes. The same is not true for the frames subjected to WNA type of earthquakes. The lower frames (2, 4 and 7-story) all exceed the rotation capacity of their connections. In the 18-story frame, the upper connections have the largest rotation demands and are stressed beyond their capacity, while some of the lower connections are still within acceptable limits of rotation depending on the analysis scenario.

CHAPTER 5

Conclusions and Recommendation

5.1 Conclusions

The following conclusions can be drawn from the observations and comparisons of the results from the numerous analyses undertaken in the present study.

- The generic buildings analyzed in the study have enough moment-resistance to ensure their survivability (as measured by drift and connection rotation) in the event of a moderate earthquake typical of Eastern North-America. This adequate moment-resistance is inherent to all four buildings considered regardless of the type of connection.
- These same generic buildings do not have adequate energy-dissipation or moment-resistance to sustain a high magnitude earthquake typical of Western North-America. The amount of retrofitting required for each connection in these buildings appears to be inversely proportional to the structures height. The total connection rotation demands are larger for the lower buildings (2, 4 and 7-stories). Furthermore, the demand over capacity ratios for the 18-story structure are smaller than the ratios of the lower buildings.
- Reduction of floor and cladding masses (through renovations for example) helps in lowering the structure's drifts and connection rotations, thus improving the survivability of the building.

- The inclusion of 2nd order effects, P-Δ did not significantly change the behavior of the structures analyzed in the present study. However, only the effects of P-Δ on reducing the building's period was considered in this study. Impact of P-Δ on hysteretic behavior and large displacement analysis were not considered here. Future research is recommended to investigate the impact of the two additional effects for which P-Δ effects may be more considerable.

5.2 Future Research

Although every effort to realistically model the existing building has been taken, additional information is required to incorporate other elements of the structure, such as cladding. The effect of the large stone cladding on the period and the damping ratio of the structure would need to be investigated. This other structural element could have an impact of the overall non-linear behavior of the structure.

Furthermore, the earthquakes chosen to represent Western North American excitation did not include the effect of subduction zones. To properly evaluate the survivability of structures located in Victoria, British Colombia subduction zones should be taken into consideration.

5.3 Recommendation

It is of great importance that the reader understands that the results presented here are for the generic buildings used in the study. They do not readily apply to existing structures and do not replace a proper structural assessment performed by a licenced engineer. The results may however be used in assisting any such engineer in his/her assessment of an existing structure, by providing general expectations of seismic behavior and a better understanding of seismic performance.

References

American Institute of Steel Construction (1957), "Iron and Steel Beams, 1873 to 1952", New York.

American Institute of Steel Construction (1962), "Steel Construction Manual", New York.

Ang, K.M. and Morris, G.A. (1984), "Analysis of three-dimensional frame with flexible beam-column connections" *Can. J. Civ. Engrg.*, 11, 245-254.

Astaneh, A., Nader, M.N. and Malik, L. (1989), "Cyclic behavior of double angle connections", *J. Struct. Div.*, ASCE, 115(5), 1101-1118.

Atkinson, G.M. (1997), "Compatible ground motion time histories for new National Seismic Hazard Maps", Report No. OCEERC 97-14, Ottawa Carleton Earthquake Engineering Research Centre

Bernuzzi, C., Zandonini, R. and Zanon, P. (1992), "Semi-Rigid Steel Connections Under Cyclic Loads", *Proceedings of the First World Conference on Constructional Steel Design*, Acapulco, Mexico.

Bruneau, M. and Bisson, M. (2000), "Cyclic Testing and Retrofitted Concrete-encased RSSA Connections", Engineering Journal (in press)

Bruneau, M. and Sarraf, M. (1996), "Cyclic Testing of existing and retrofitted stiffened seat angle connections", *ASCE Structural Journal,* Vol.122 No. 7, pp. 762-775

Bruneau, M. and Sarraf, M. (1994), "Experimental study on cyclic behavior of riveted stiffened seat angle connections", Report No. OCEERC 94-01, Ottawa Carleton Earthquake Engineering Research Centre

Canadian Institute of Steel Construction (1997), "Handbook of Steel Construction", Toronto.

Carr, A.J. (1998), "Ruaumoko", University of Canterbury, New Zealand.

Chopra, A.K. (1995), "Dynamics of Structures", Englewood Cliffs, New Jersey.

Clough, R.W. and Penzien, J. (1975), "Dynamics of Structures", McGraw-Hill, New York.

Council on tall buildings and urban habitat (1993), "Semi-rigid connections in steel frames", McGraw-Hill, New York.

De Stephano, M., De Luca, A. and Astaneh-Asl, A. (1994), "Modelling of Cyclic Moment-Rotation Response of Double-Angle Connections", *J. Struct. Engrg.*, ASCE, 120(1), 212-223.

De Luca, A. (1995), "Behaviour and Modelling of Top and Seat, Top and Seat and Web Angle Connections", *Connections in Steel Structures III: Behaviour, Strength and Design*; Proceedings of the third International Workshop, Trento, Italy, 289-297.

Frye, M.J. and Morris, G.A. (1976), "Analysis of flexibly connected steel frames", *Can. J. Civ. Engrg.*, 2(3), 280-291

Gaylord, E.H. and Gaylord C.N. (1972), "Design of Steel Structures", McGraw-Hill, New York.

Gaylord, E.H., Gaylord C.N. and Stallmeyer, J.E. (1992), "Design of Steel Structures", McGraw-Hill, New York.

Goel, R.K. and Chopra, A.K. (1997), "Vibration properties of buildings determined from recorded earthquake motions", *Report No. UCB/EERC-97/14*, Earthquake Engineering Research Centre, University of California, Berkley.

Hetchman, R.A., and Johnston, B.G. (1947), "Riveted semi-rigid beam-to-column building connections, progress report no. 1", AISC Research at Leigh Univ., Bethlehem, Pa.

Keshavarzian, M. and Schnobrich, W. (1984), "Computed Nonlinear Seismic Response of R/C Wall-frame Structures", University of Illinois.

Ketchum, M.S. (1924), "Structural Engineer's Handbook", McGraw-Hill, New York.

Ketchum, M.S. (1932), "The Design of Steel Mill Buildings and the Calculation of Stresses in Framed Strucures", McGraw-Hill, New York.

Kishi, N. and Chen, W.F. (1990), "Moment-rotation relations of semi-rigid connections with angles", *J. Struc. Engrg.*, ASCE, 116(7), 1813-1834.

Kulak, G.L. and Gilmor, M.I. (1998), "Limit States Design in Structural Steel", Canadian Institute of Steel Construction, Toronto.

Kulak, G.L., Fisher, J.W. and Struik, J.H. (1987), "Guide to Design Criteria for Bolted and Riveted Joints", J. Wiley & Sons, New York.

Lightfoot, E., et al. (1974), "Elastic analysis of frameworks with elastic connections", *J. Struct. Engrg.*, ASCE, 100(ST6), 1297-1309.

Lewitt, C.W., Chesson, E. and Munse, W.H. (1969), "Restraint characteristics of flexible riveted and bolted beam-to-column connections", *Engineering Experiment Station Bulletin 500,* College of Engineering, University of Illinois.

Marley, M.J., et al. (1982), "Analysis and test of flexibly-connected steel frames", *Report to AISC under Project 199,* AISC, Chicago, Ill.

Maxwell, S.M., et al. (1981), "A realistic approach to the performance and application of semi-rigid joints in steel structures", *Joints in Structural Steel Work,* Pentech Press, 2.71-2.98.

Monforton, A.R., et al. (1963), "Matrix analysis of semi-rigidly connected frames", *J. Struct. Engrg.,* ASCE, 87(ST6), 13-42.

Munse, W.H., Bell, W.G. and Chesson, E. (1959), "Behaviour of Rivetted and Bolted Beam-to-Column Connections", *Journal of the Structural Division,* ASCE, No. ST3, 29-51.

Munse, W.H., Petersen, K.S. and Chesson, E. (1959), "Strength of the American Society of Civil Engineers", *Journal of the Structural Division,* ASCE, No. ST3, 7-28.

National Building Code of Canada 1995 (1995), Canadian Commission on Building and Fire Codes, National Research Council of Canada, Ottawa.

National Building Code of Canada 1995, Structural Commentaries (Part 4) (1995), Canadian Commission on Building and Fire Codes, National Research Council of Canada, Ottawa.

Norris, C. and Wilbur, J. (1960), "Elementary Structural Analysis", McGraw-Hill, New York.

Picard, A. and Beaulieu, D. (1991), "Calcul des charpentes d'acier", Institut Canadien de la Construction en Acier, Toronto.

Popov, E.P. and Stephen R.M. (1972), "Cyclic loading of full-size steel connections", *Steel Research for construction*, Bulletin No. 21.

Popov, E.P., Tsai, K.-C. and Engelhardt, D. (1989), "On seismic steel joints and connections", Engineering Structures, 11(3), 148-162

Radziminski, J.B. and Azizinamini, A. (1986), "Low cyclic fatigue of semi-rigid steel beam-to-column connections", *Proceeding of the third U.S. National Conference on Earthquake Engineering,* 1285-1296.

Rathbun, J.C. (1936), "Elastic properties of riveted connections", *Trans. ASCE,* Paper No. 1933, Vol. 101, 524-563.

Redwood, R.G., Lu, F., Bouchard, G. and Paultre, P. (1991), "Seismic response of concentrically braced steel frames", Can. J. Civ. Engrg. 18, 1062-1077

Reynolds, T. and Lewis, K. (1955), "Structural Steelwork", English Universities Press, London.

Roeder, C.W., Leon, R.T. and Preece, F.R. (1994), "Strength, stiffness and ductility of older steel structures under seismic loading", Report No. SGEM 94-4, Dept. Civ. Engrg, Univ. of Washington, Seattle, Washington.

Salmon, C.G. and Johnson, J.E. (1980), "Steel Structures, Design Behavior", Harper & Row, New York.

Stelmack, T.W. , Marley, M.J. and Gerstle, K.H. (1986), "Analysis and tests of flexibly connected steel frames", J. Struct. Engrg., ASCE, 112(7), 1573-1586.

Tall, L. (1974), "Structural Steel Design", The Ronald Press Company, New York.

Wilson, W.M. and Moore, H.F. (1917), "Tests to determine the rigidity of riveted joints of steel structures", *Engineering Experiment Station, Bulletin No. 104,* Univ. of Illinois, Urbana, Ill.

Wu, F.-H. and Chen, W.-F. (1990), "A design model for semi-rigid connections" *Engineering Structures,* 12(2), 88-97.

Yee, Y.L. and Jackson K.B. (1934), "The relative rigidity of welded and riveted connections", *Canadian Journal of research,* vol. 11, 62-100.

Young, C.R., and Jackson, K.B. (1934), "The relative rigidity of welded and riveted connections", *Canadian Journal of Research,* vol. 11, 62-100.

Youssef-Agha, W., Aktan, H.M. and Olowokere, O.D. (1989), "Seismic response of low-rise steel frames", *J.Struct. Engrg.,* ASCE, 115(3), 594-605.

Floor	Beam	Tee section					Stiffeners (2 back-to-back angles)		
		D	W	L	$t_{avg\ flange}$	t_{stem}	Size	Thickness	Length
3	exterior	13	15.0	29	1.07	0.66	6 x 3 1/2	0.3125	13
	interior	13	15.0	29	1.07	0.66	6 x 3 1/2	0.3125	13
4	exterior	13	15.0	29	1.07	0.66	6 x 3 1/2	0.3125	13
	interior	13	15.0	29	1.07	0.66	6 x 3 1/2	0.3125	13
5	exterior	13	14.2	25	0.96	0.59	5 x 3 1/2	0.3125	10
	interior	13	14.2	25	0.96	0.59	6 x 3 1/2	0.3125	10
6	exterior	13	14.2	25	0.96	0.59	5 x 3 1/2	0.3125	10
	interior	13	14.2	25	0.96	0.59	6 x 3 1/2	0.3125	10
7	exterior	13	12.3	22	0.95	0.54	5 x 3 1/2	0.3125	10
	interior	13	12.3	22	0.95	0.54	6 x 3 1/2	0.3125	10
8	exterior	13	12.7	20	1.04	0.60	5 x 3 1/2	0.3125	10
	interior	13	12.7	20	1.04	0.60	5 x 3 1/2	0.3125	10
9	exterior	13	12.7	20	1.04	0.60	5 x 3 1/2	0.3125	10
	interior	13	12.7	20	1.04	0.60	5 x 3 1/2	0.3125	10
10	exterior	8	15.7	17	1.18	0.70	5 x 3 1/2	0.3125	10
	interior	8	15.7	17	1.18	0.70	5 x 3 1/2	0.3125	10
11	exterior	8	15.7	17	1.18	0.70	4 x 3 1/2	0.3125	10
	interior	8	15.7	17	1.18	0.70	5 x 3 1/2	0.3125	10
12	exterior	8	15.7	17	1.18	0.70	4 x 3 1/2	0.3125	10
	interior	8	14.2	14	1.02	0.64	4 x 3 1/2	0.3125	10
13	all	8	15.7	17	1.18	0.70	4 x 3 1/2	0.3125	10
14	exterior	8	8.0	10	0.58	0.38	4 x 3 1/2	0.3125	10
	interior	8	14.2	14	1.02	0.64	4 x 3 1/2	0.3125	10
15	exterior	8	7.0	7	0.74	0.41	4 x 3 1/2	0.3125	10
	interior	8	15.7	17	1.18	0.70	4 x 3 1/2	0.3125	10
16	all	8	8.0	10	0.58	0.38	3 1/2x3 1/2	0.156	10
17	all	8	8.0	10	0.58	0.38	3 1/2x3 1/2	0.156	10
roof	all	8	7.2	8	0.41	0.29	3 1/2x3 1/2	0.1875	10

all sizes are in inches

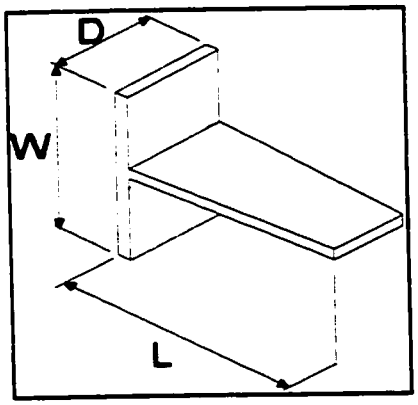

Table 3.1: Redesigned connection sizes

Positive Bending		
I	Tensile yielding of rivets	yield
II	Formation of hinge mechanism in tee	yield
III	Net section yield of stem	yield
IV	Tensile rupture of rivets	rupture
V	Shear failure of rivets	rupture
VI	Net section rupture of stem	rupture
Negative Bending		
I	Formation of hinge mechanism in stiffeners	yield
II	Net section yield of stem	yield
III	Shear failure of rivets in stem of tee	rupture
IV	Net section rupture of stem	rupture

Table 3.2: Calculated Failure Modes, Riveted Stiffened Tee-Stub Connection

Floor	Beam	Positive Bending				Negative Bending			
		M^{+}_{yield} [kN·m]	Failure Type	$M^{+}_{rupture}$ [kN·m]	Failure Type	M^{-}_{yield} [kN·m]	Failure Type	$M^{+}_{rupture}$ [kN·m]	Failure Type
3	exterior	460	III	980	VI	460	II	890	IV
	interior	230	III	485	VI	230	II	445	IV
4	exterior	460	III	980	VI	460	II	890	IV
	interior	230	III	485	VI	230	II	445	IV
5	exterior	450	III	870	VI	450	II	790	IV
	interior	220	III	430	VI	220	II	395	IV
6	exterior	450	III	870	VI	450	II	790	IV
	interior	220	III	430	VI	220	II	395	IV
7	exterior	295	I	800	VI	375	II	730	IV
	interior	145	I	400	VI	185	II	365	IV
8	exterior	300	I	735	V	420	II	735	III
	interior	150	I	365	V	210	II	365	III
9	exterior	300	I	735	V	420	II	735	III
	interior	150	I	365	V	210	II	365	III
10	exterior	300	I	580	VI	300	II	580	IV
	interior	150	I	290	VI	150	II	290	IV
11	exterior	300	I	580	VI	300	I	580	IV
	interior	150	I	290	VI	170	I	290	IV
12	exterior	300	I	580	VI	300	I	580	IV
	interior	135	III	245	V	155	I	245	III
13	all	150	II	290	V	155	I	290	IV
14	exterior	65	III	80	IV	160	II	220	IV
	interior	135	III	245	V	155	I	245	III
15	exterior	25	I	120	IV	170	II	175	III
	interior	135	III	265	VI	145	I	265	IV
16	all	75	II	90	IV	155	I	250	IV
17	all	75	II	90	IV	155	I	250	IV
roof	all	30	II	55	IV	100	I*	100	III*

* both failure modes are reached simultaneously

Table 3.3: Connection yield and rupture moments

Earthquake	Year	PGA (g)	Scaling factor
Western North American type of Earthquakes			
Kobe	1995	0.84	0.4
New Hall	1994	0.59	0.6
Olympia	1949	0.28	1.2
Pacoima Dam	1994	1.28	0.3
Parkfield	1966	0.49	0.7
San fernando	1971	1.17	0.3
Eastern North American type of Earthquakes			
Atkinson long period *	1997	0.09	2
Atkinson short period *	1997	0.15	1.2
Nahanni	1985	0.95	0.2
Saguenay	1988	0.17	1.1

* Synthetic time-history (Atkinson 1997)

Table 3.4: Earthquake records

Analysis Configuration	Frame			
	2 story	4 story	7 story	18 story
Stiffened tee-stub connections				
As is	1.23	2.30	2.33	5.04
P-Δ	1.30	2.56	2.47	5.74
Modern mass	0.90	1.54	1.74	3.39
Stiffened seat angle connections				
As is	1.81	2.83	2.95	5.97
P-Δ	2.00	3.23	3.22	6.65
Modern mass	1.38	1.93	2.20	4.01

Table 3.5: Periods of the frames analyzed

Analysis Scenario	Location	Maximum Drift		Mean Drift	
As-built	Quebec City	0.62	-0.73	0.46	-0.54
	Victoria	3.43	-3.57	2.17	-2.16
P-Δ	Quebec City	0.66	-0.82	0.46	-0.57
	Victoria	3.38	-2.46	1.99	-1.91
Modern Construction	Quebec City	0.41	-0.36	0.28	-0.24
	Victoria	2.95	-2.14	1.67	-1.62
As-built, seat angle	Quebec City	0.66	-0.80	0.49	-0.51
	Victoria	3.07	-3.57	2.16	-2.38
P-Δ, seat angle	Quebec City	0.70	-0.80	0.50	-0.54
	Victoria	5.38	-3.02	2.98	-2.13
Modern Construction, seat angle	Quebec City	0.61	-0.75	0.44	-0.51
	Victoria	3.21	-3.37	2.21	-2.39
Non-scaled Eqs	Quebec City	1.63	-1.75	0.66	-0.75
	Victoria	7.56	-4.51	4.72	-3.29

Table 4.1: Averaged maximum and mean drift results for the 2 story frame

Analysis Scenario	Location	Maximum Drift		Mean Drift	
As-built	Quebec City	0.26	-0.27	0.16	-0.18
	Victoria	2.00	-1.82	1.14	-1.08
P-Δ	Quebec City	0.29	-0.25	0.17	-0.17
	Victoria	2.06	-1.93	1.15	-1.03
Modern Construction	Quebec City	0.24	-0.28	0.16	-0.17
	Victoria	1.26	-1.65	0.87	-0.96
As-built, seat angle	Quebec City	0.37	-0.34	0.24	-0.25
	Victoria	2.37	-2.26	1.51	-1.42
P-Δ, seat angle	Quebec City	0.43	-0.33	0.27	-0.22
	Victoria	2.56	-2.46	1.58	-1.38
Modern Construction, seat angle	Quebec City	0.30	-0.31	0.20	-0.21
	Victoria	1.98	-2.15	1.15	-1.23
Non-scaled Eqs	Quebec City	0.85	-0.81	0.32	-0.31
	Victoria	3.99	-3.53	2.07	-2.38

Table 4.2: Averaged maximum and mean drift results for the 4 story frame

Analysis Scenario	Location	Maximum Drift		Mean Drift	
As-built	Quebec City	0.21	-0.22	0.14	-0.14
	Victoria	1.47	-0.86	0.80	-0.54
P-Δ	Quebec City	0.23	-0.21	0.14	-0.14
	Victoria	1.67	-0.83	0.90	-0.49
Modern Construction	Quebec City	0.17	-0.20	0.12	-0.12
	Victoria	1.25	-0.78	0.67	-0.55
As-built, seat angle	Quebec City	0.25	-0.23	0.17	-0.17
	Victoria	1.60	-1.27	0.94	-0.68
P-Δ, seat angle	Quebec City	0.31	-0.26	0.18	-0.17
	Victoria	1.50	-0.97	0.93	-0.62
Modern Construction, seat angle	Quebec City	0.21	-0.22	0.13	-0.14
	Victoria	1.40	-1.02	0.79	-0.69
Non-scaled Eqs	Quebec City	0.75	-0.64	0.27	-0.24
	Victoria	2.63	-1.49	1.57	-1.03

Table 4.3: Averaged maximum and mean drift results for the 7 story frame

Analysis Scenario	Location	Maximum Drift		Mean Drift	
As-built	Quebec City	0.18	-0.22	0.09	-0.10
	Victoria	0.79	-0.51	0.45	-0.28
P-Δ	Quebec City	0.22	-0.26	0.09	-0.11
	Victoria	0.78	-0.43	0.44	-0.22
Modern Construction	Quebec City	0.13	-0.16	0.08	-0.09
	Victoria	0.73	-0.67	0.44	-0.35
As-built, seat angle	Quebec City	0.25	-0.32	0.10	-0.13
	Victoria	0.99	-0.65	0.51	-0.33
P-Δ, seat angle	Quebec City	0.30	-0.37	0.11	-0.15
	Victoria	0.95	-0.54	0.58	-0.30
Modern Construction, seat angle	Quebec City	0.14	-0.18	0.08	-0.10
	Victoria	0.84	-0.68	0.49	-0.39
Non-scaled Eqs	Quebec City	0.38	-0.34	0.15	-0.15
	Victoria	1.55	-0.86	0.73	-0.37

Table 4.4: Averaged maximum and mean drift results for the 18 story frame

Comparison	Location	Maximum Drift		Mean Drift	
As-built vs P-Δ	Quebec City	6.5	12.3	0.0	5.6
	Victoria	-1.5	-31.1	-8.3	-11.6
As-built vs As-built, seat angle	Quebec City	6.5	9.6	6.5	-5.6
	Victoria	-10.5	0.0	-0.5	10.2
As-built vs Modern masses	Quebec City	-33.9	-50.7	-39.1	-55.6
	Victoria	-14.0	-40.1	-23.0	-25.0
As-built, seat angle vs P-Δ, seat angle	Quebec City	6.1	0.0	2.0	5.9
	Victoria	75.2	-15.4	38.0	-10.5
As-built, seat angle vs Modern masses, seat angle	Quebec City	-7.6	-6.3	-10.2	0.0
	Victoria	4.6	-5.6	2.3	0.4
P-Δ vs P-Δ, seat angle	Quebec City	6.1	-2.4	8.7	-5.3
	Victoria	59.2	22.8	49.7	11.5
Modern masses vs Modern masses, seat angle	Quebec City	48.8	108.3	57.1	112.5
	Victoria	8.8	57.5	32.3	47.5
As-built structure Scaled vs Non-scaled Eqs	Quebec City	162.9	139.7	43.5	38.9
	Victoria	120.4	26.3	117.5	52.3

Table 4.5: Differences in drift for the 2 story frame, percentage

Comparison	Location	Maximum Drift		Mean Drift	
As-built vs P-Δ	Quebec City	11.5	-7.4	6.3	-5.6
	Victoria	3.0	6.0	0.9	-4.6
As-built vs As-built, seat angle	Quebec City	42.3	25.9	50.0	38.9
	Victoria	18.5	24.2	32.5	31.5
As-built vs Modern masses	Quebec City	-7.7	3.7	0.0	-5.6
	Victoria	-37.0	-9.3	-23.7	-11.1
As-built, seat angle vs P-Δ, seat angle	Quebec City	16.2	-2.9	12.5	-12.0
	Victoria	8.0	8.8	4.6	-2.8
As-built, seat angle vs Modern masses, seat angle	Quebec City	-18.9	-8.8	-16.7	-16.0
	Victoria	-16.5	-4.9	-23.8	-13.4
P-Δ vs P-Δ, seat angle	Quebec City	48.3	32.0	58.8	29.4
	Victoria	24.3	27.5	37.4	34.0
Modern masses vs Modern masses, seat angle	Quebec City	25.0	10.7	25.0	23.5
	Victoria	57.1	30.3	32.2	28.1
As-built structure Scaled vs Non-scaled Eqs	Quebec City	226.9	200.0	100.0	72.2
	Victoria	99.5	94.0	81.6	120.4

Table 4.6: Differences in drift for the 4 story frame, percentage

Comparison	Location	Maximum Drift		Mean Drift	
As-built vs P-Δ	Quebec City	9.5	-4.5	0.0	0.0
	Victoria	13.6	-3.5	12.5	-9.3
As-built vs As-built, seat angle	Quebec City	19.0	4.5	21.4	21.4
	Victoria	8.8	47.7	17.5	25.9
As-built vs Modern masses	Quebec City	-19.0	-9.1	-14.3	-14.3
	Victoria	-15.0	-9.3	-16.3	1.9
As-built, seat angle vs P-Δ, seat angle	Quebec City	24.0	13.0	5.9	0.0
	Victoria	-6.3	-23.6	-1.1	-8.8
As-built, seat angle vs Modern masses, seat angle	Quebec City	-16.0	-4.3	-23.5	-17.6
	Victoria	-12.5	-19.7	-16.0	1.5
P-Δ vs P-Δ, seat angle	Quebec City	34.8	23.8	28.6	21.4
	Victoria	-10.2	16.9	3.3	26.5
Modern masses vs Modern masses, seat angle	Quebec City	23.5	10.0	8.3	16.7
	Victoria	12.0	30.8	17.9	25.5
As-built structure Scaled vs Non-scaled Eqs	Quebec City	257.1	190.9	92.9	71.4
	Victoria	78.9	73.3	96.3	90.7

Table 4.7: Differences in drift for the 7 story frame, percentage

Comparison	Location	Maximum Drift		Mean Drift	
As-built vs P-Δ	Quebec City	22.2	18.2	0.0	10.0
	Victoria	-1.3	-15.7	-2.2	-21.4
As-built vs As-built, seat angle	Quebec City	38.9	45.5	11.1	30.0
	Victoria	25.3	27.5	13.3	17.9
As-built vs Modern masses	Quebec City	-27.8	-27.3	-11.1	-10.0
	Victoria	-7.6	31.4	-2.2	25.0
As-built, seat angle vs P-Δ, seat angle	Quebec City	20.0	15.6	10.0	15.4
	Victoria	-4.0	-16.9	13.7	-9.1
As-built, seat angle vs Modern masses, seat angle	Quebec City	-44.0	-43.8	-20.0	-23.1
	Victoria	-15.2	4.6	-3.9	18.2
P-Δ vs P-Δ, seat angle	Quebec City	36.4	42.3	22.2	36.4
	Victoria	21.8	25.6	31.8	36.4
Modern masses vs Modern masses, seat angle	Quebec City	7.7	12.5	0.0	11.1
	Victoria	15.1	1.5	11.4	11.4
As-built structure Scaled vs Non-scaled Eqs	Quebec City	111.1	54.5	66.7	50.0
	Victoria	96.2	68.6	62.2	32.1

Table 4.8: Differences in drift for the 18 story frame, percentage

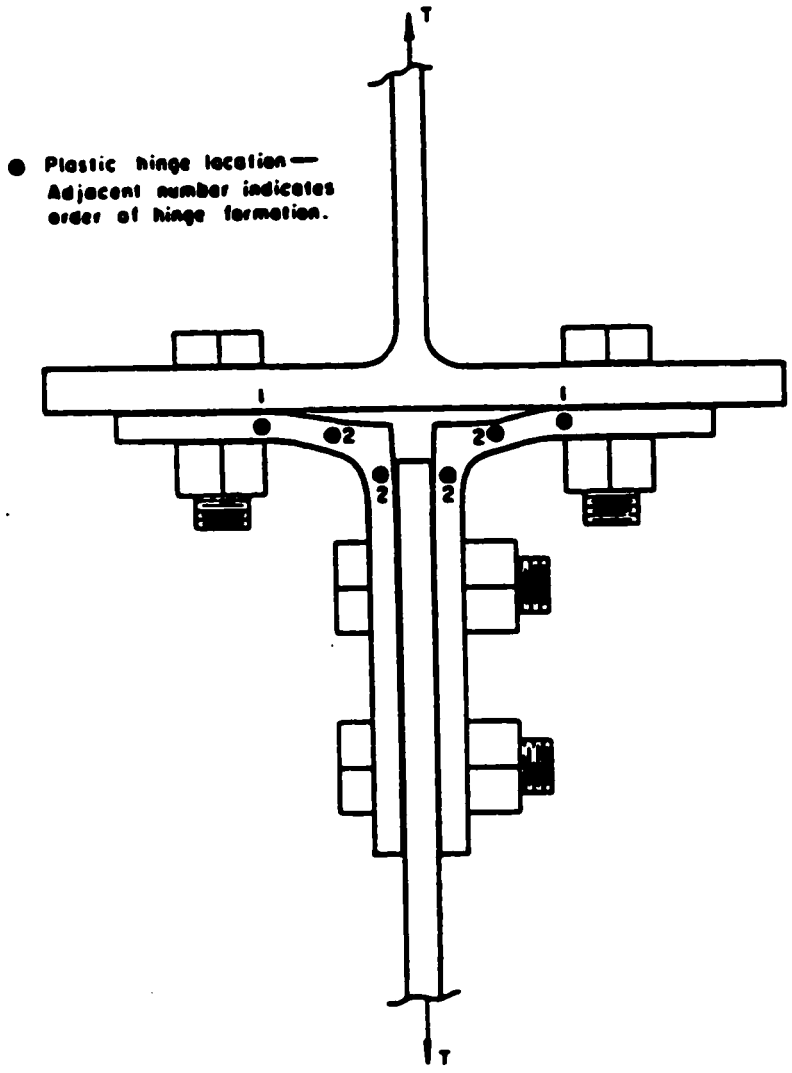

Figure 2.1: Plastic hinging of angles under tension (Lewitt et al., 1966)

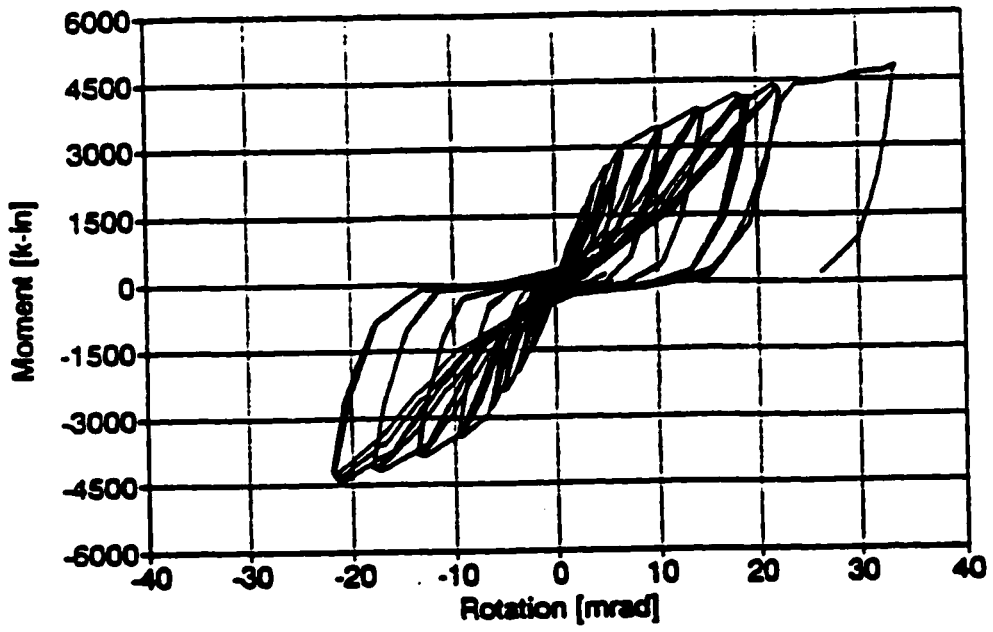

Figure 2.2: Moment-rotation ($M-\theta$) curve, tee-stub connection (Roeder et al., 1994)

Figure 2.3: Deformation of top tee in tee-stub connection (Roeder et al., 1994)

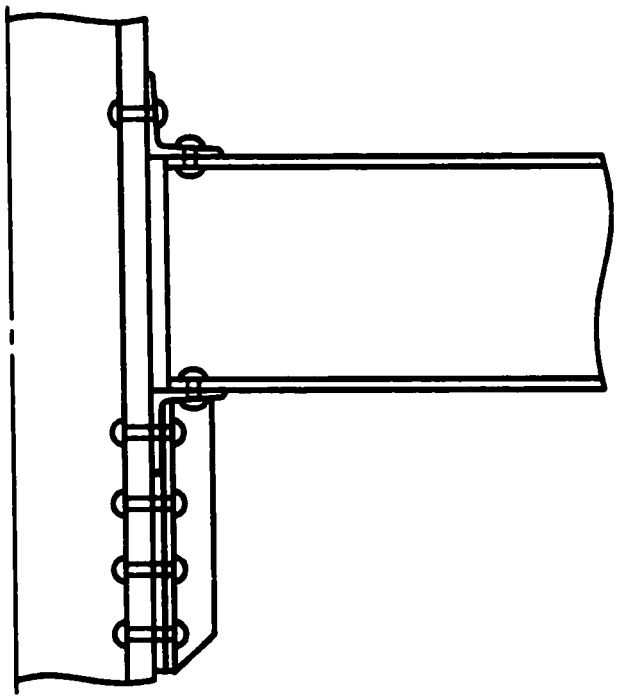

Figure 2.4: Riveted stiffened seat angle connection, as tested by Bruneau and Sarraf (1996)

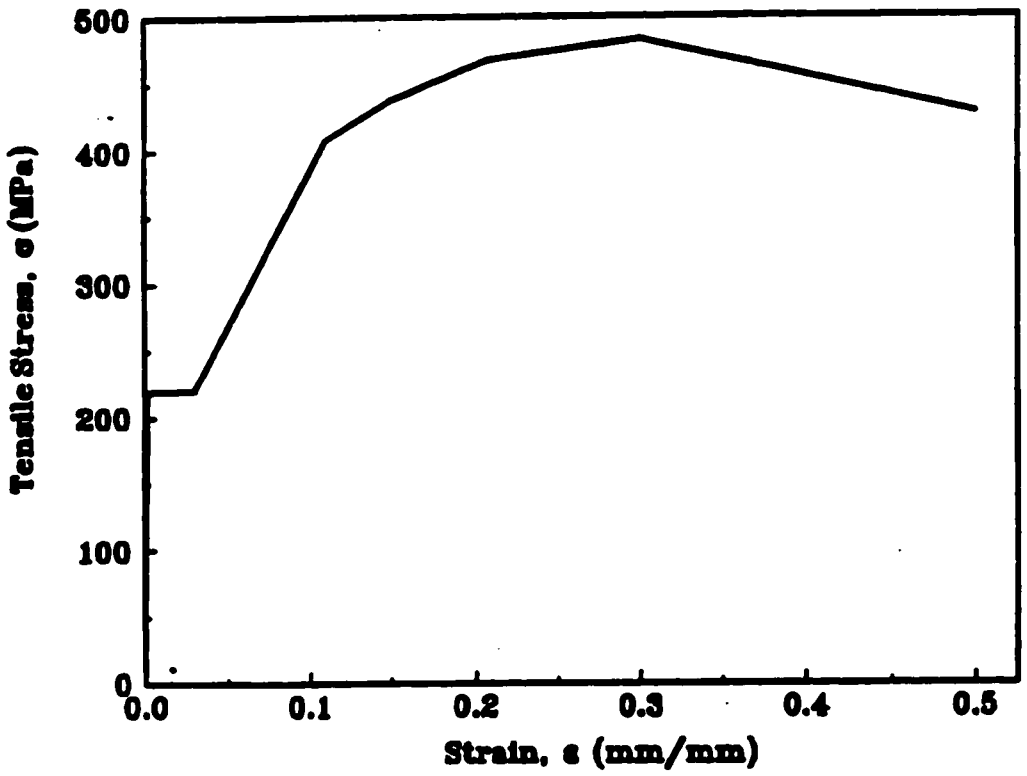

Figure 2.5: Stress-strain relationship obtained from tensile test of 3/4" rivet (Bruneau and Sarraf, 1996)

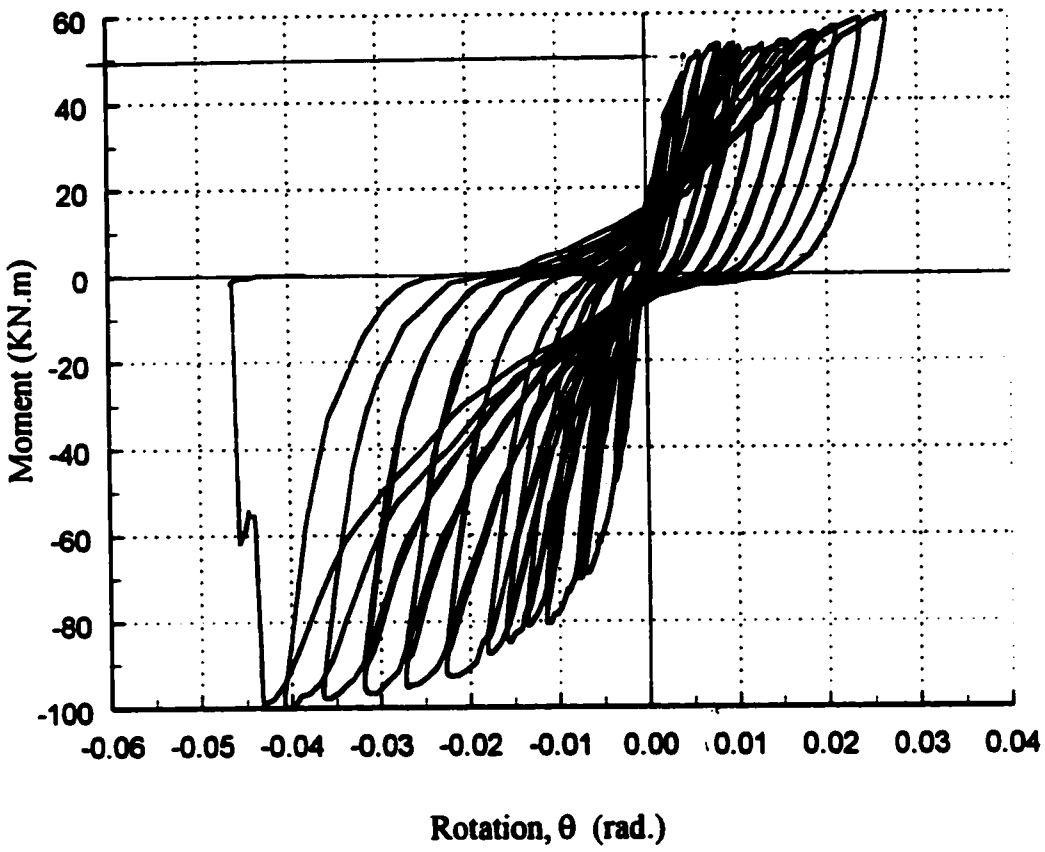

Figure 2.6: Moment-rotation curve, riveted stiffened seat angle connection (Bruneau and Bisson, 2000)

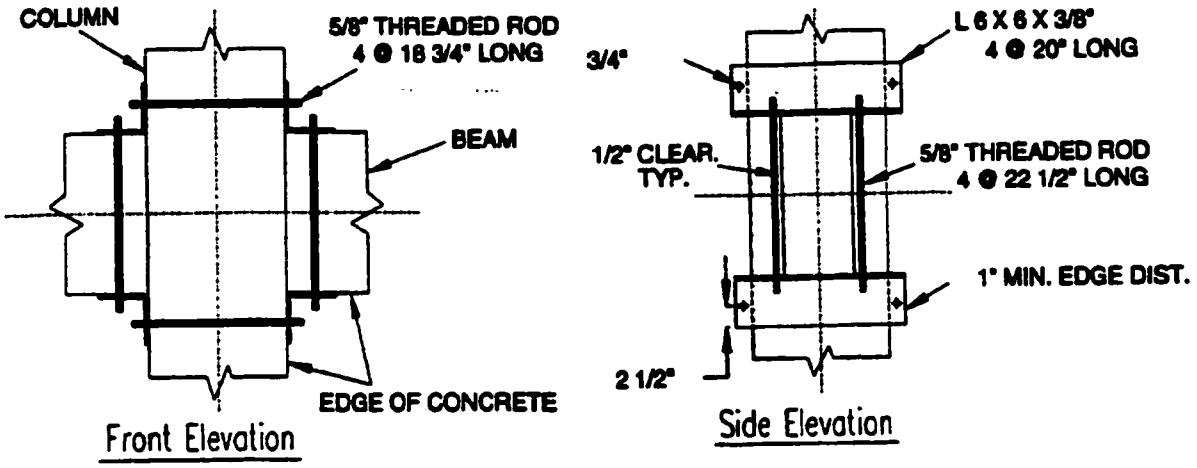

Figure 2.7: Retrofit strategy, concrete encased connection (Roeder et al., 1994)

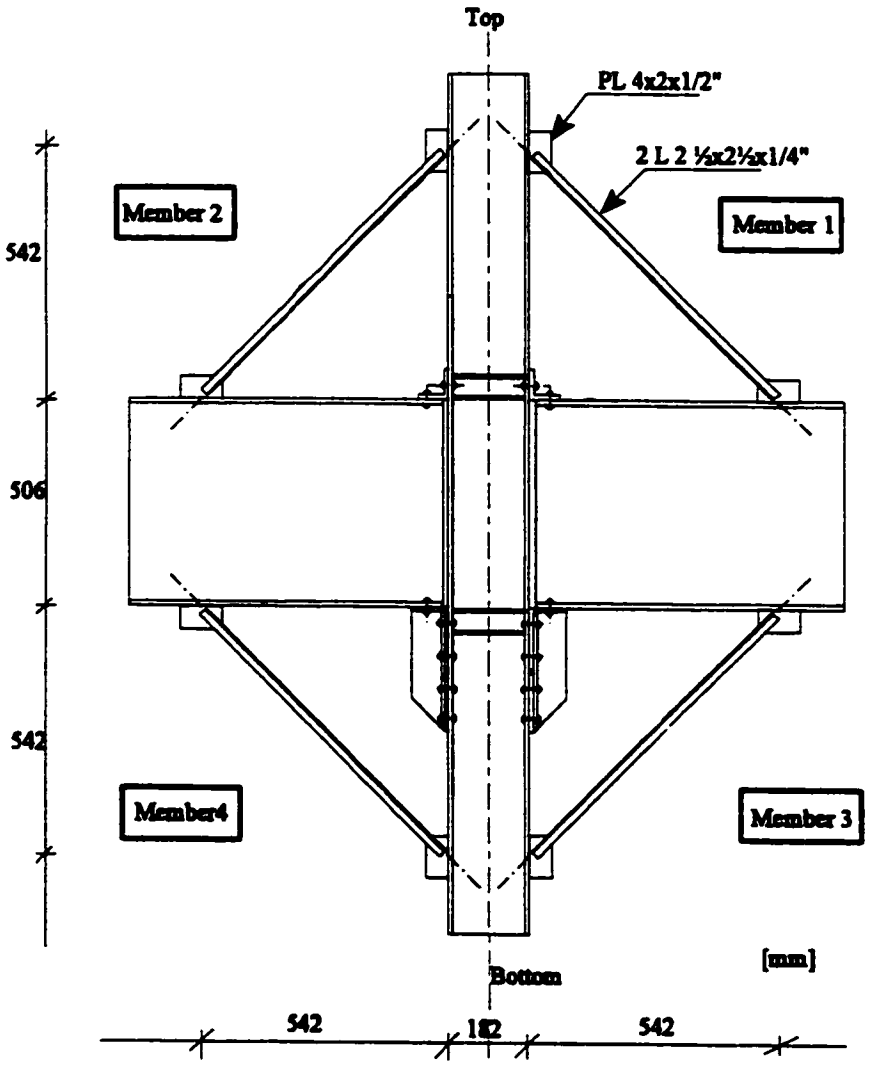

Figure 2.8: Retrofit strategy, knee braces (Bruneau and Sarraf, 1996)

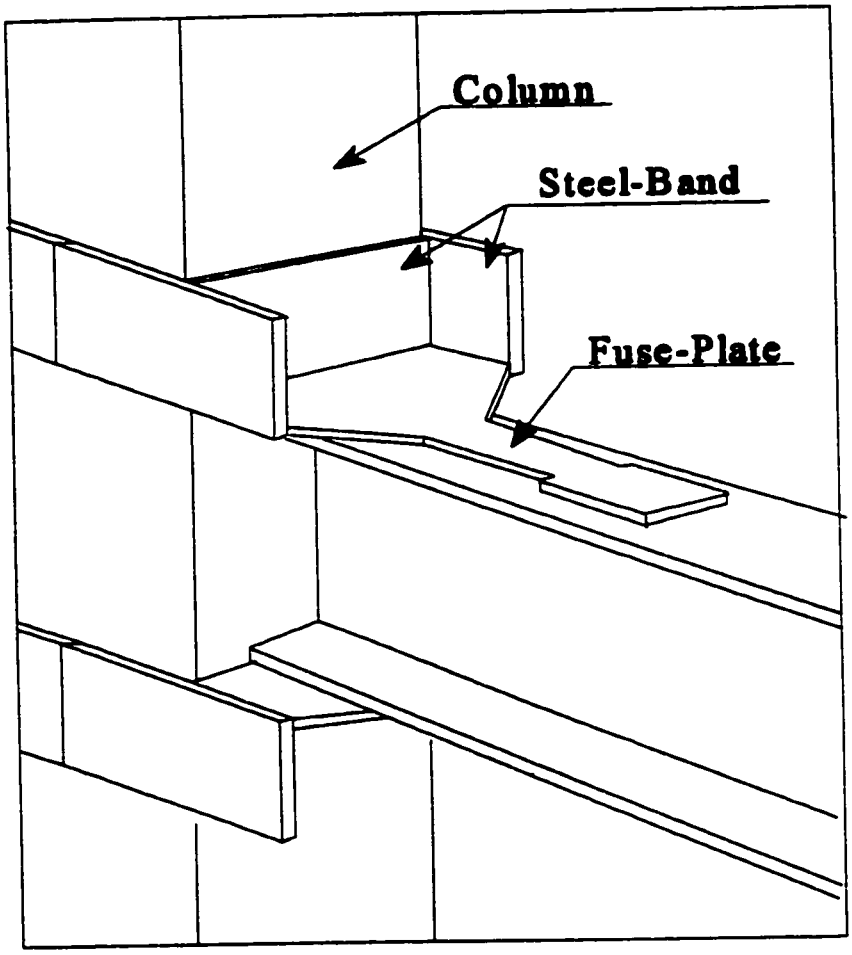

Figure 2.9: Retrofit strategy, steel-band fuse plate (Bruneau and Bisson, 2000)

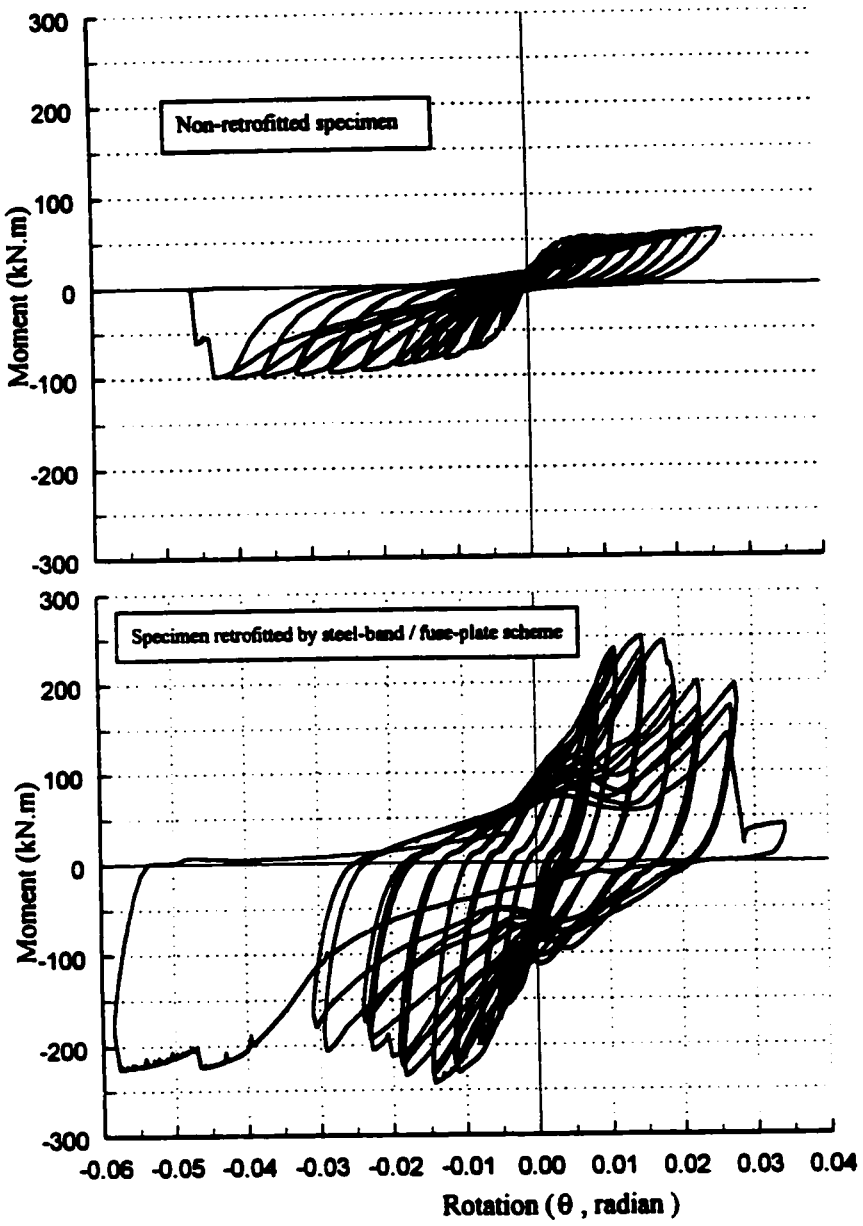

Figure 2.10: Comparison of non-retrofitted and retrofitted moment-rotation curves (Bruneau and Bisson, 2000)

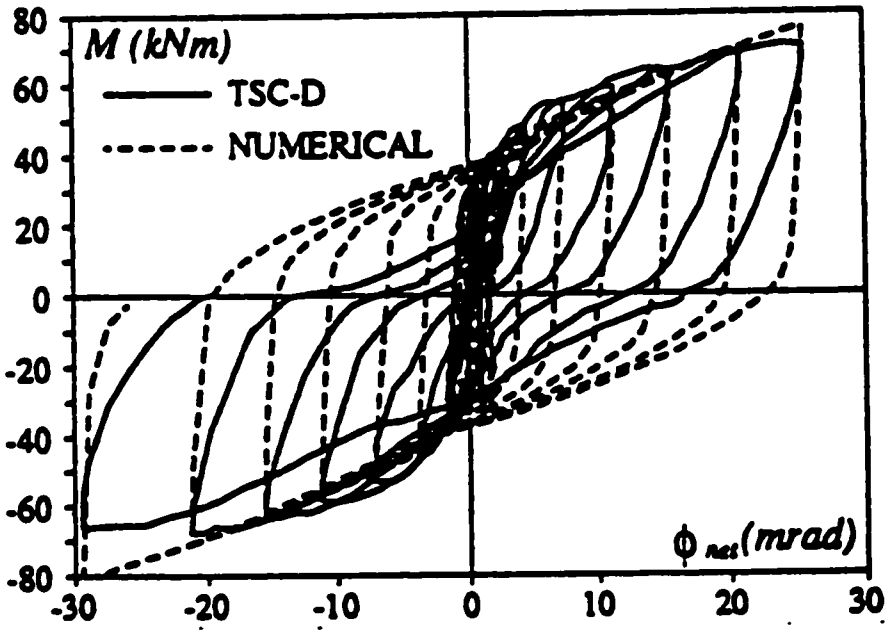

Figure 2.11: Comparison between experimental and modeled moment-rotation curves (De Luca, 1995)

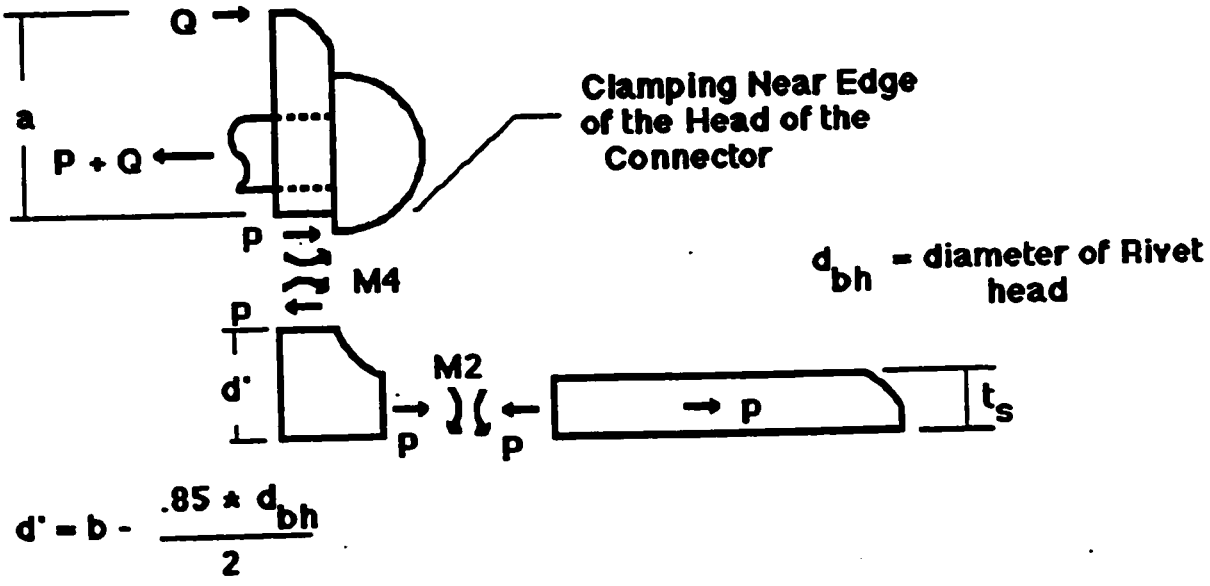

Figure 2.12: Force equilibrium in clip angle connection (Roeder et al., 1994)

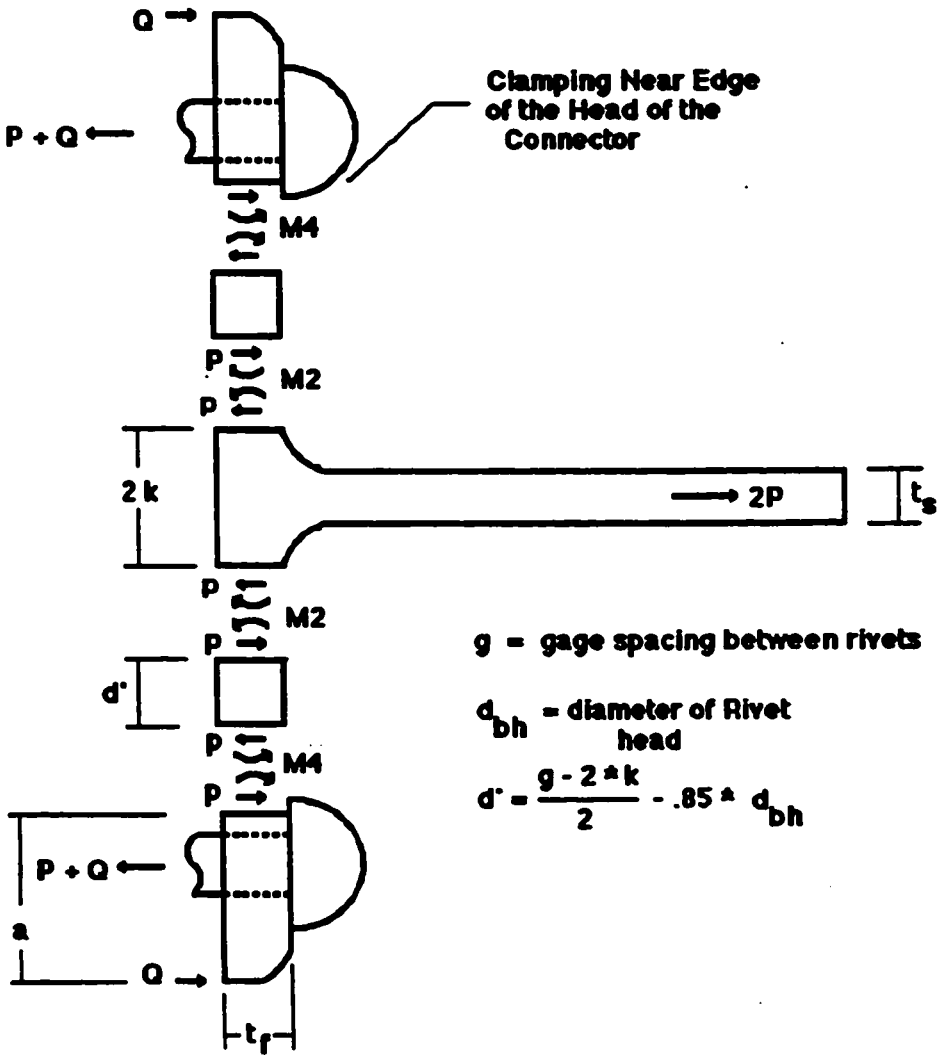

Figure 2.13: Force equilibrium in tee-stub connection (Roeder et al., 1994)

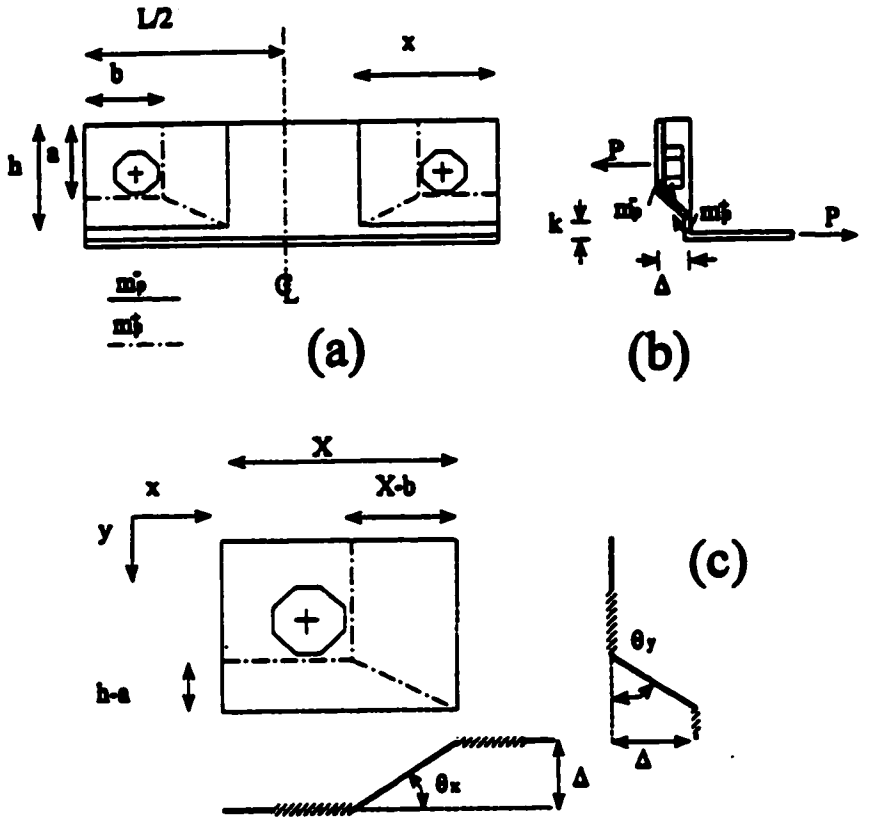

Figure 2.14: Plastic yield mechanism of top angle (Bruneau and Sarraf, 1996)

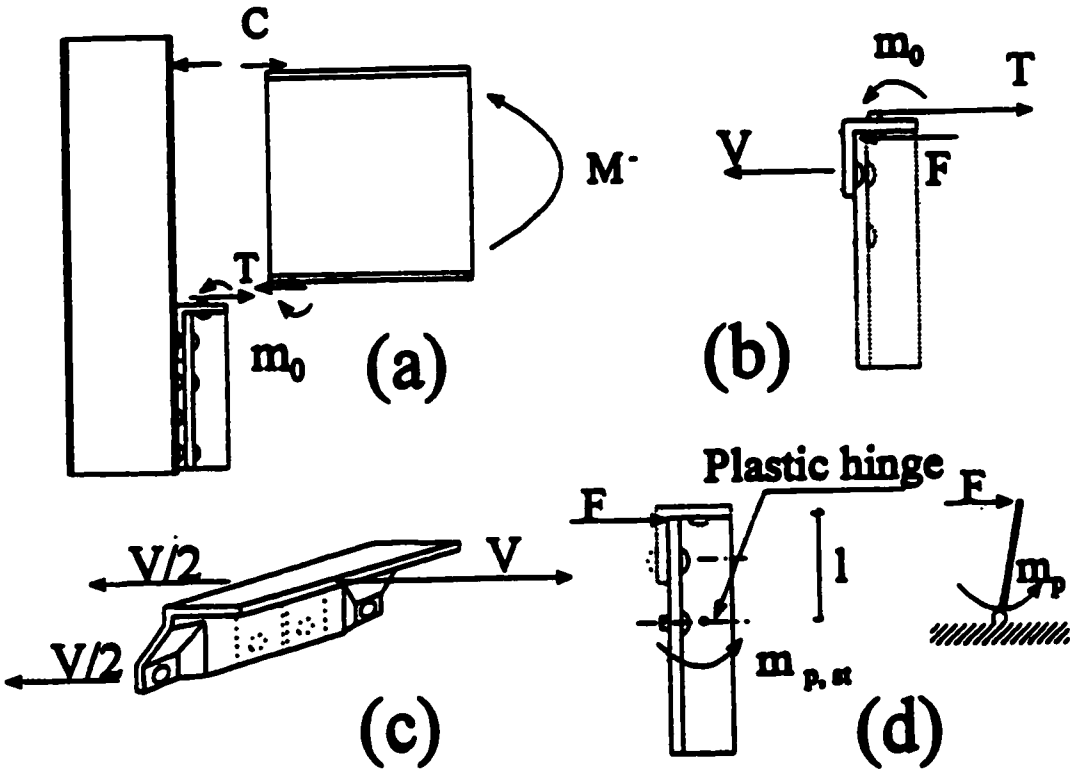

Figure 2.15: Plastic yield mechanism of stiffened seat angle (Bruneau and Sarraf, 1996)

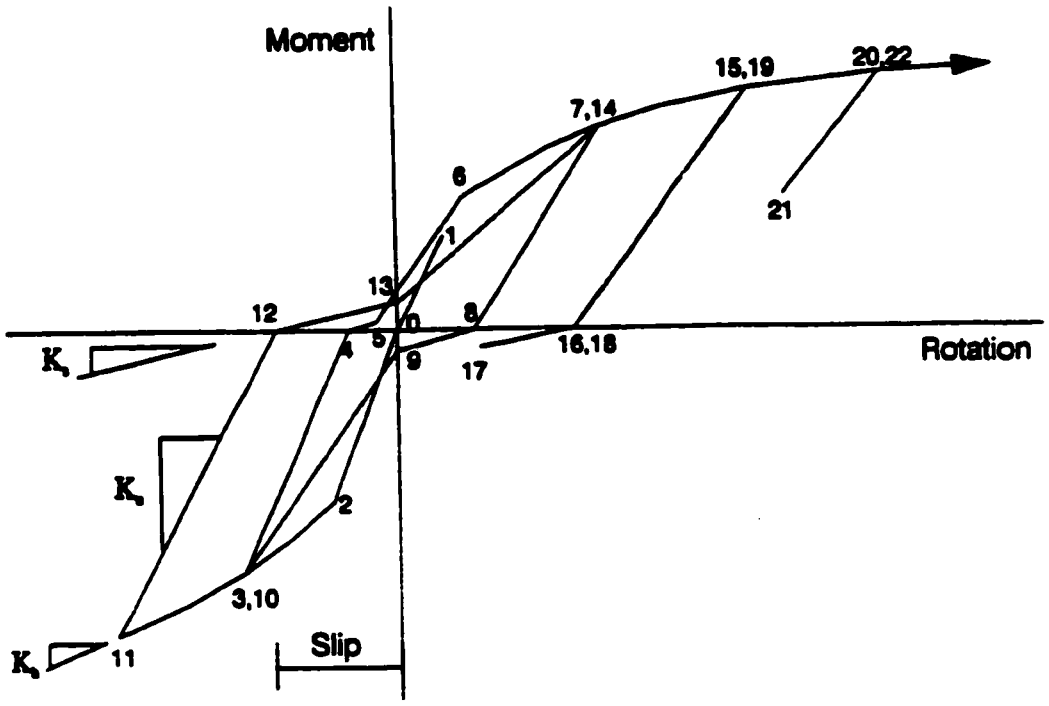

Figure 2.16: Riveted connection Hysteresis rule (Roeder et al., 1994)

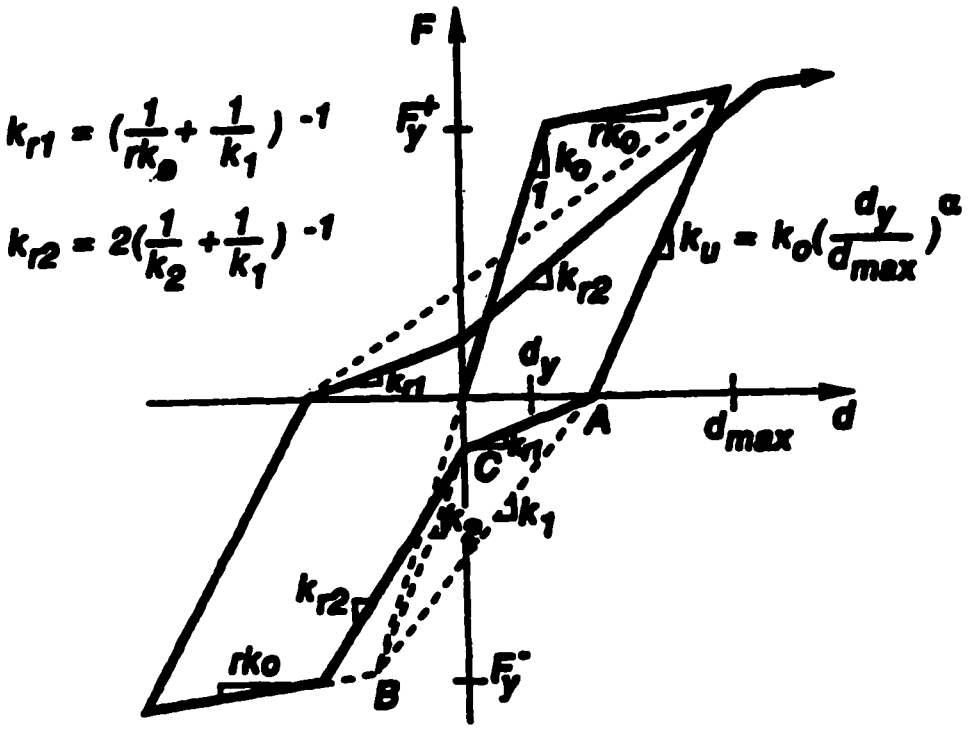

Mehran Keshavarian Hysteresis

Figure 2.17: Mehran Keshavarzian degrading and pinching hysterisis rule (Carr, 1998)

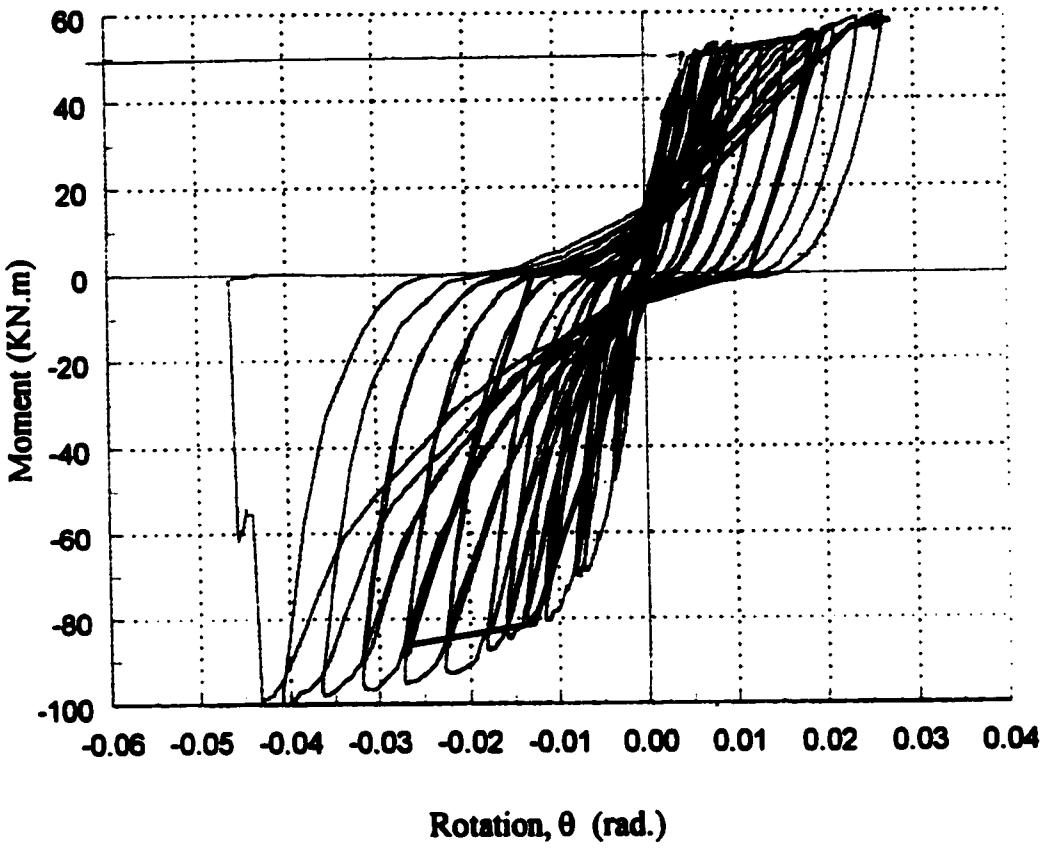

Figure 2.18: Comparison of hysteretic curves, experimental (Bruneau and Bisson, 2000) vs model (Carr, 1998)

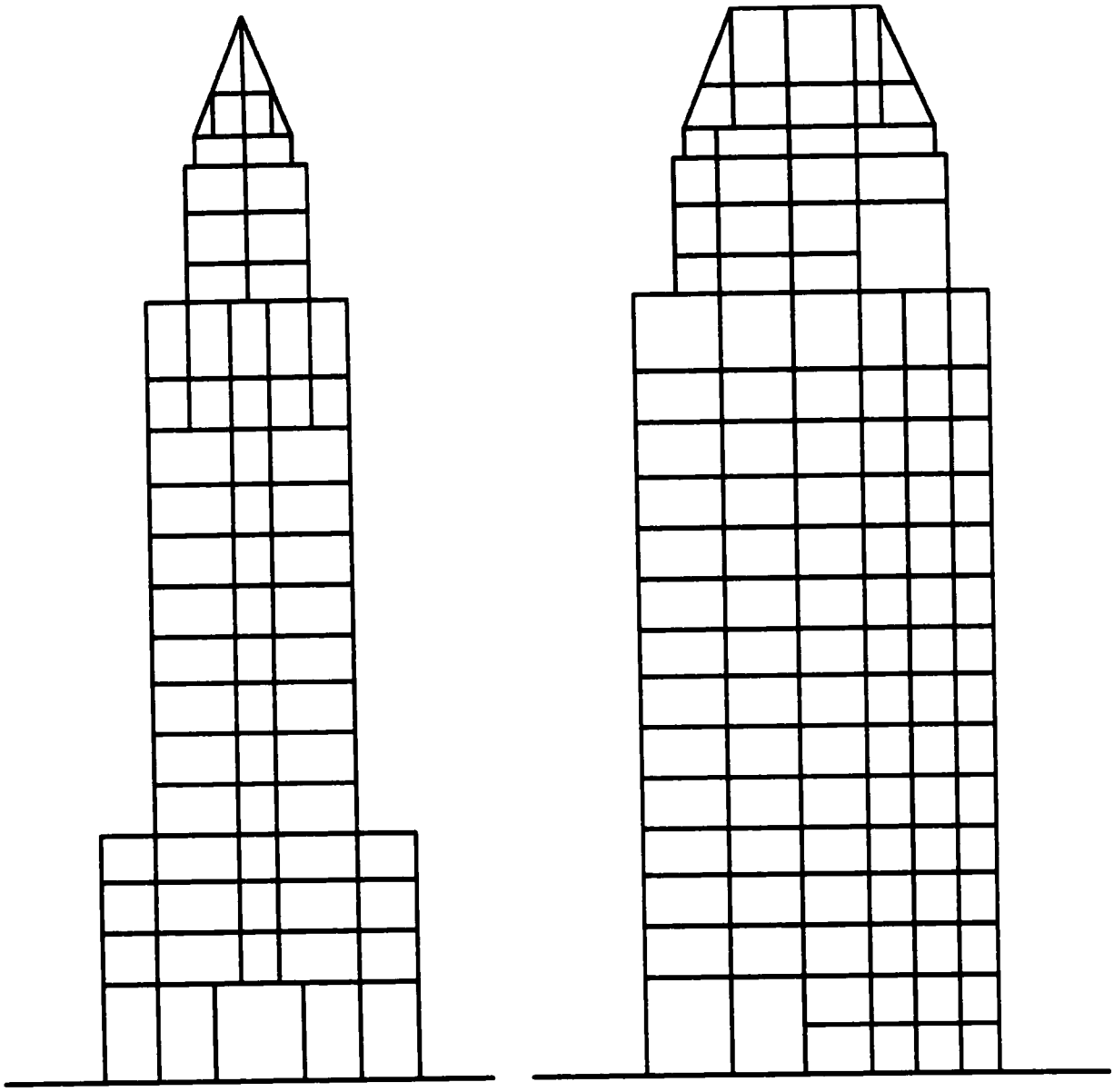

East-West frame

North-South frame

Figure 3.1: Existing Structure

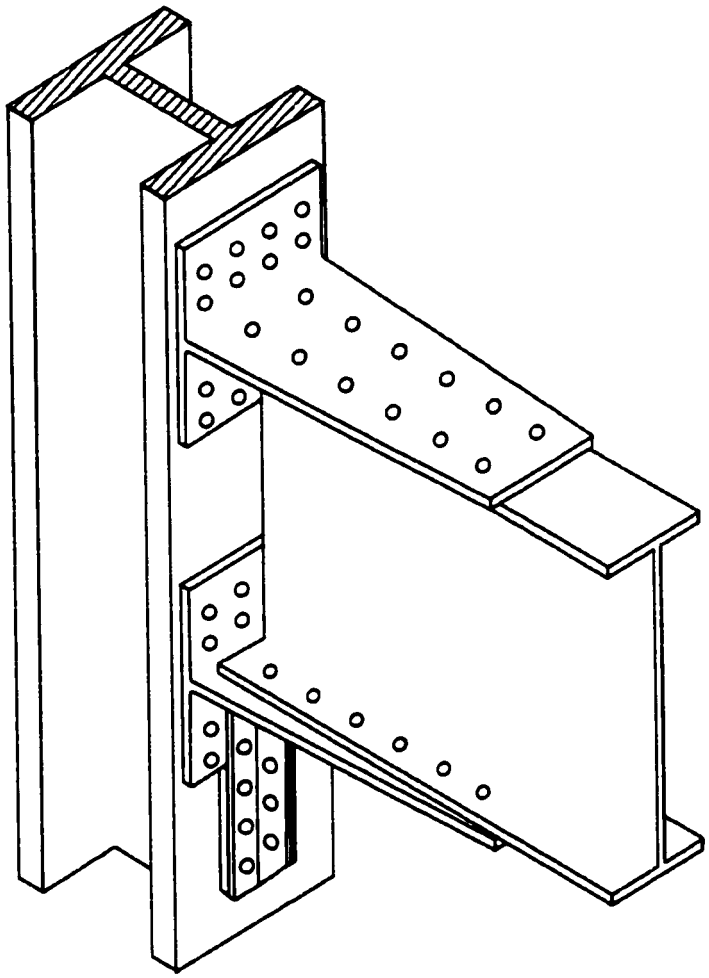

Figure 3.2: Riveted stiffened tee-stub connection

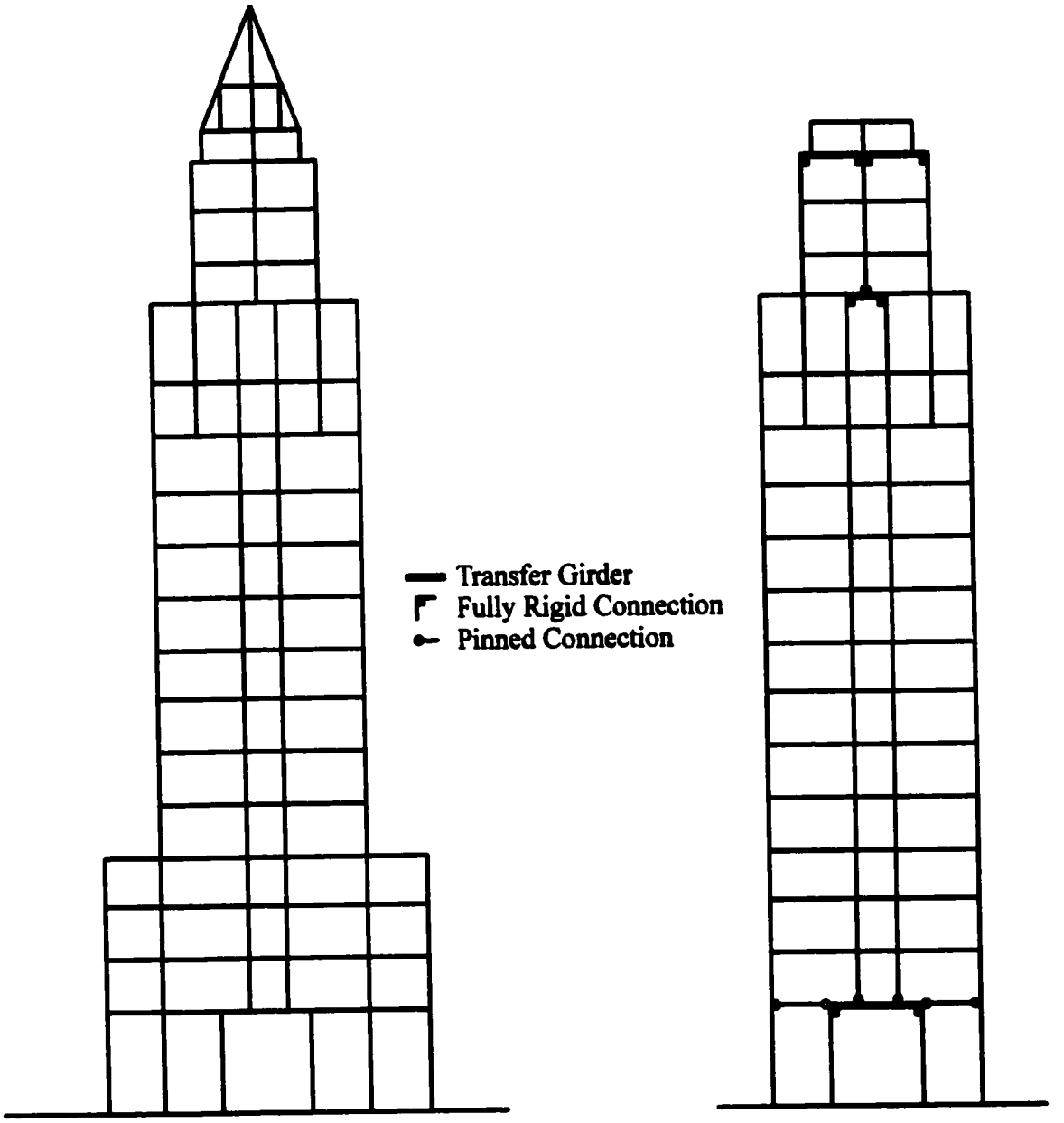

Figure 3.3: Simplification of input model

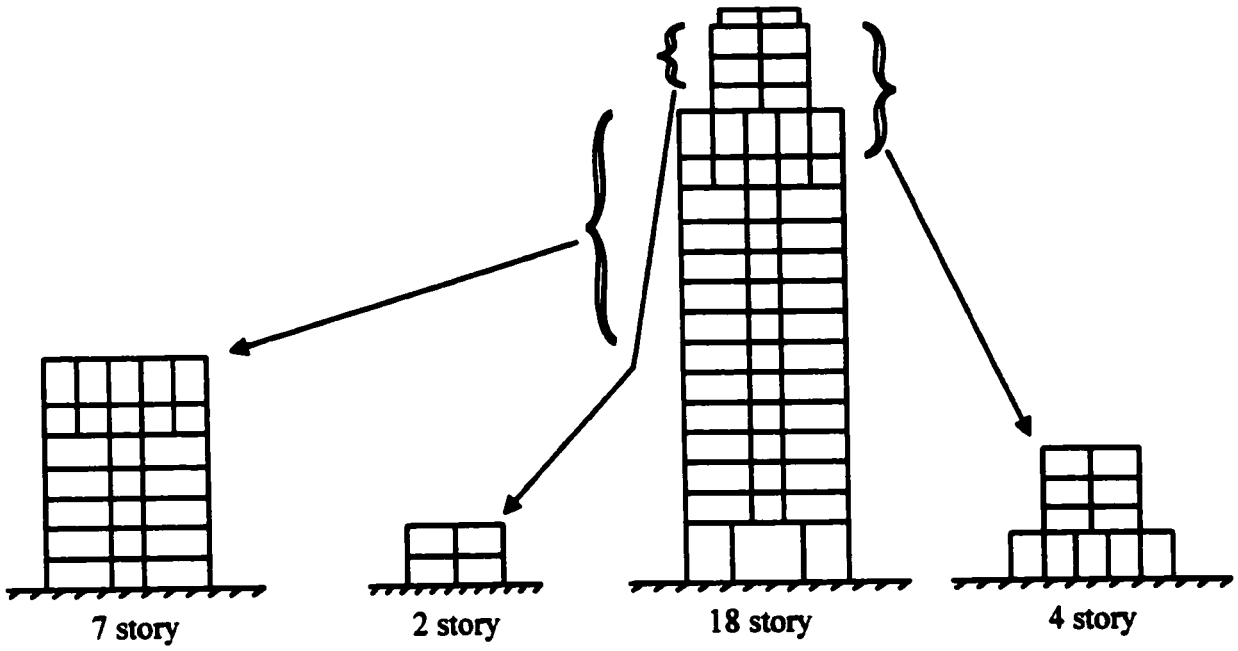

Figure 3.4: Generic frames analyzed

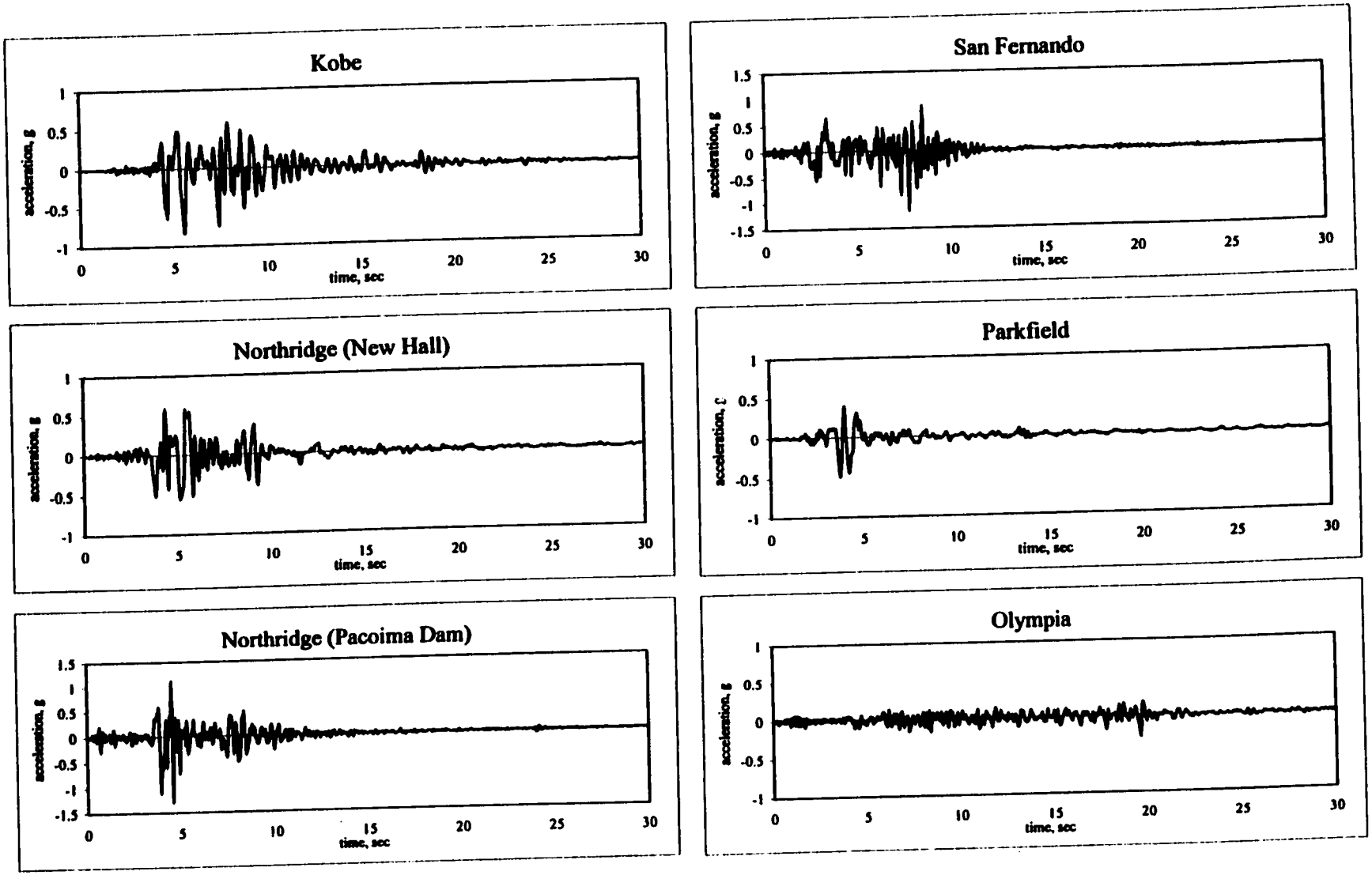

Figure 3.5: Western earthquakes, non-scaled

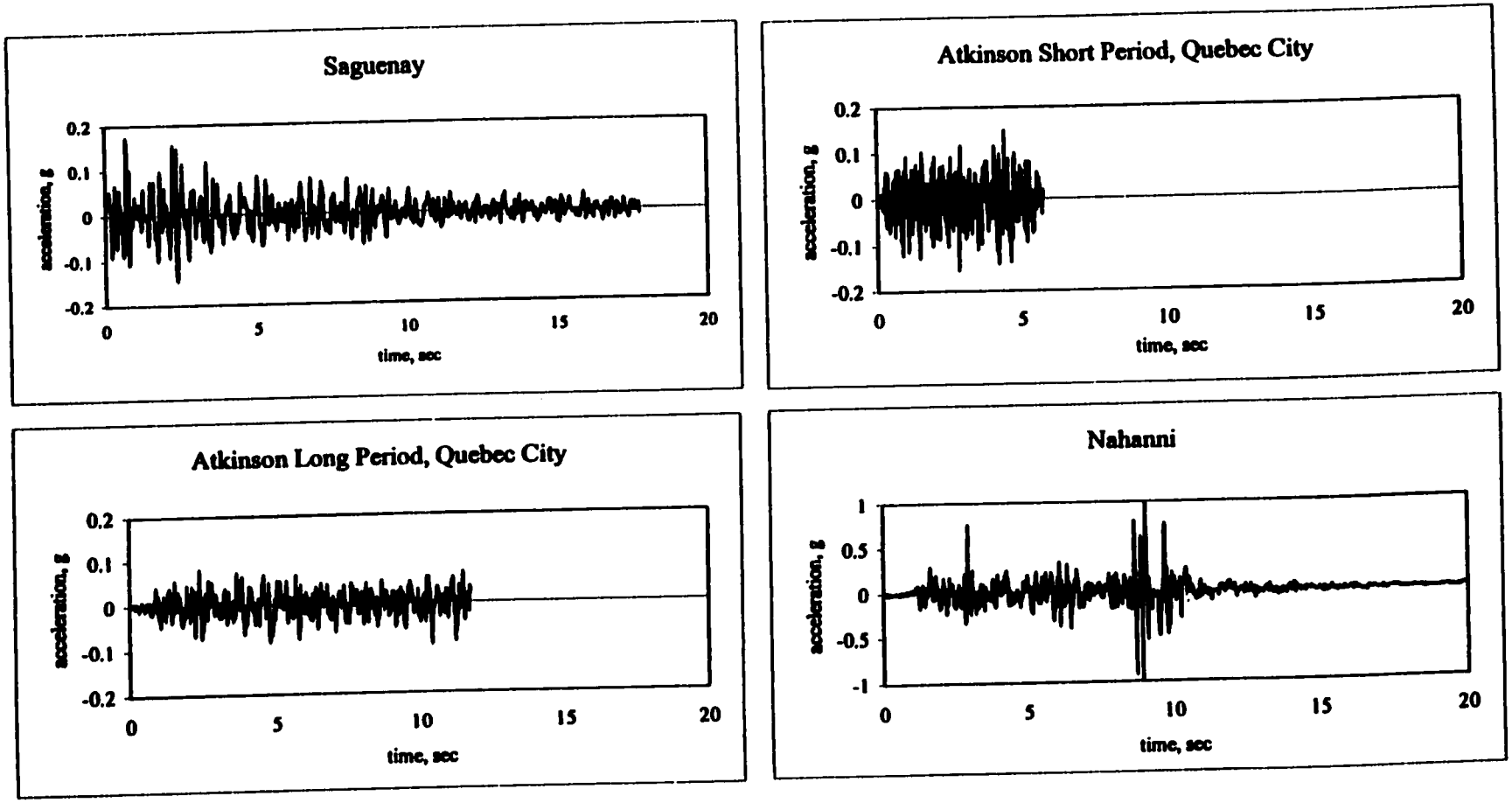

Figure 3.6: Eastern earthquakes, non-scaled

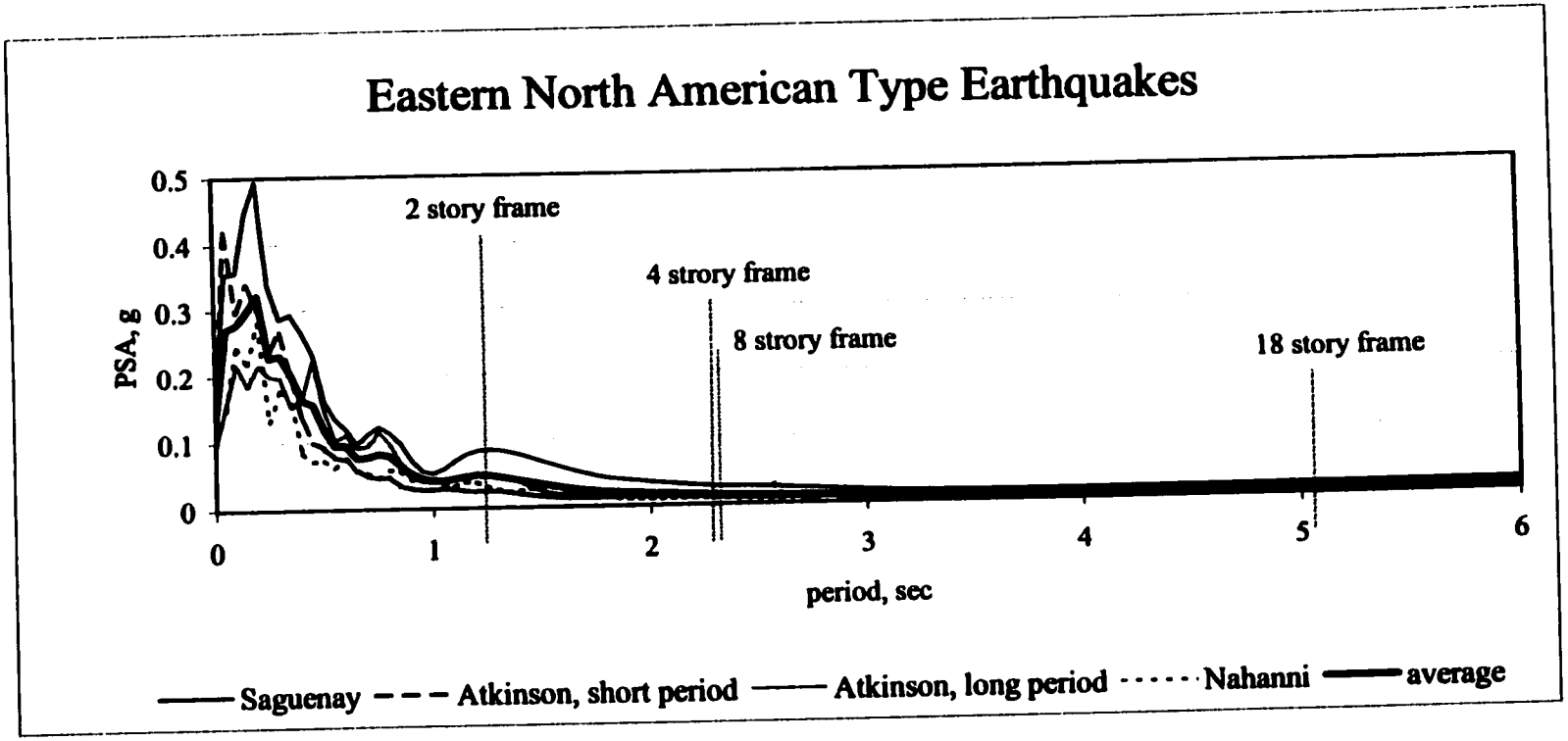

Figure 3.7: Spectral acceleration, Eastern North American type earthquake

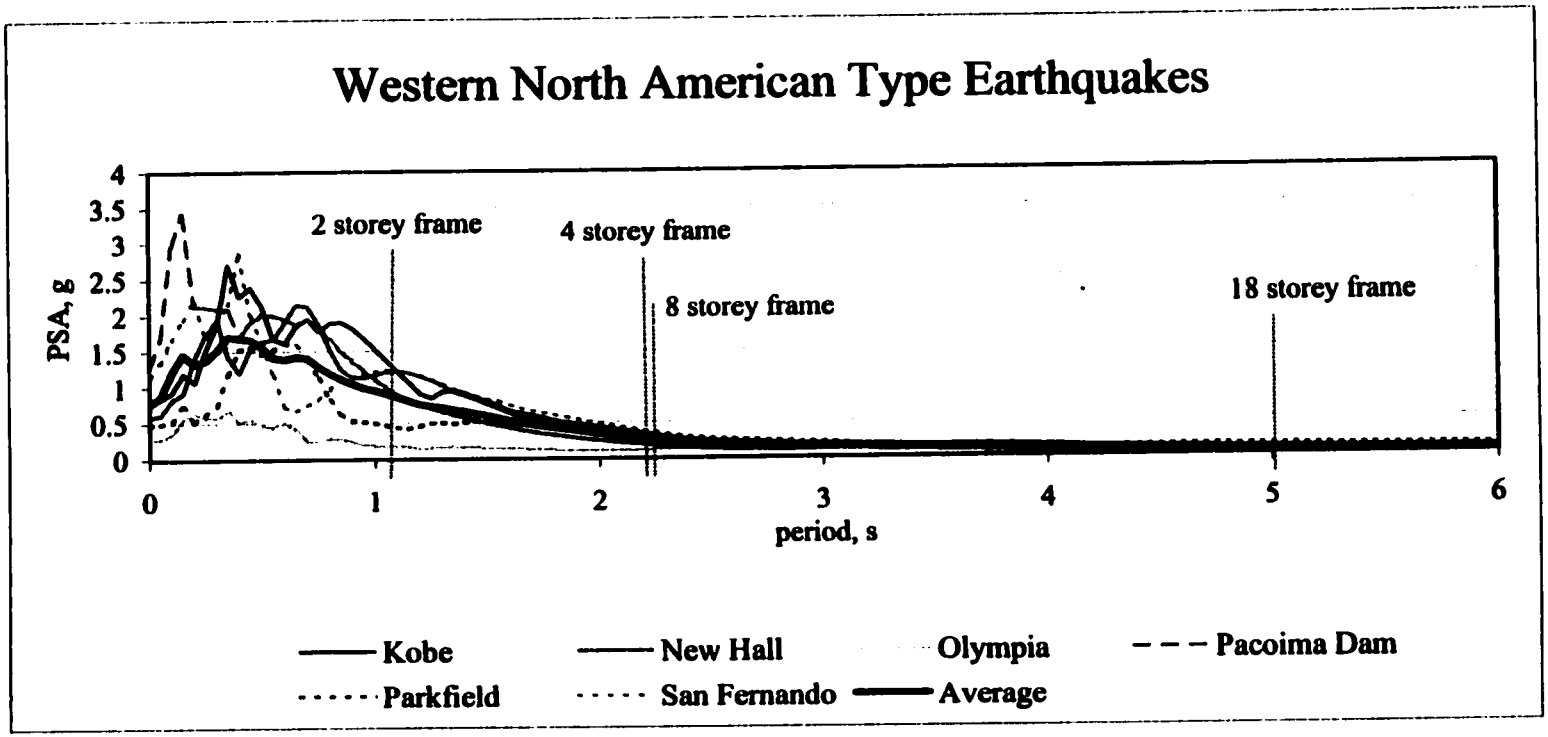

Figure 3.8: Spectral acceleration, Western North American type earthquake

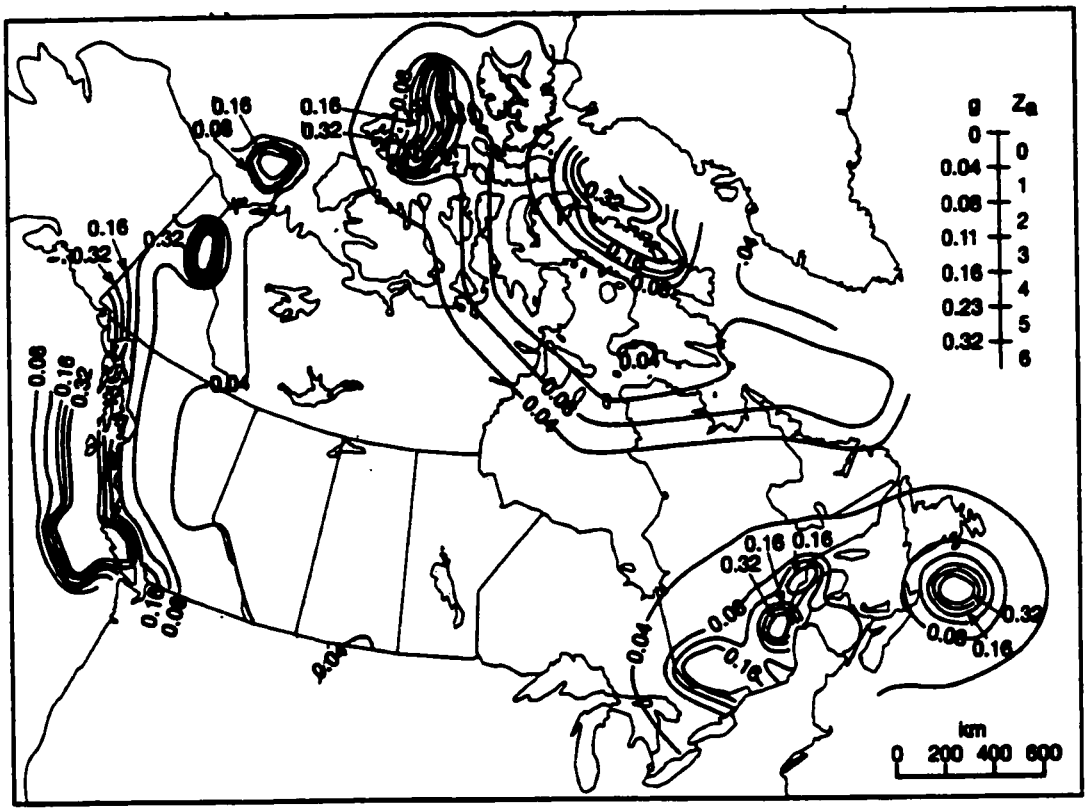

Figure J-1
Contours of peak horizontal ground accelerations, in units of g, having a probability of exceedance of 10% in 50 years.

Figure 3.9: NBCC Seismic Hazard map (10% probability of exceedance in 50 years)

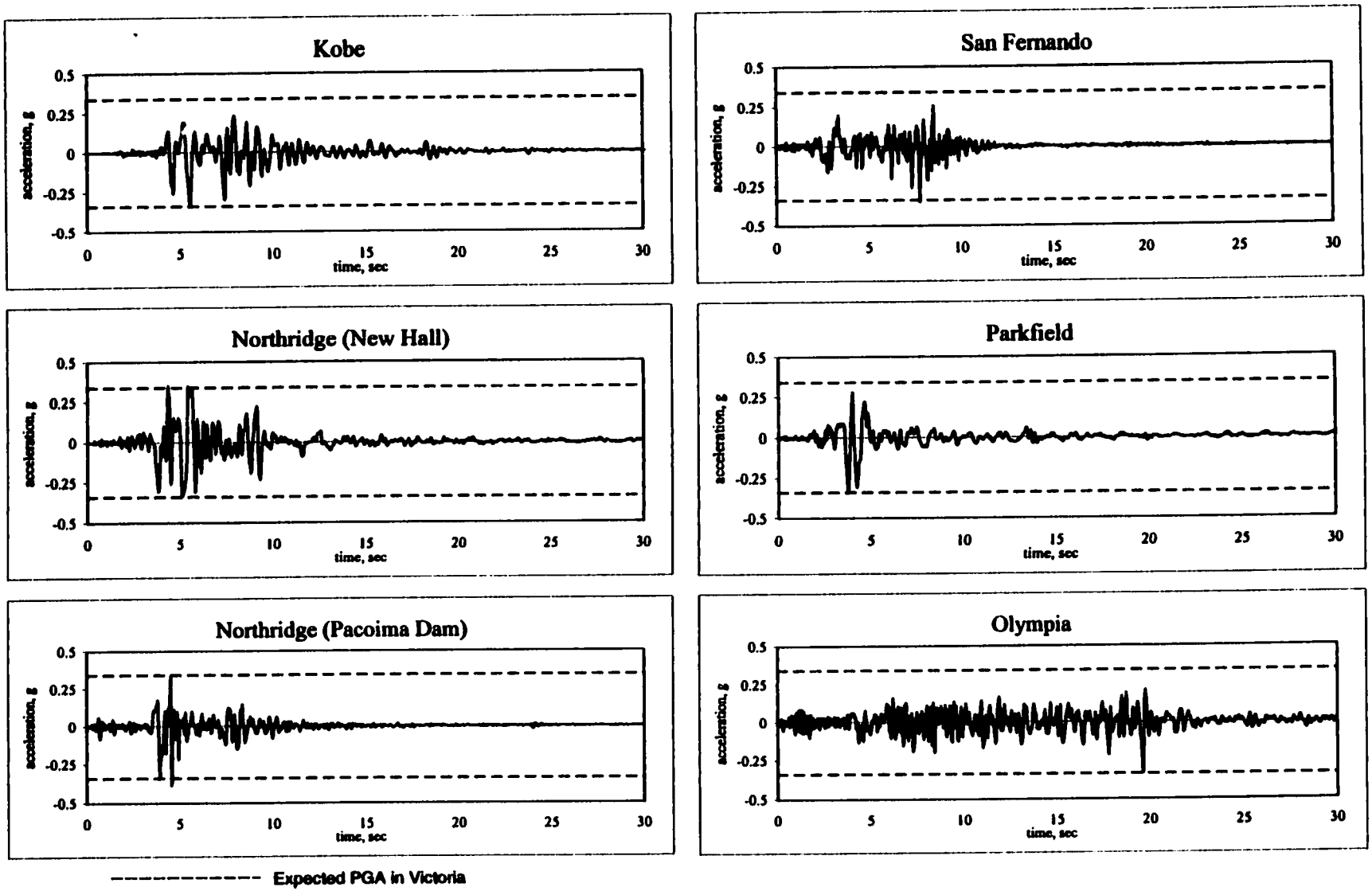

Figure 3.10: Western earthquakes, scaled

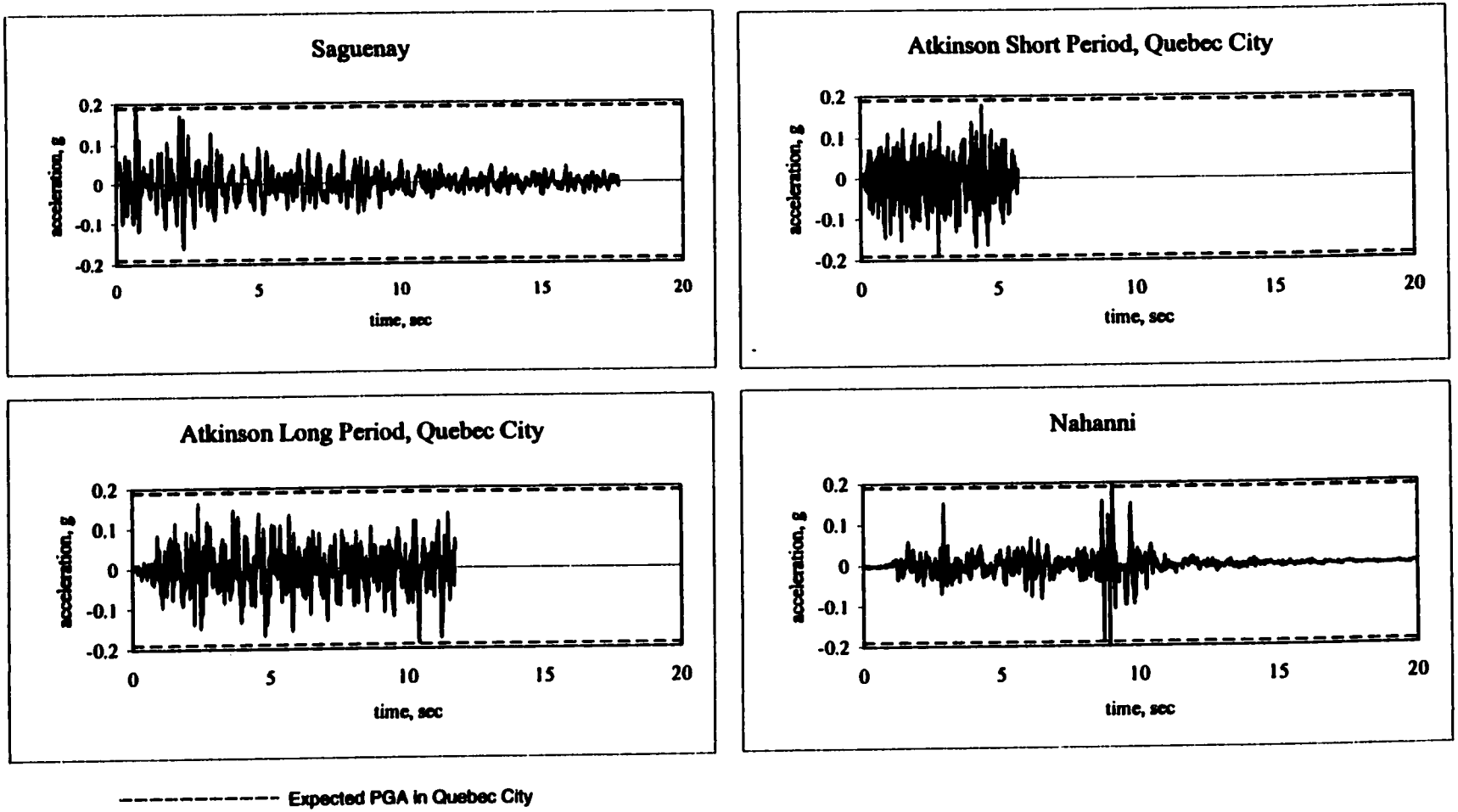

Figure 3.11: Eastern earthquakes, scaled

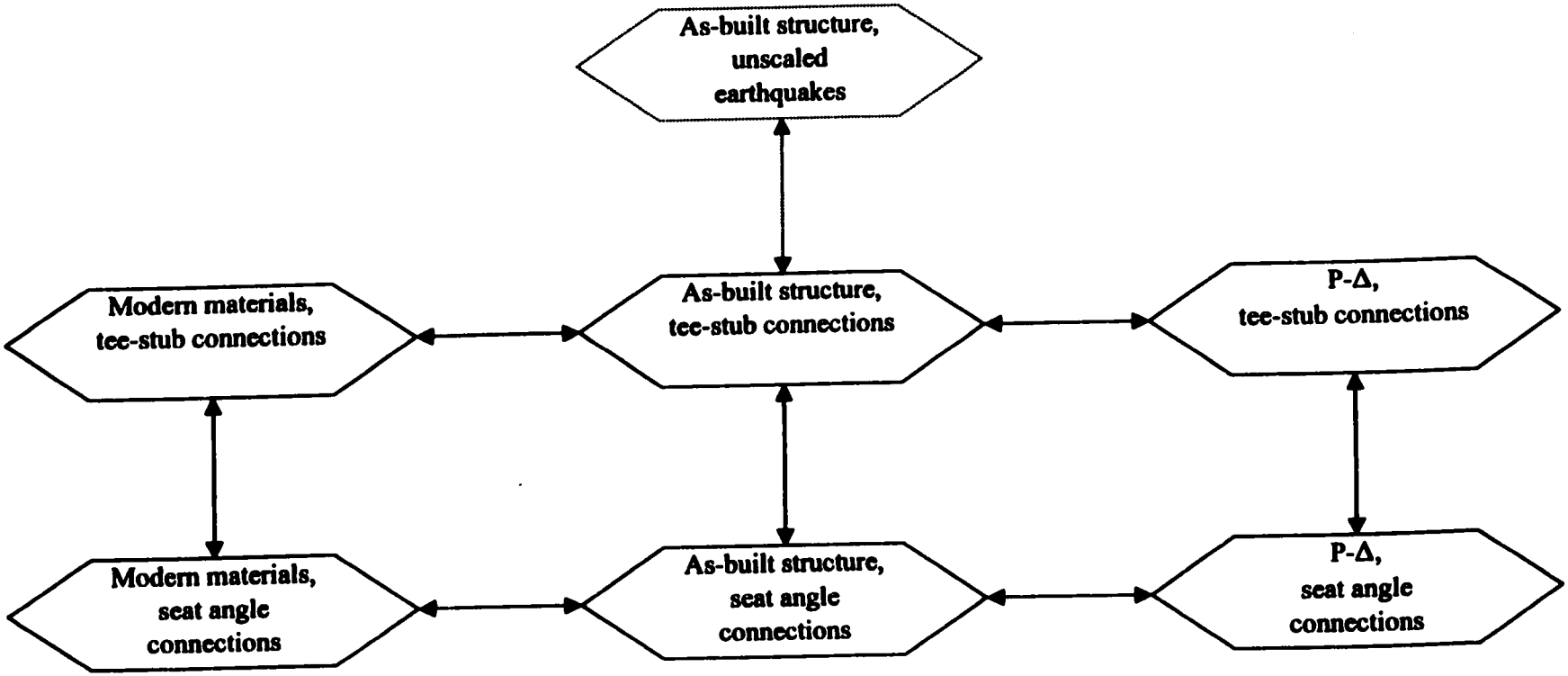

Figure 3.12: Comparison matrix

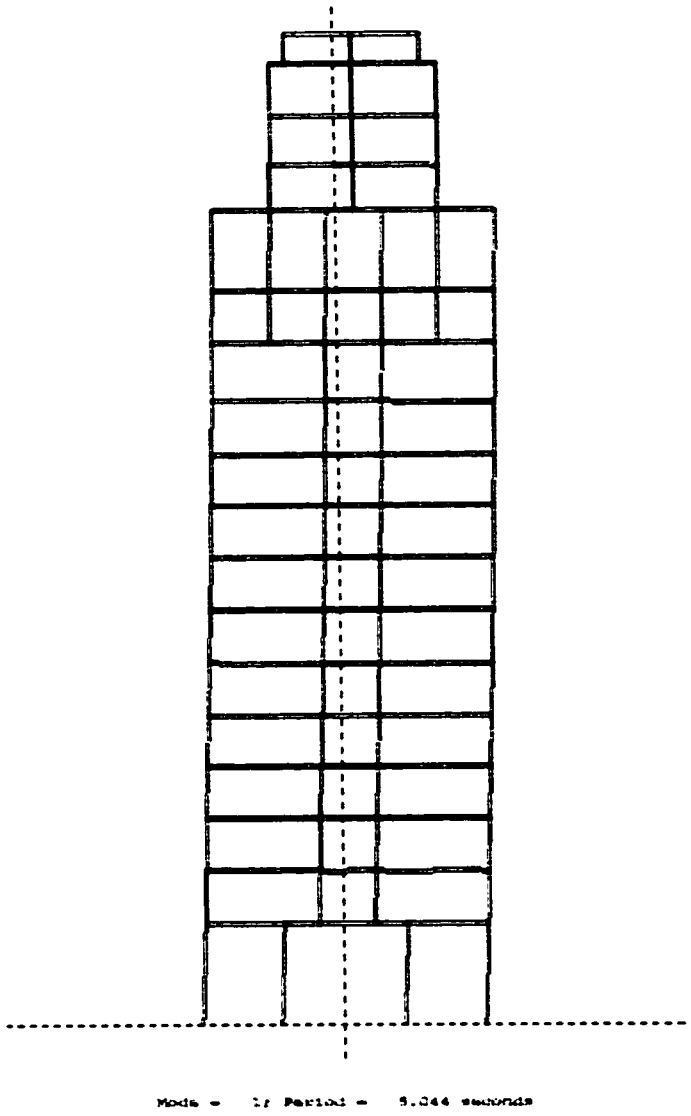

Figure 4.1: Mode shape and period, 18 story frame, As-built scenario

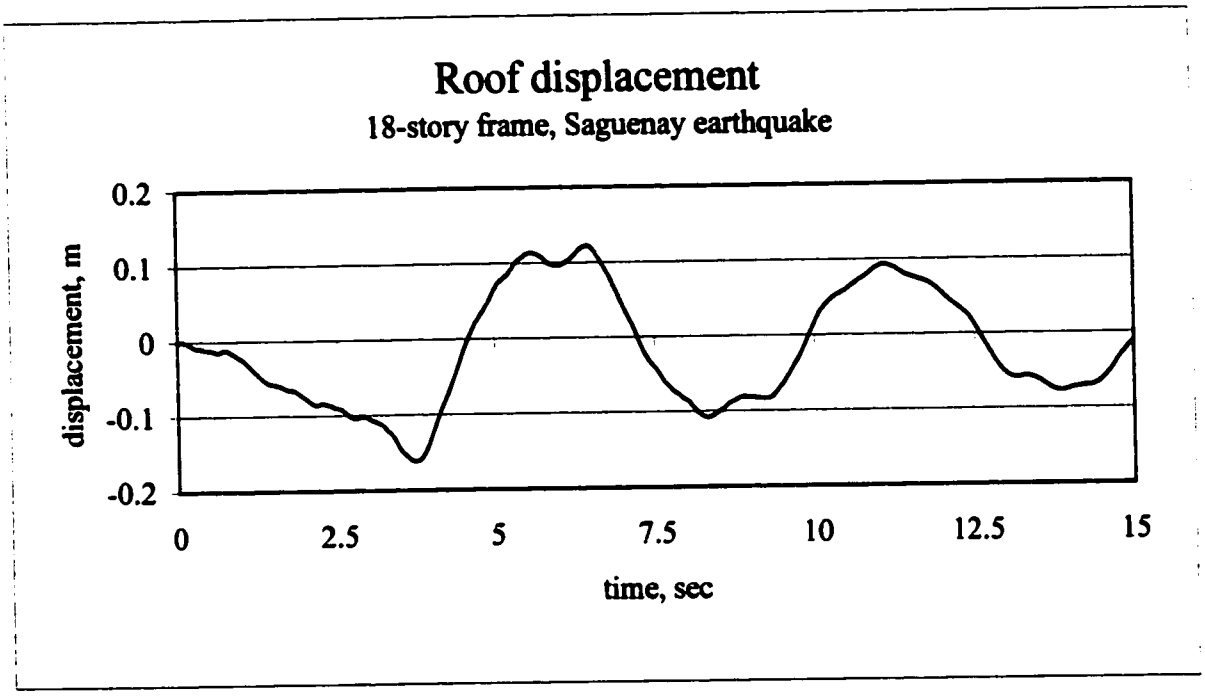

Figure 4.2: Time-history plot of roof displacement, 18-story frame, Saguenay earthquake

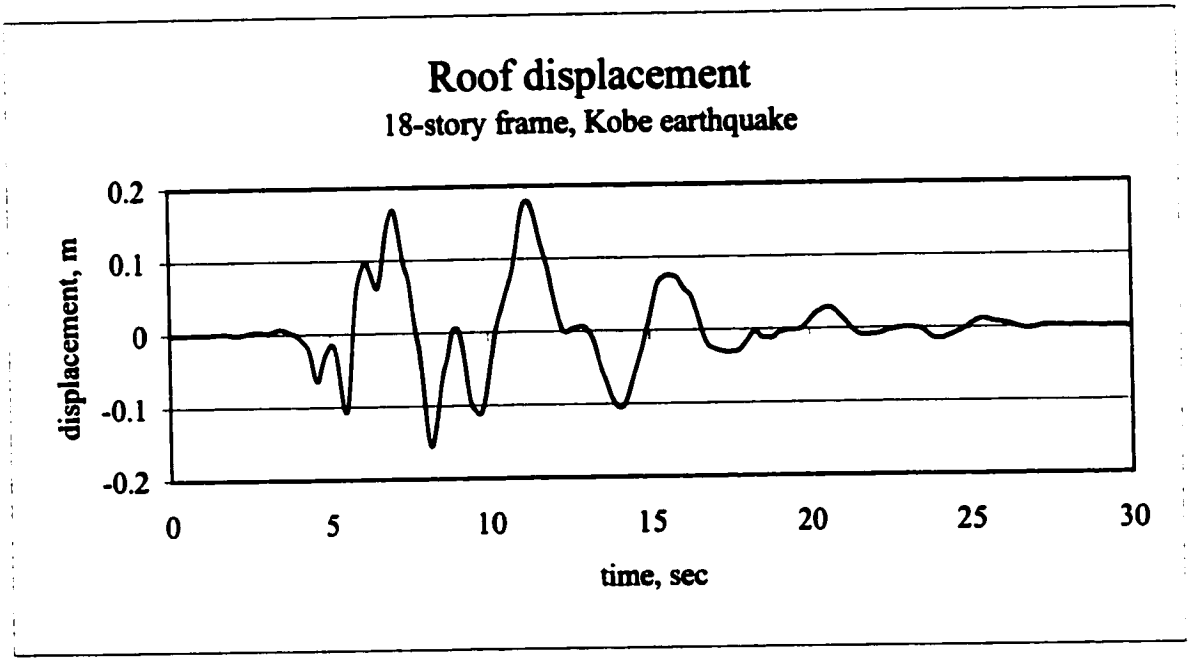

Figure 4.3: Time-history plot of roof displacement, 18-story frame, Kobe earthquake

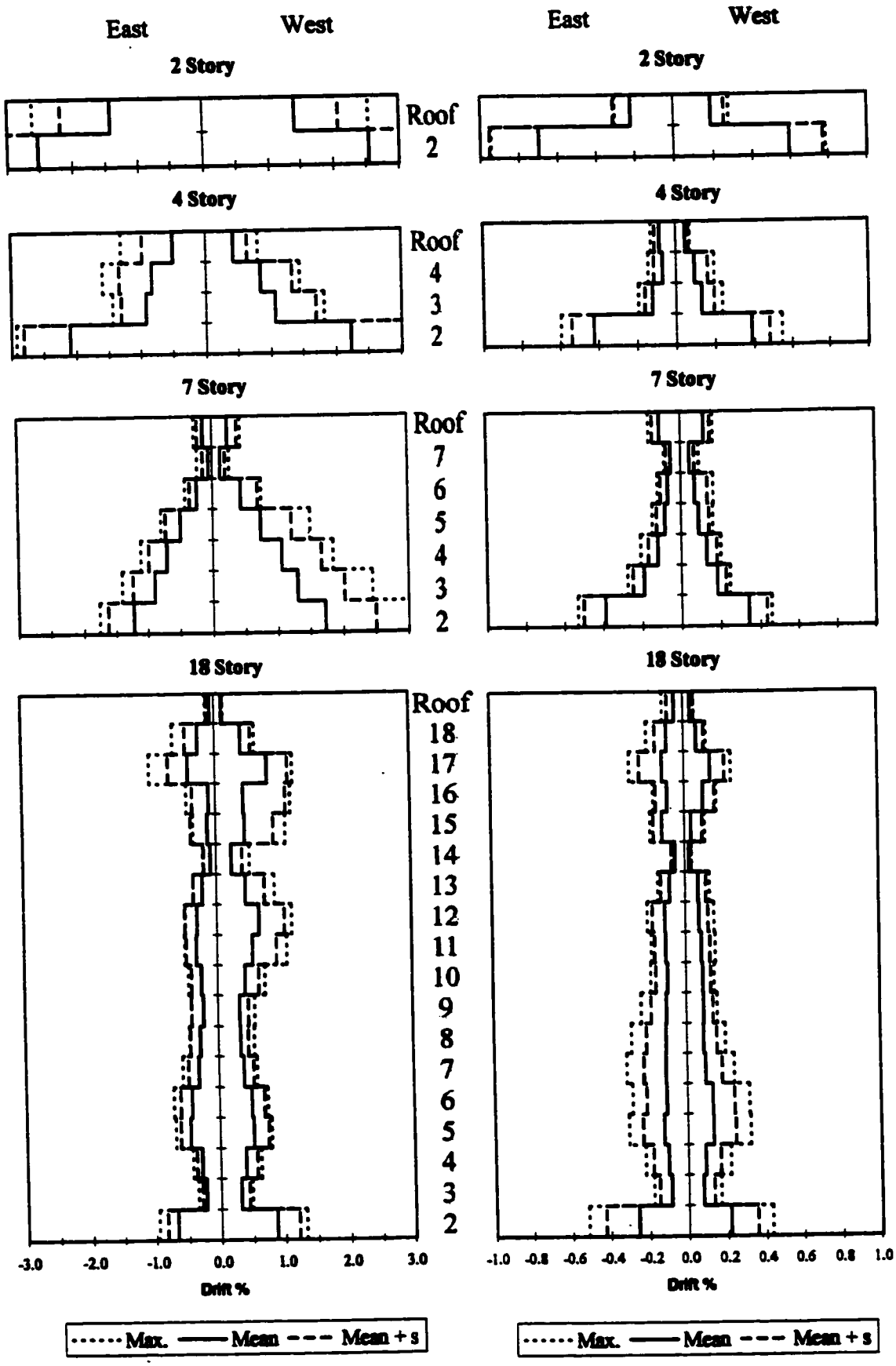

Figure 4.4: Inter-story drifts for tee-stub connections, As-built scenario

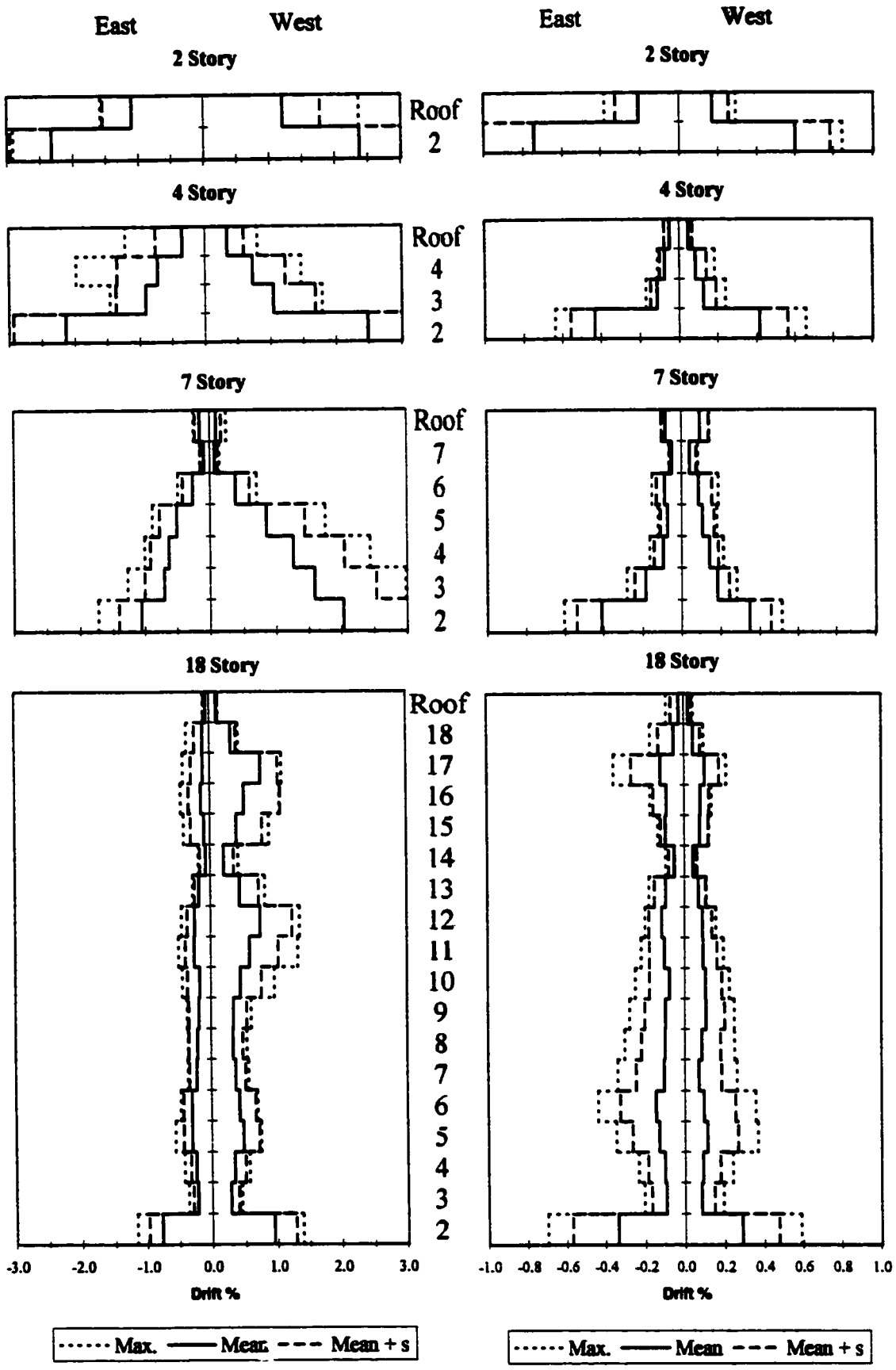

Figure 4.5: Inter-story drifts for tee-stub connections, P-Δ scenario

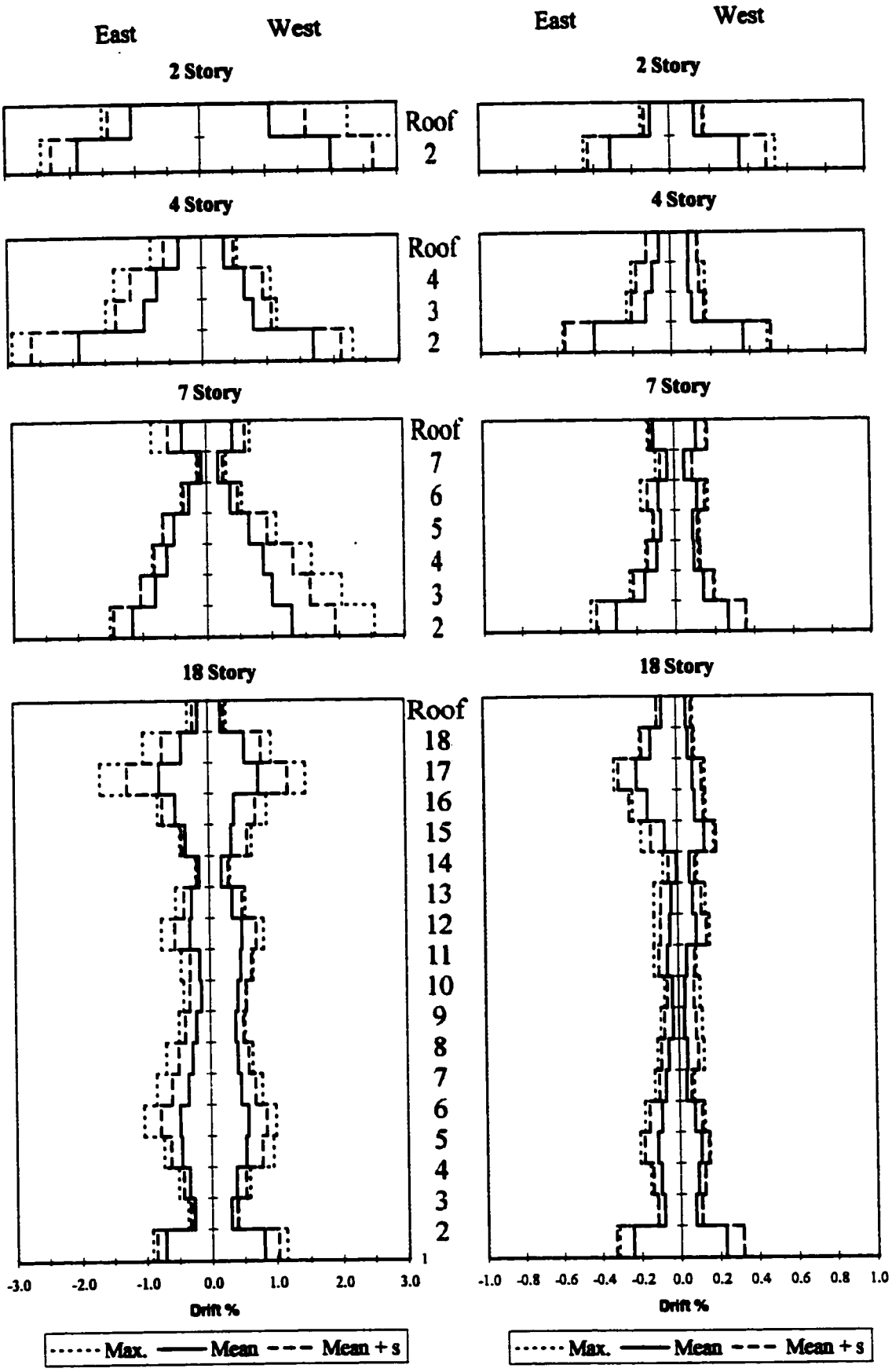

Figure 4.6: Inter-story drifts for tee-stub connections, Modern mass scenario

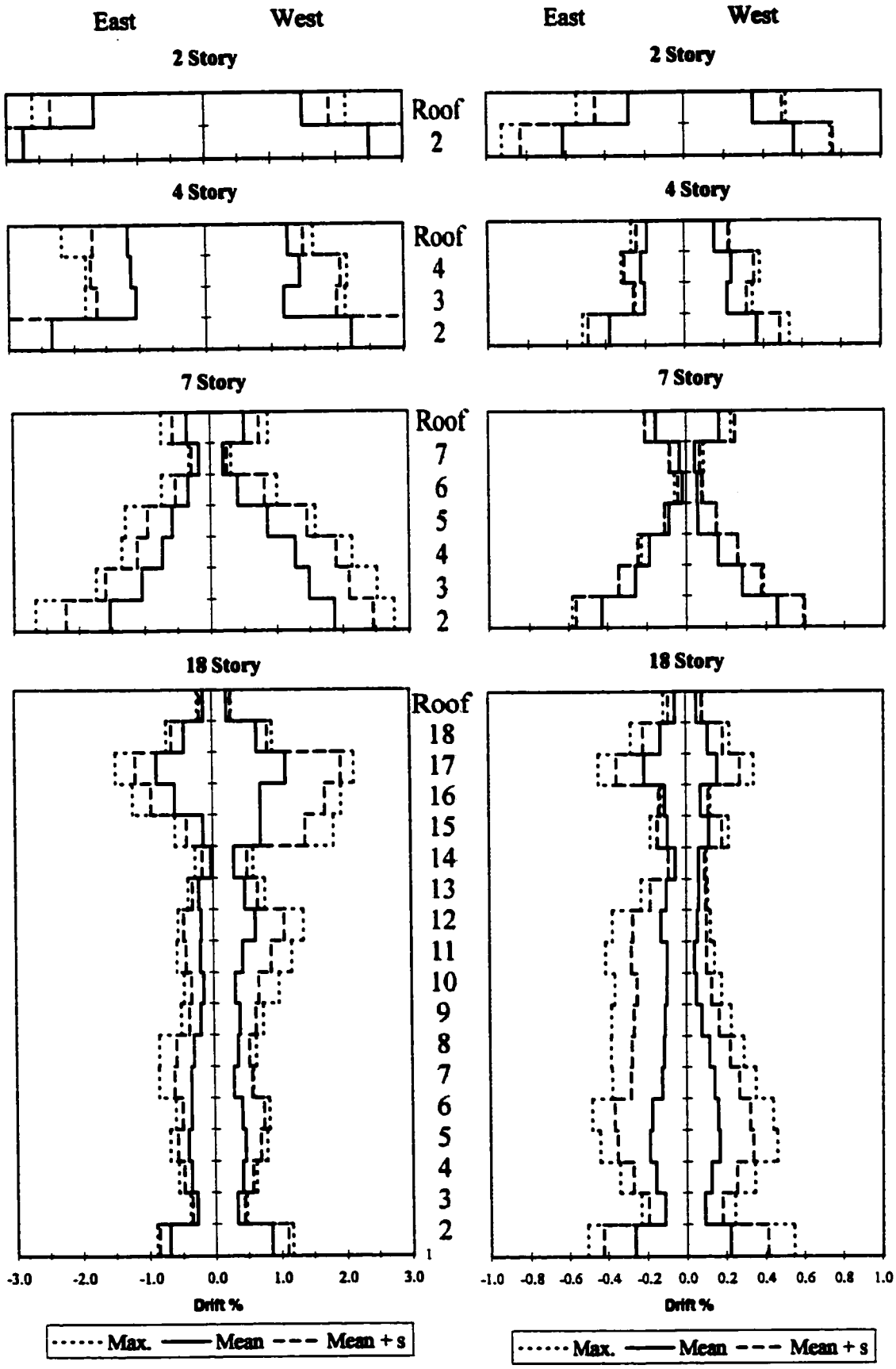

Figure 4.7: Inter-story drifts for seat-angle connections, As-built scenario

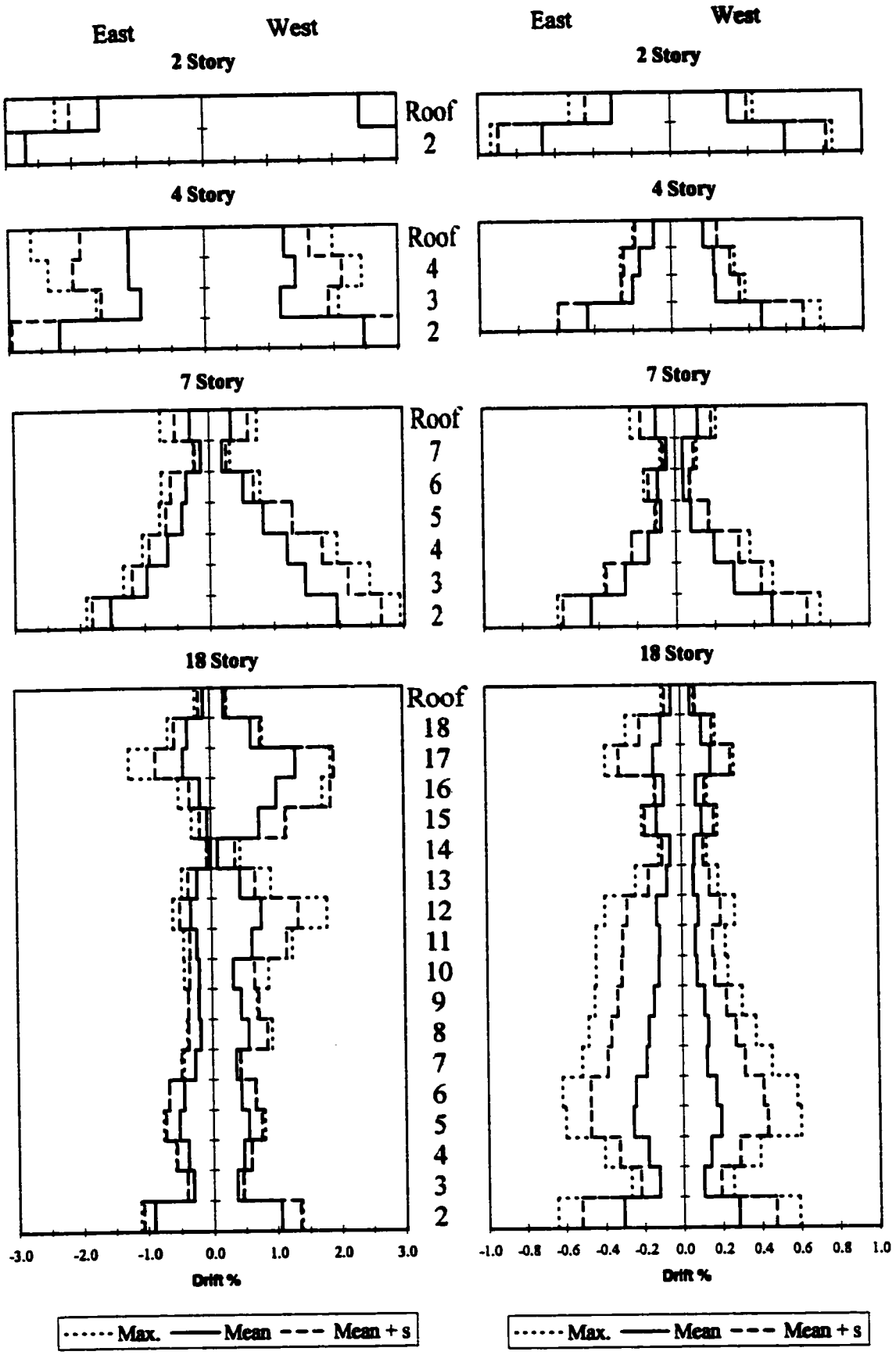

Figure 4.8: Inter-story drifts for seat-angle connections, P-Δ scenario

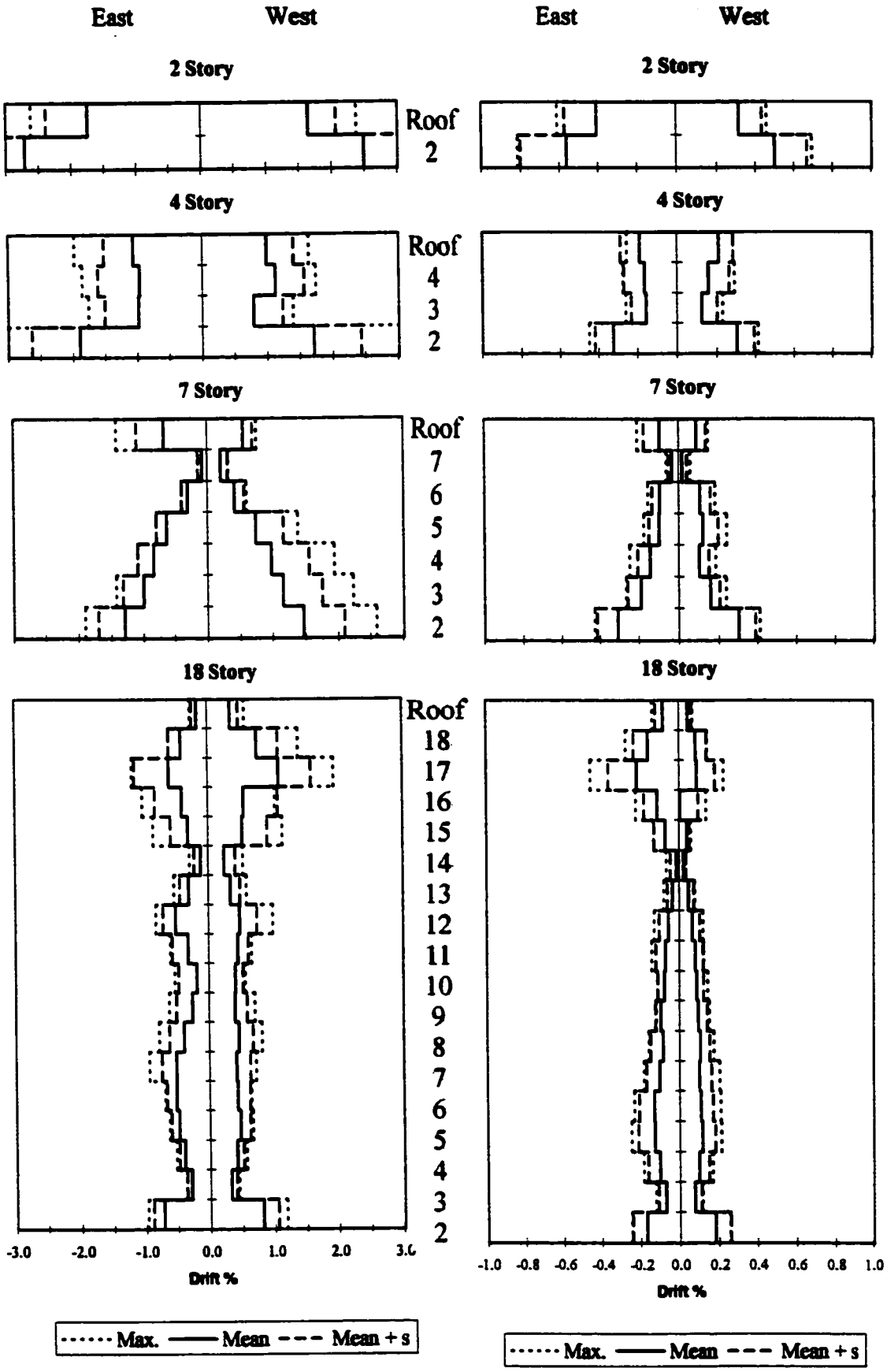

Figure 4.9: Inter-story drifts for seat-angle connections, Modern mass scenario

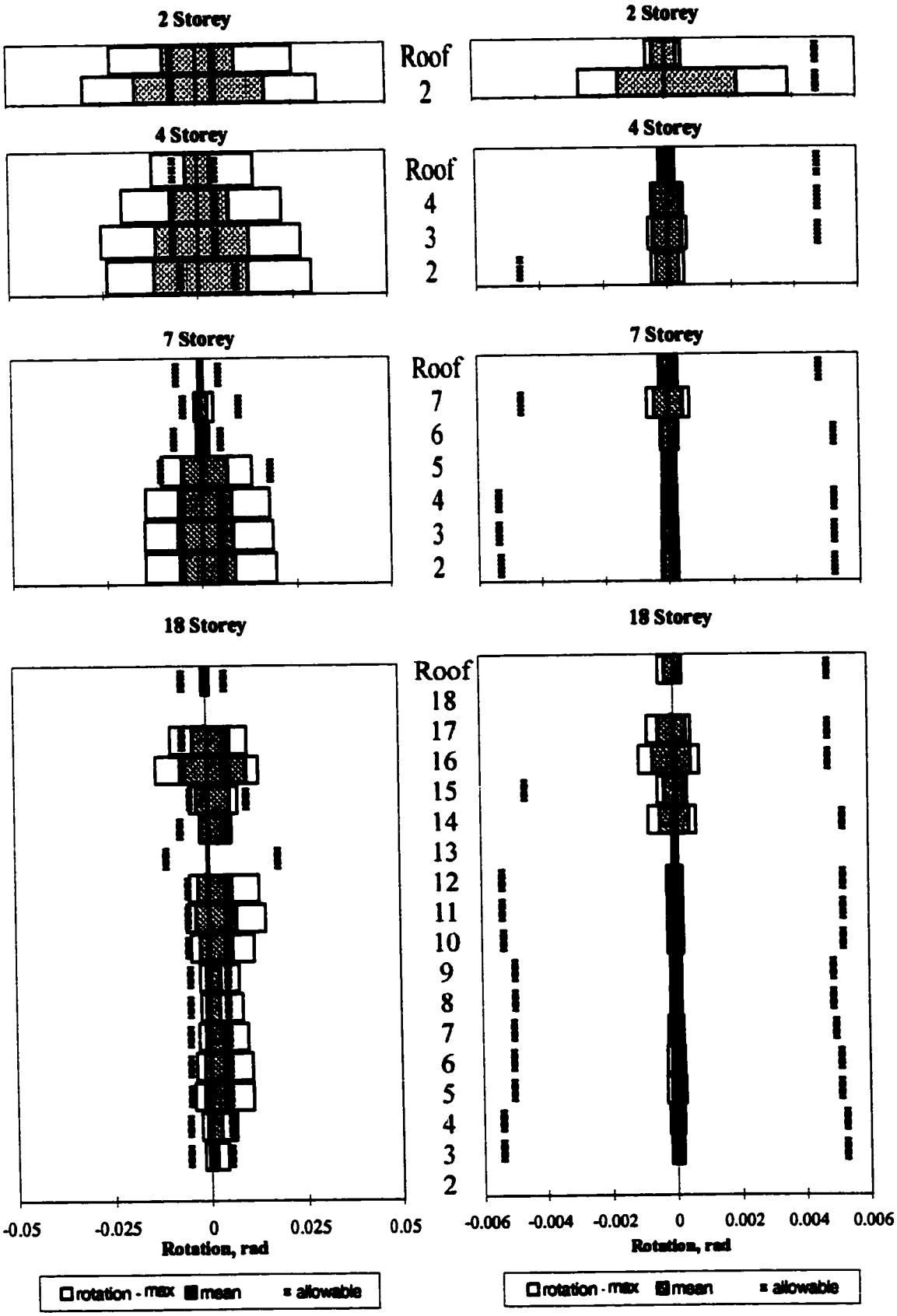

Figure 4.10: Rotation of critical tee-stub connections, As-built scenario

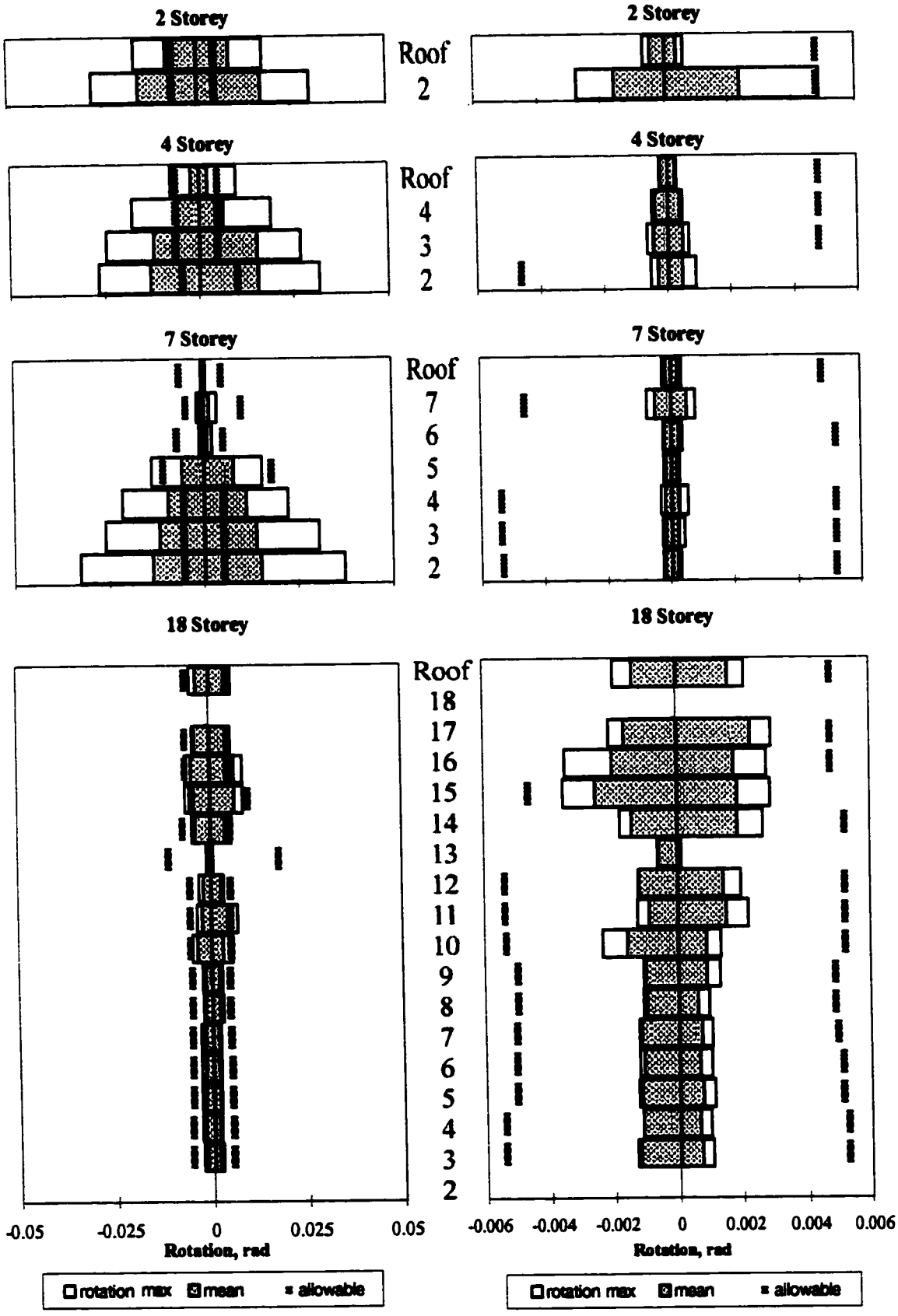

Figure 4.11: Rotation of critical tee-stub connections, P-Δ scenario

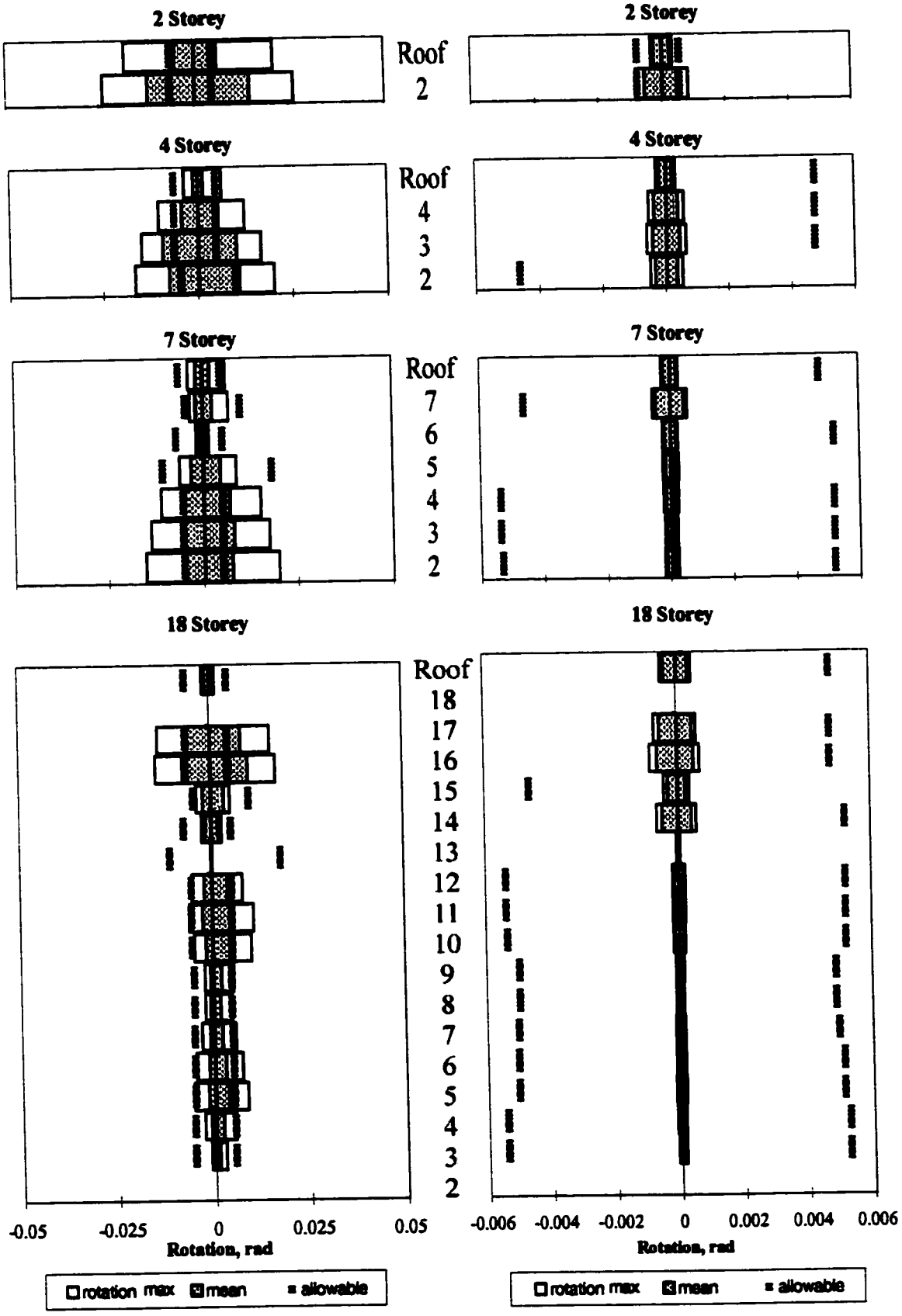

Figure 4.12: Rotation of critical tee-stub connections, Modern mass scenario

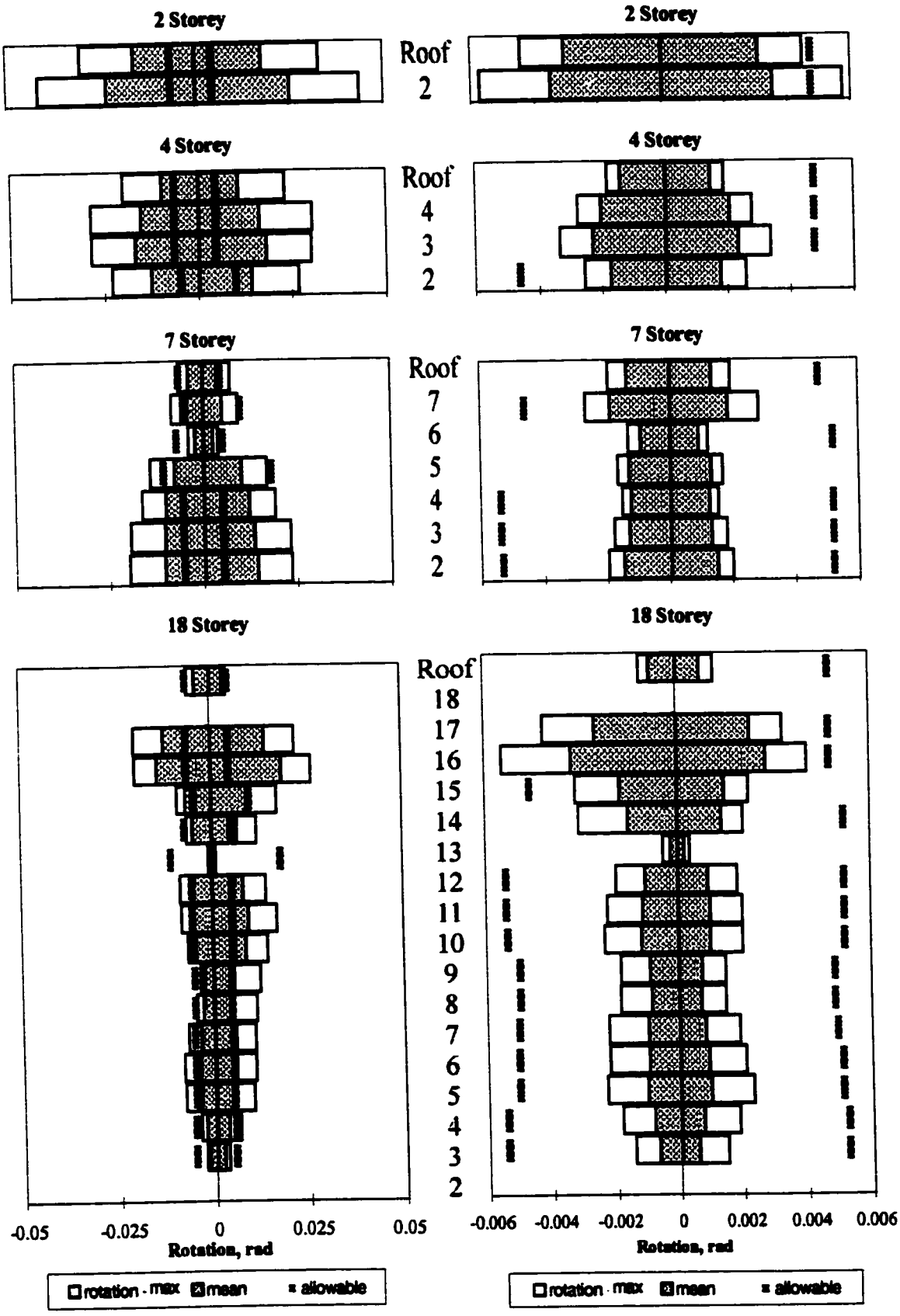

Figure 4.13: Rotation of critical seat angle connections, As-built scenario

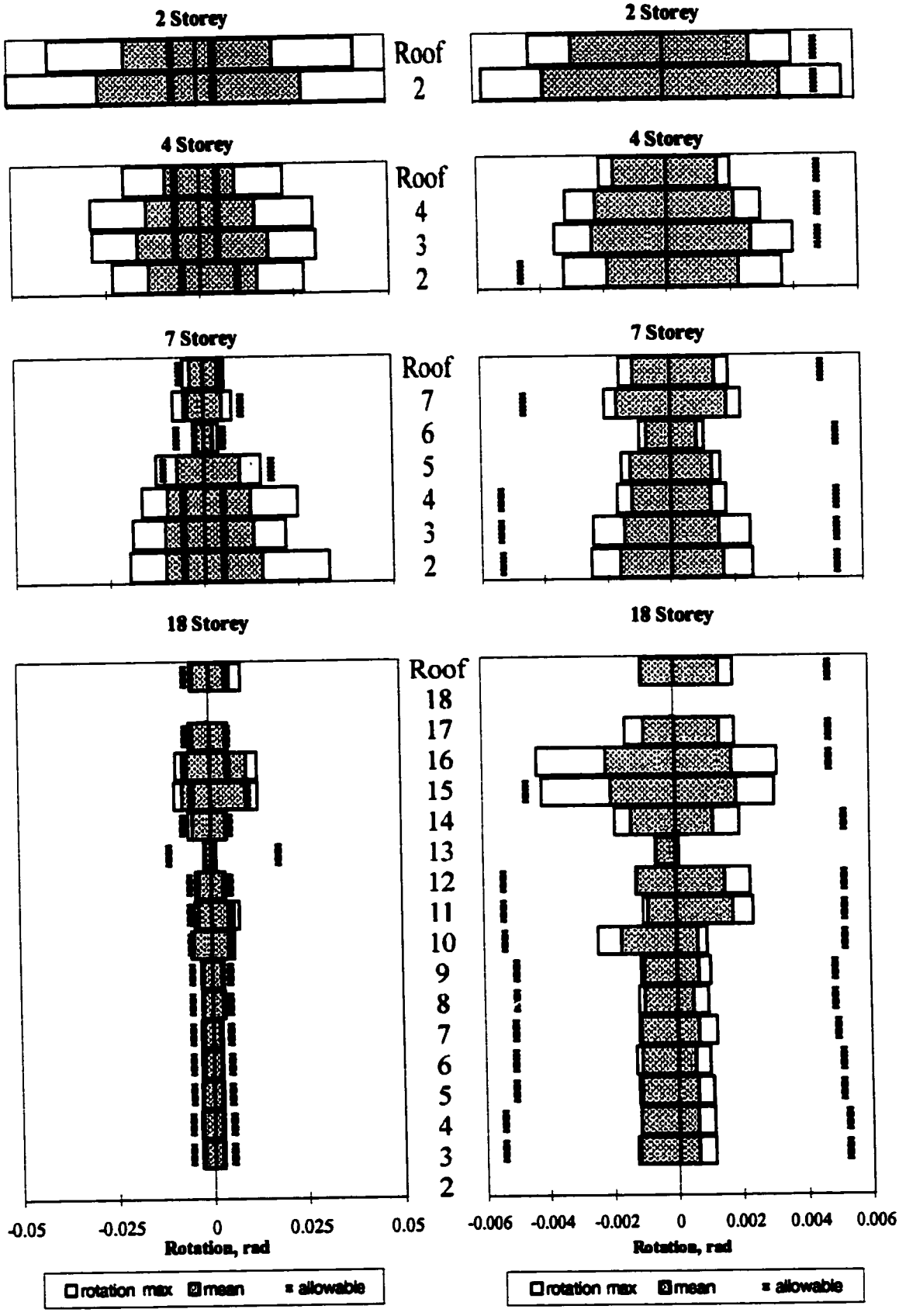

Figure 4.14: Rotation of critical seat angle connections, P-Δ scenario

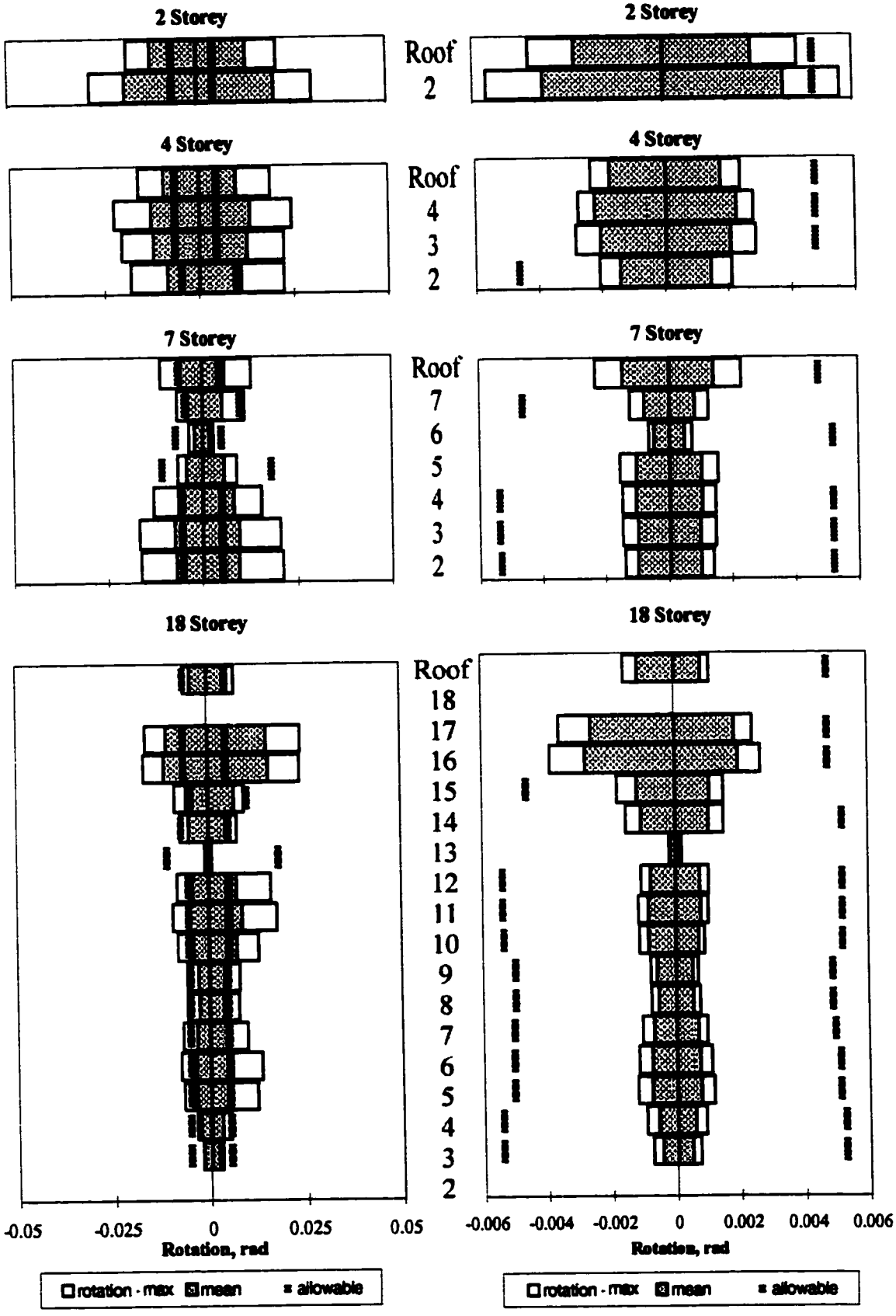

Figure 4.15: Rotation of critical seat angle connections, Modern mass scenario

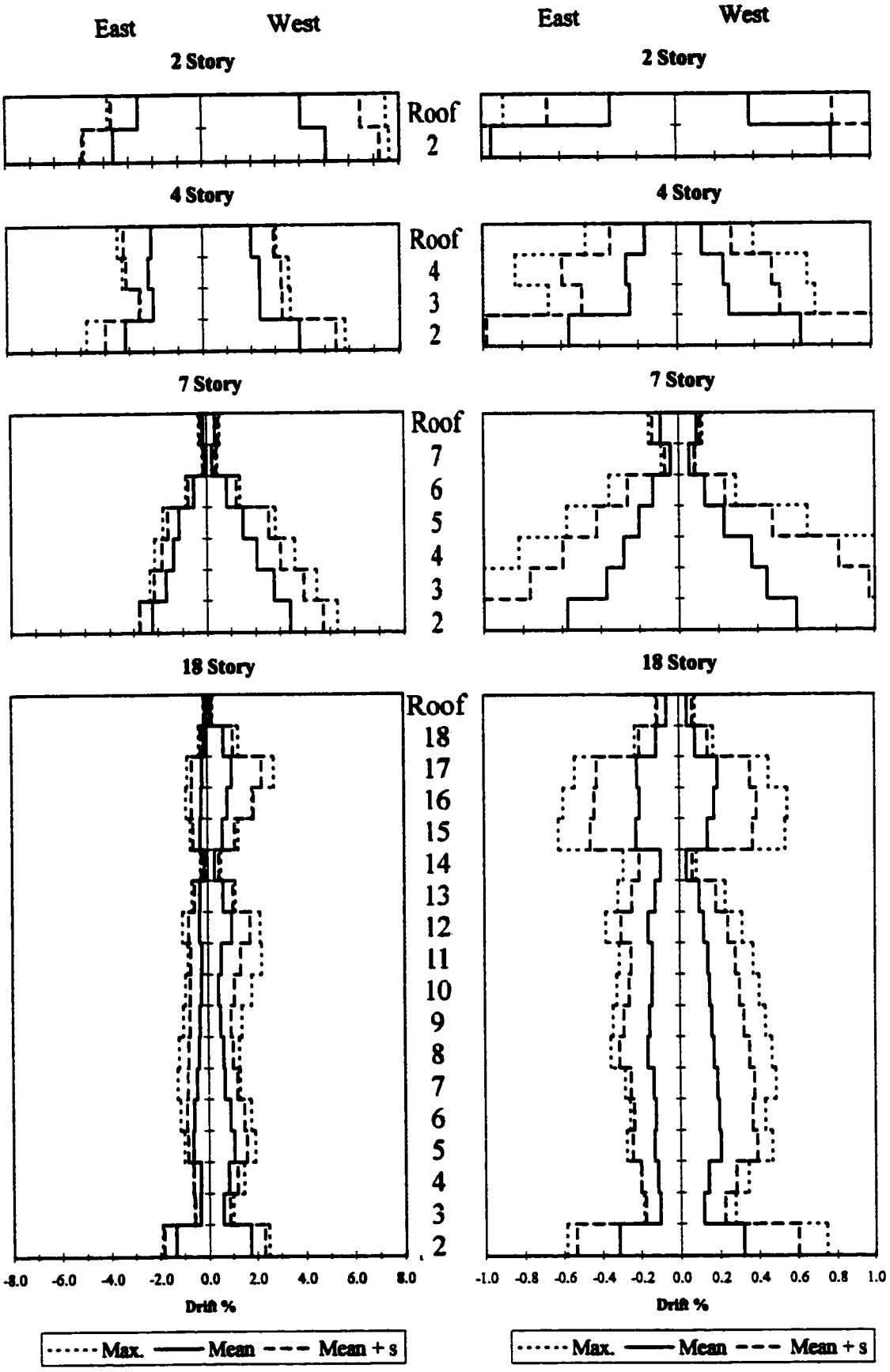

Figure 4.16: Inter-story drifts for tee-stub connections, Non-scaled earthquake scenario

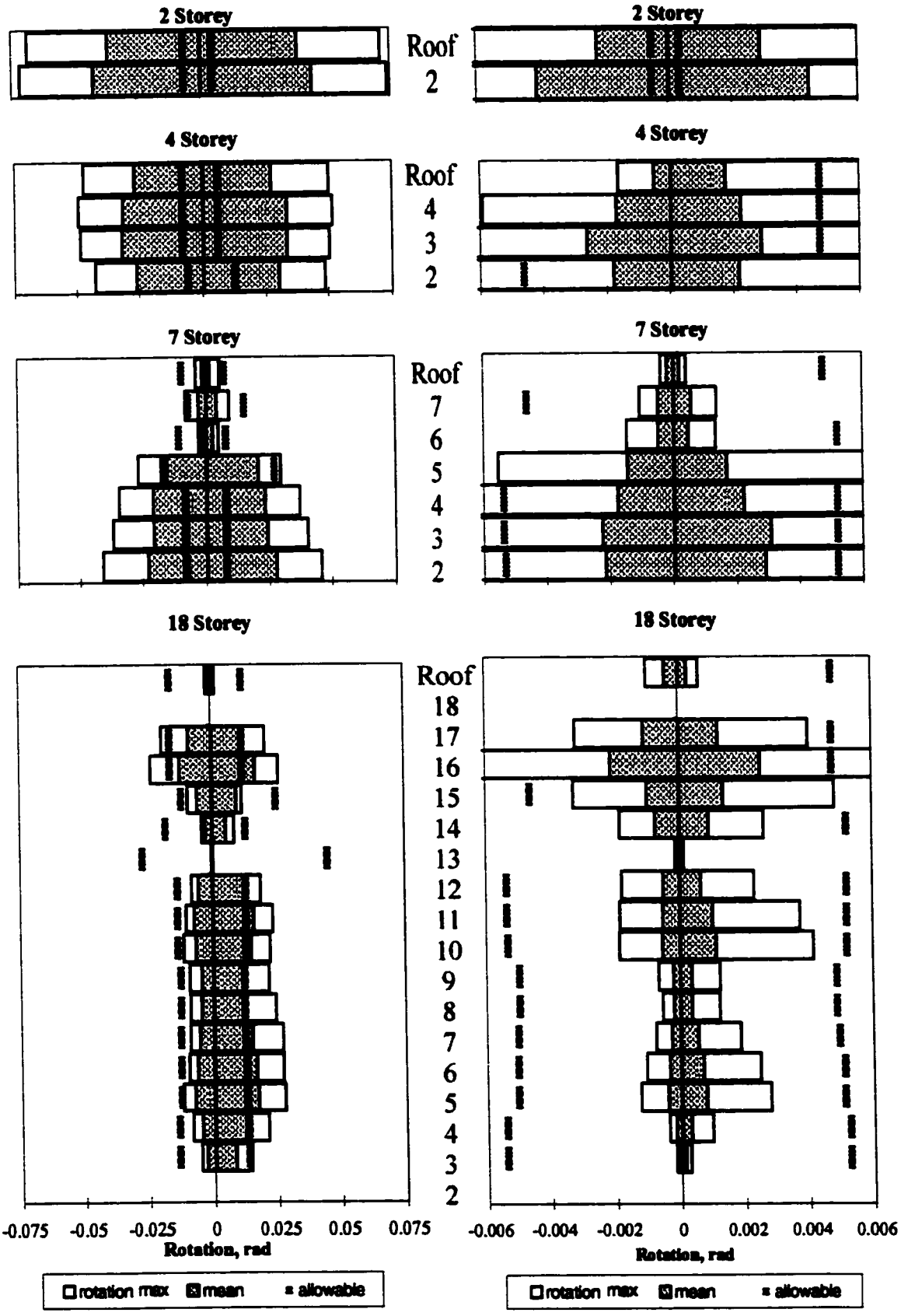

Figure 4.17: Rotation of critical tee-stub connections, Non-scaled earthquake scenario

Appendix A

Connection Redesign

A.1 Connection Redesign

The connections of the existing structure were redesigned based on the specifications given by the architect.

> *Wind is to be taken at 30 lbs. per. sq. ft. on exposed area of building blowing in any direction and will be assumed as distributed to all the columns in the building by the floor slabs.*

The following is an example of the design method followed for all the connections of the structure. The calculations are for the typical 5th floor connection.

A.2 Connection Moments and Shears

The distribution of wind loads in the frame follows the portal method described in *Structural Steel Design* by Tall (1974). The moment and shear from the wind loads acting on the connections were calculated assuming points of inflection at the column and beam mid-points. The values of moment and shear obtained for the wind loading are added to that of the gravity loads. The values calculated for the typical 5th floor connection are 167.3 kip·ft and 38.1 kips for the moment and shear respectively.

A.3 Assumptions for Connection Design

Certain assumptions were required to re-design the connections of the existing building. They are all listed below:

- The architect had specified that all the steel members were to be from Bethlehem or Carnegie steel mills. All the member sizes identified on the structural drawings were verified against the tables found in *Iron and Steel Beams 1873 To 1952* to obtain the

physical properties of each section, as in the early part of the century, beam sizes were not all standardized.

- A steel grade of 30 ksi was assumed, and the rivet yield strength of 33 ksi observed in the Bruneau and Sarraf (1996) study was used.
- All the rivets in the connections were assumed to be of constant diameter, $^{3}/_{4}$". The rivets holes were set at $^{13}/_{16}$" as given in the shop drawings.
- The tees used in the connections were assumed to come from split W shapes available from Bethlehem or Carnegie steel, if possible.
- A safety factor (SF) was set at 0.6 throughout the design. This safety factor was only used in the redesign of the connections, it was not included in the capacity calculations presented in Appendix B.

A.4 Connection Design

Basic properties:
Column flange width = 15 in.
Beam depth = 19.88 in.
Beam width = 8 in.

Applied forces:
V = 38.1 kips
M = 167.2 kip·ft

The moment applied to the connection can be divided into a force couple as shown in Figure A.1.

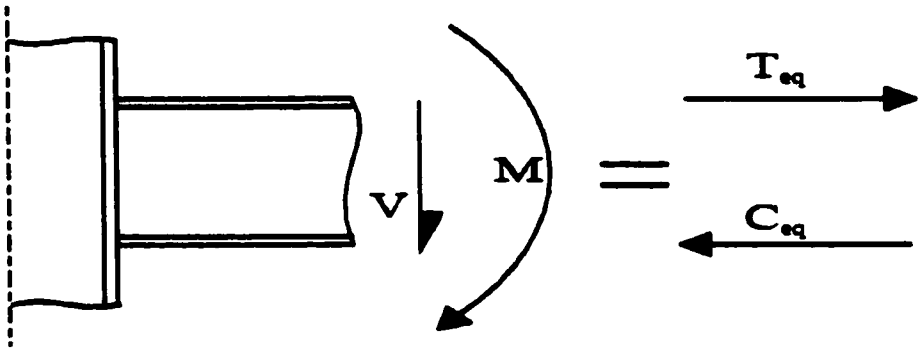

Figure A.1

T_{eq} = M / beam depth
= 167.2 / (19.88 / 12)
= 101.0 kips

Rivet strength:

Maximum rivet tensile resistance:
SF·A·Fy = 0.6·0.44·33
= 8.7 kips

Maximum rivet shear resistance:
0.75·SF·A·Fy = 0.75·0.6·0.44·33
= 6.5 kips

Minimum amount of rivets:

flange of tee to column (tension)
n = T / 8.7
= 11.4 rivets (The shop drawings gave 16 rivets.)

Stem of tee to beam (shear)
n = T / 6.5
= 15.2 rivets (use 16 rivets, 8 rows of two rivets)

It was assumed that the shear is transferred from the beam to the column via the stiffener and its rivets.

Stiffener to column (shear)
n = V / 6.5
= 5.7 rivets (use 6 rivets)

Tee size:
The rivet spacing is given in Figure A.2, which gives a 13" wide tee. The stem length of the tee was determined using the same 3" gage for the rivets, giving a length of 25".

Using the 13" wide stem it was possible to calculate the minimum stem thickness.

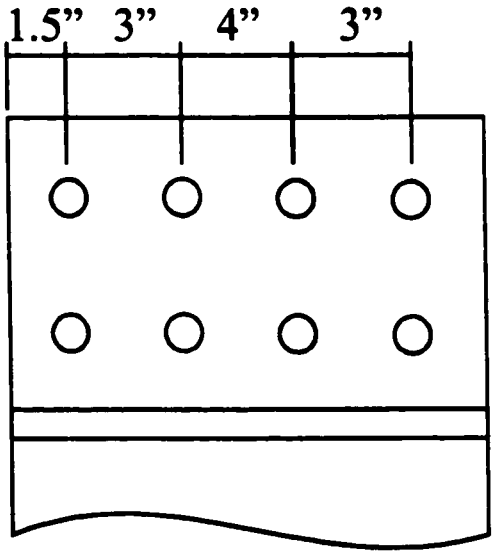

Figure A.2

$t_{stem} = T_{eq} / (SF \cdot Fy(13\text{-}2 \cdot holes))$
$= 0.493$ in.

The dimensions obtained for this connection were too large to have the tee come from a split W shape. Therefore, the tee was obtained by cutting the flange off a W shape. Based on the *Iron and Steel beams* book, the flange of the tee has a width of 14.16".

The same tee size was used for the bottom assembly in the connection.

Stiffener size:

The method described in Salmon and Johnson (1980) was followed to obtain the stiffener thickness, t_s.

The required bearing length was given as:

$$N = \frac{P}{0.75 \cdot F_y \cdot t_w} - k = 4.4in.$$

Where: N = bearing length
P = shear force acting on stiffener
t_w = beam web thickness
k = distance from outer face of flange to web toe of fillet

Total width of stiffener = N + k + setback = 5.0 in.

The stiffener thickness:
i- t_s must be at least the same thickness as the web of the beam = 0.375 in.

ii- also, $t_s \geq \frac{P}{0.90F_y(W - 0.5)2} = 0.21in.$

Therefore t_s must be at least 0.375 in. (Total stiffener tickness)

The minimum length of the stiffener is calculated based on rivet layout, although shear capacity was also considered but did not govern in this case. The rivet layout dictated a minimum length of 10".

The stiffener sizes obtained for this connection are two 3 $^1/_2$" x 6" angles (long legs back-to-back) with a thickness of 0.3125" and a length of 10".

The sizes obtained for all the connections of the existing structure are given in Table 3.1.

Appendix B

Connection Failure Modes

B.1 Failure modes

The following sections describe the failure modes calculated for all the connections in the existing structure. The sample calculations provided are for the 5th floor connections. The size of the tees and stiffeners are given in Table 3.1.

B.2 Positive moment failure modes

B.2.1 Tensile yielding of rivets

According to Picard and Beaulieu the prying action in a tee can be evaluated using the following methodology. It is assumed that the tensile force applied to the tee is distributed evenly among the rivets. The prying action is applicable only to the interior line of rivets.

$$Q = P_f\left(\frac{\alpha\delta}{1+\alpha\delta}\right)\left(\frac{b'}{a'}\right) = prying\,action$$

Where: P_f = total tensile force on tee / 16

$$\alpha = \frac{1}{\delta}\left[\frac{4P_f b'}{pt_r^2 F_{y\,steel}} - 1\right]$$

$$\delta = \frac{(p - dia)t_2}{pt_1} = 0.64$$

dia = hole diameter = 20.6 mm

t_r = average flange thickness between stem and 1st rivet line = 29 mm

t_1 = flange thickness at stem = 31.5 mm

t_2 = flange thickness at 1st rivet line = 27 mm

p = width of tee ÷ rivet rows = 330/4 = 82.5 mm

b = stem face to center of rivet hole = 56 mm

a = lesser of: center of rivet hole to flange edge or 1.25 b = 70 mm

a' = a + 0.5 dia = 80 mm

b' = b - 0.5dia = 46 mm

$F_{y\,steel}$ = 206 MPa

To obtain the yield point of the connection, $P_{int.\ rivet} = P_f + Q = P_{yield}$

Where: $P_{yield} = A_{rivet} \cdot F_{y\ rivet} = 74$ kN

$A_{rivet} = 335$ mm

$F_{y\ rivet} = 225$ MPa

By iteration, the load required to yield the rivets were calculated, however, in this connection the flange offered more resistance to bending than the rivets could sustain (i.e no prying action).

Therefore, $T = 16 \cdot P_{yield} = 1180$ kN, and

$$M^+ = T \cdot d$$
$$= 595 \text{ kN} \cdot \text{m}$$

Where: d = beam depth = 505 mm

Note: the lower floor connections have thick flanges making prying action not very significant. Prying action is nonetheless verified for all the connections and accounted for in the upper floors.

B.2.2 Hinge mechanism in tee

The location of the plastic hinges are shown in Figure B.2.2.

Using the virtual work method,

$$T = 2(M_{p1} + M_{p2}) / a = 945 \text{ kN}$$

Where: M_{p1} = plastic moment at stem = 16.9 kN ·m

M_{p2} = plastic moment at rivet line

= 9.2 kN ·m

a = distance between stem face and rivet line

= 55 mm

Therefore: $M^+ = 475$ kN ·m

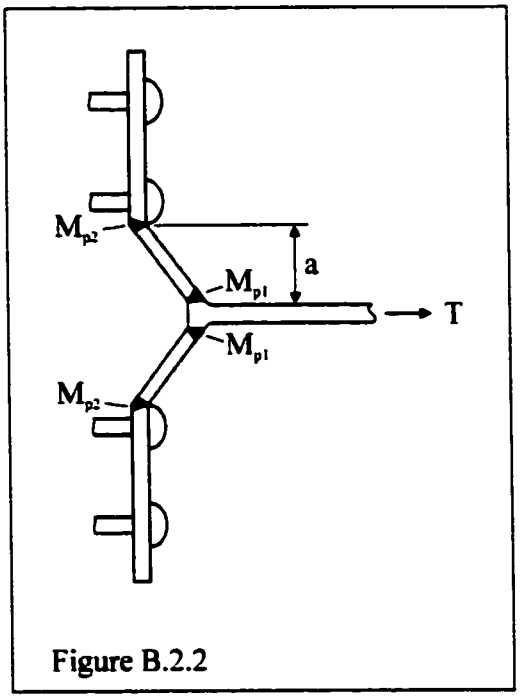

Figure B.2.2

B.2.3 Net section yield of stem

$$T = A_{net} \cdot F_{y\,steel} = 890 \text{ kN}$$

Where: A_{net} = Area of stem - 2 rivet holes = $(330 - 2 \cdot 21)15 = 4320 \text{ mm}^2$

$F_{y\,steel}$ = 206 MPa

Therefore the failure moment is $M^+ = 450 \text{ kN} \cdot \text{m}$

B.2.4 Tensile rupture of rivets

The tensile rupture of the rivets was calculated the same way as for their tensile yielding (Section B.2.1), substituting $F_{y\ rivet}$ with $F_{u\,rivet} = 485$ MPa.

Substitution gives T = 2600 kN and $M^+ = 1310 \text{ kN} \cdot \text{m}$.

B.2.5 Shear failure of rivets

Taking the shear to tension ratio of rivets as 0.75 as given by (Kulak et al.), the shear capacity of the rivets in the stem of the top tee is:

$$V = 0.75\, A_{rivet} \cdot F_{u\,rivet} \cdot n$$
$$= 1940 \text{ kN}$$

Where: $A_{rivet} = 335 \text{ mm}^2$

$F_{u\,rivet} = 485$ MPa

n = number of rivets = 16

Therefore: $M^+ = V \cdot d$

$= 970 \text{ kN} \cdot \text{m}$

B.2.6 Net section rupture of stem

$$T_{ultimate} = A_{net} \cdot F_{u\ steel}$$
$$= 1730\ kN$$

Where: $F_{u\ steel} = 400$ Mpa

Therefore: $M^{+} = T_{ultimate} \cdot d$
$$= 870\ kN \cdot m$$

B.3 Negative moment failure modes

B.3.1 Formation of hinge mechanism in stiffeners

The model developed by Bruneau and Sarraf (1996) is modified and applied to this connection. The capacity of the bottom assembly is divided in two components: the tee and the stiffener. The total capacity is given by:

$$T_{total} = T_{tee} + T_{stiffener.}$$

Where: T_{tee} = same as section B.2.1 = 1180 kN

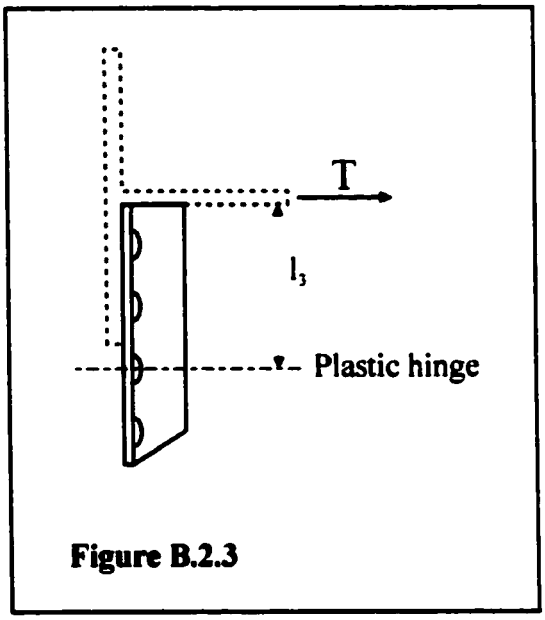

Figure B.2.3

A plastic hinge will form in the stiffener (Figure B.3.1) along the third rivet line. There is no contribution from the top two rows of rivets since they move with the tee.

$$T_{stiffener} = M_{p\ stiffener} / l_3 = 80\ kN$$

Where: $M_{p\ stiffener} = 22\ kN \cdot m$ (for 2 back to back stiffeners)

$l_3 = 279$ mm

Therefore: $T_{total} = 1180 + 80 = 1260$ kN ; and

$M^- = 635$ kN·m

B.3.2 Net section yield of stem

This mode of failure is the same as for the top tee (B.2.3).

Therefore, the failure moment is $M^- = 450$ kN ·m

B.3.3 Shear failure of rivets in stem of tee

This mode of failure is the same as for the top tee .

Therefore: $M^- = 970$ kN ·m

B.3.4 Net section rupture of stem

This mode of failure is the same as for the top tee.

Therefore: $M^- = 870$ kN ·m

B.4 Critical modes of failure

The point of initial yield and the governing mode of failure for each connection is based on the comparison of the modes of failure calculated. For the 5th floor connection, they are listed in Table B.4.

Positive Bending		
I	Tensile yielding of rivets	595 kN ·m
II	Formation of hinge mechanism in tee	475 kN ·m
III	Net section yield of stem	**450 kN ·m**
IV	Tensile rupture of rivets	1310 kN ·m
V	Shear failure of rivets	970 kN ·m
VI	Net section rupture of stem	**870 kN ·m**

Negative Bending		
I	Formation of hinge mechanism in stiffeners	635 kN ·m
II	Net section yield of stem	**450 kN ·m**
III	Shear failure of rivets in stem of tee	970 kN ·m
IV	Net section rupture of stem	**870 kN ·m**

Table B.4: Calculated failure modes for 5th floor connection

The initial onset of yield in positive bending, for the 5th floor connection, is caused by the yielding of the net area of the stem and occurs at a moment of 450 kN·m, the mode of failure governing the positive bending is the rupture of the net section of the stem occurring at 870 kN·m. In negative bending, for this connection, the initial yield point and the mode of rupture occurs at the same moment as the top tee. The top and bottom assemblies do not always yield or fail in the same manner.

The initial yield point and failure modes for all the connections are listed in Table 3.3.